July 2016

Design, Synthesis, and Applications of Nano-assemblies Based on Amphiphilic Macromolecules

Hui Wang
University of Massachusetts Amherst

DESIGN, SYNTHESIS, AND APPLICATIONS OF NANO-ASSEMBLIES BASED ON AMPHIPHILIC MACROMOLECULES

A Dissertation Presented

by

HUI WANG

Submitted to the Graduate School of the
University of Massachusetts Amherst in partial fulfillment
of the requirements for the degree of

DOCTOR OF PHILOSOPHY

May 2016

Chemistry

DESIGN, SYNTHESIS, AND APPLICATIONS OF NANO-ASSEMBLIES BASED ON AMPHIPHILIC MACROMOLECULES

A Dissertation Presented

by

Hui Wang

Approved as to style and content by:

_____

Sankaran Thayumanavan, Chair

_____

Min Chen, Member

_____

James J. Chambers, Member

_____

Harry Bermudez, Member

_____

Craig T. Martin, Department Head

Chemistry Department

DEDICATION

To my parents

ACKNOWLEDGMENTS

I would like to take this opportunity to express my sincere gratitude to those who have helped and supported me to make this dissertation possible.

First of all, I would like to thank my advisor, Professor Sankaran Thayumanavan, for his training, guidance, inspiration and support throughout my doctoral degree. I appreciate the freedom he has given me to come up with my own research ideas and execute them and the training he has provided for me to approach scientific problems critically and creatively. I really appreciate his constant efforts to push all of his students, including myself, to become better scientists.

I would like to extend my gratitude to my committee members, Professor Min Chen, Professor James Chambers, and Professor Harry Bermudez, for their valuable suggestions and inputs during my Prospectus, ORP and Final defense. I would also like thank Prof. Min Chen and Professor Harry Bermudez for writing reference letters for me.

I would like to acknowledge all my collaborator and colleagues for their contributions to my research and all sorts of help: Dr. Krishna R. Raguphathi, Dr. Jiaming Zhuang, Dr. Reuben Chacko, Dr. Bhooshan Popere, Dr. Rajasekhar Reddy Rami Reddy, Dr. Ambata Poe, Dr. Andrea Della Pelle, Dr. Feng Wang, Dr. Jing Guo, Dr. Longyu Li, Dr. Wei Bai, Bo Zhao, Kishore Raghupathi, Bin Liu, Huan He, Poornima Rangadurai, Uma Sridhar, Priyaa Prasad, Vikash Kumar. Thank you all for your tremendous help in my research work and creating a fun and friendly research environment. It has been a great experience working with all of you.

I would like to express my special thanks to Dr. Krishna R. Raguphathi, Dr. Jiaming Zhuang. Both of them are my seniors (by one year). They have been very helpful and

resourceful to me since I joined the group and have continued to give valuable suggestions and advice throughout most of my PhD career. Thank you for being such wonderful seniors. I could not have done so much without your help.

I would like to thank our group assistant Karen Hakala for her help, as well as UMass Chemistry staff J.M. Stowe and Robert Sabola.

Finally, I could not have gone so far without the support and care of my family and friends. To my parents: thank you for your unconditional love and always encouraging me of pursuing higher education. Thank you for your occasional financial support even though I should be the one doing this at this age. To my girlfriend and friends: thank you for your encouragements and being there with me and when I was frustrated and confused. I enjoyed all the fun time we had at Amherst.

ABSTRACT

DESIGN, SYNTHESIS, AND APPLICATIONS OF NANO-ASSEMBLIES BASED ON AMPHIPHILIC MACROMOLECULES

May 2016

HUI WANG, B.S., STONY BROOK UNIVERSITY

Ph.D., UNIVERSITY OF MASSACHUSETTS AMHERST

Directed by: Professor Sankaran Thayumanavan

Recent progress in nanotechnology has been significantly impacting a variety of areas such as utilization in microelectronics, multiphase catalysis, sensing and therapeutics. Our interests are to develop new nanomaterials to understand their structure-property relationships and to utilize them for various applications. In this thesis, we discuss our findings on the design, synthesis and applications of nanomaterials formed by self-assembly of amphiphilic molecules.

Micelles are self-assembled nanostructures formed by amphiphilic molecules. They are capable of sequestering hydrophobic guest molecules in an aqueous environment. Other than surfactants, micelles can also be formed by amphiphilic polymers or dendrimers, which are macromolecular surfactants in a linear or branched fashion. We are interested in creating various functional materials based on self-assembled micelles that could be tuned by modifying the amphiphilic building blocks during their synthesis. We showed that utilizing the container property and dynamic equilibrium of small molecule surfactants, we were able to develop a protein nanosensor by non-covalently encapsulating a fluorophore-tethered ligand and a quencher in the micelle core. By incorporating an enzyme substrate on an amphiphilic dendrimer, we developed a nanoprobe that was capable of detecting

enzyme activities based on ^{19}F NMR spectroscopy. Last but not least, employing the convenience of polymer synthesis, we invented a new methodology of forming polymer nanoparticles by covalently crosslinking the hydrophobic components of micelles formed by amphiphilic random copolymers.

TABLE OF CONTENTS

LIST OF TABLES

Table Page

LIST OF FIGURES

Figure Page

LIST OF SCHEMES

Scheme Page

LIST OF CHARTS

Chart Page

CHAPTER 1

INTRODUCTION

Supramolecular assemblies such as micelles, vesicles, fibers, and helical structures are often formed by the spontaneous self-organization of amphiphilic molecules through non-covalent interactions.[1-5] The self-assembled structures form as a system reaches thermodynamic equilibrim, minimizing its free energy. Among various self-assembled systems, strcutures displaying container properties have found tremendous implications in the field of sensing, drug delivery and diagnostics because of their abilities to retain guest molecules such as drug molecules and reporter units.[6-9] For example, micelles are capable of solubilizing lipophilic guest molecules in an aqueous environment by localizing them into their water excluded lipophilic cores, while vesicles are capable of sequestering both lipophilic and hydrophilic molecules.

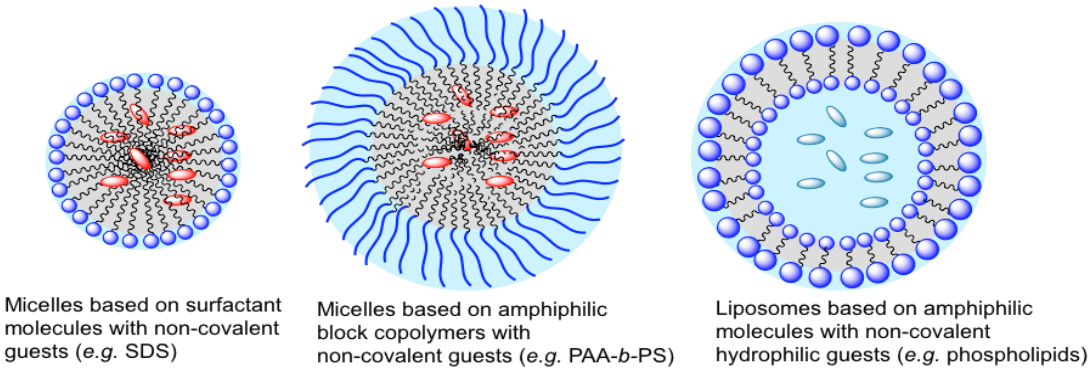

Figure 1.1: Assemblies made from amphiphilic molecules capable of non-covalently binding guest molecules.

The self-assembly of an amphiphilic molecule is dictated by the differential interactions of hydrophilic and hydrophobic functionalities with the bulk solvent and among themselves. [1-5, 10-17] For example, micelles form when the hydrophilic functionalies

of the amphiphiles can effectively shield the lipophilic functionalities from the aqueous medium to form a water-excluded hydrophobic enviroment. In addition, the type of assembly an amphiphile forms, such as a micelle, a vesicle, or another assembly, is determined by the relative position and volume of its functional groups.[18-20] Besides the requirements for functional group, amhiphiles must be above a certain concentration to form assemblies. The minimum concentration of an amphiphile, above which the molecule aggregates into amphiphilic assemblies, is called its critical aggregation concentration (CAC).

Self-assembled structures can be formed from both amphiphilic small molecules and macromolecules. Amphiphilic small molecules, known as surfactants, are often used as detergents, emulsifiers, foaming and anti-foaming agents, and etc. They generally have large CAC values and form assemblies with relatively low mechanical stabilities. On the other hand, assemblies formed from amphiphilic macromolecules have higher stabilities and considerably lower CAC values. These assemblies generally are more stable in retaining guest molecules and have therefore found applications in many areas.[10-16] This dissertation will primarily focus on the assemblies formed by macromolecular surfactants which may be broadly classified into two categories, amphiphilic polymers and dendrimers.

1.1 Stimuli Responsive Supramolecular Assemblies

Stimuli responsive assemblies are materials capable of responding to changes in the local environment. These materials have generated great interests in a variety of fields, including controlled drug delivery vehicles,[21-25] sensing,[26-30] tissue engineering,[31-33] coatings,[34, 35] catalysis,[36, 37] and separations.[38, 39] The types of stimuli that trigger these

materials are diverse and can be broadly divided into three categories: physical, chemical and biological stimuli.[40] Physical stimuli include magnetic fields, light, ultrasound, temperature, electric fields and mechanical forces; chemical stimuli can be pH, ionic strength, and redox potential changes, while biological stimuli include enzymes, proteins, nucleic acids, sugars and etc. Because the levels of biological stimuli are often indicative of one's pathological state, systems that respond to these stimuli have important therapeutic and diagnostic values. Our interests lie in designing macromolecular assemblies that respond to biological stimuli, especially proteins and enzymes.

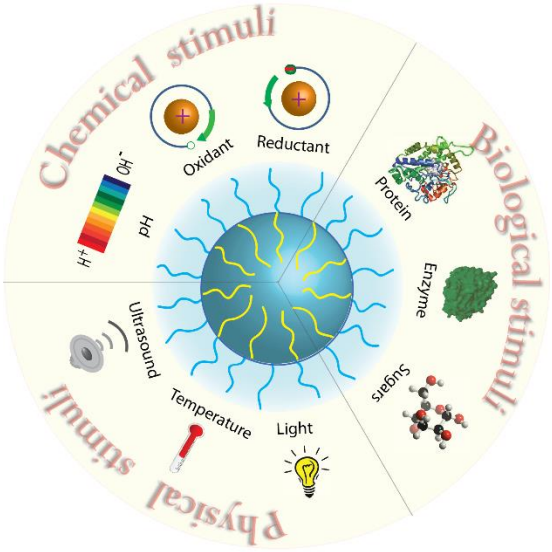

Figure 1.2: Three categories of stimuli for responsive materials: physical, chemical and biological.

1.2 Stimuli Responsive Supramolecular Assemblies Based On Polymers

Amphiphilic polymer is an attractive material for constructing protein responsive assemblies because of the enhaced binding efficiency between the polymer and the protein surfaces through multivalent interactions. In addition, polymeric assemblies generally

exhibit higher structural stability compared to assemblies formed by small molecules. While binding of proteins to micelles formed by surfactants often causes the disruption of the assemblies, polymeric micelles can retain intact upon protein binding. Utilizing the high integrity of polymeric micelles, our group developed a novel approach for detecting proteins based on micellar assemblies formed by an amphiphilic polymer.[41]

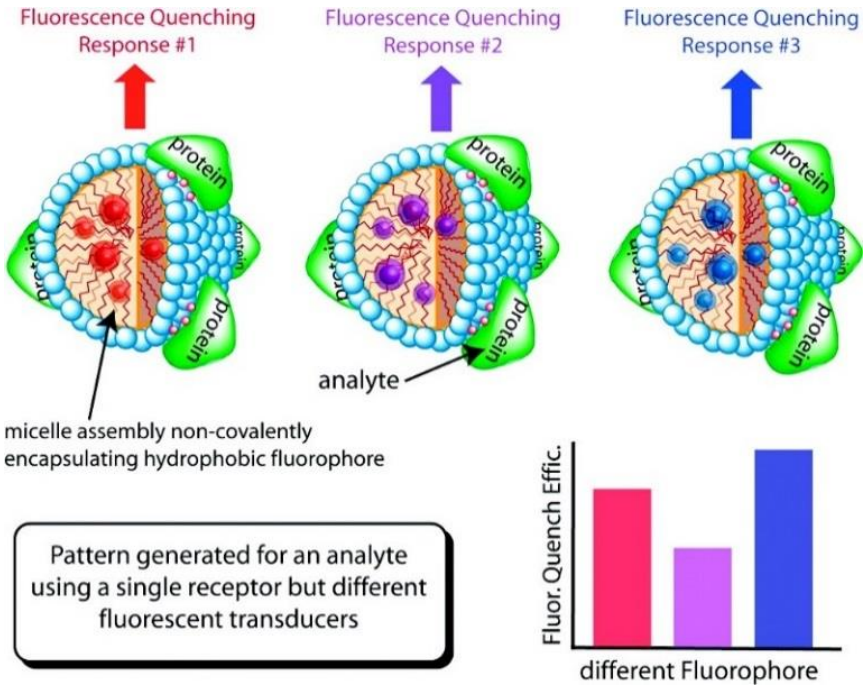

Figure 1.3: Schematic of the differential transducer approach using amphiphilic polymeric micelles.

In this approach, we designed an amphiphilic polymer that is able to (i) form micelles with high stability, (ii) encapsulate hydrophobic guest molecules, and (iii) bind to proteins. Because protein cofactors can quench the fluorescence of dye molecules by accept energy or electrons from the excited state of these fluorophores, dye molecules were encapsulated in these micellar assemblies. Upon binding to different metalloproteins through nonspecific interactions, the fluorescence intensities were quenched to different extents. By simply varying the encapsulated dye molecule, we were able to generate

fluorencent patterns for detecting different metalloproteins (Figure 3). Note that it's important that the protein binding does not disrupt the container property of these assemblies, as release of dye molecule also causes reduction of fluorescent intensity. In this case, an assembly with high stability is required for the success of the sensing design.

1.3 Stimuli Responsive Supramolecular Assemblies Based On Dendrimers

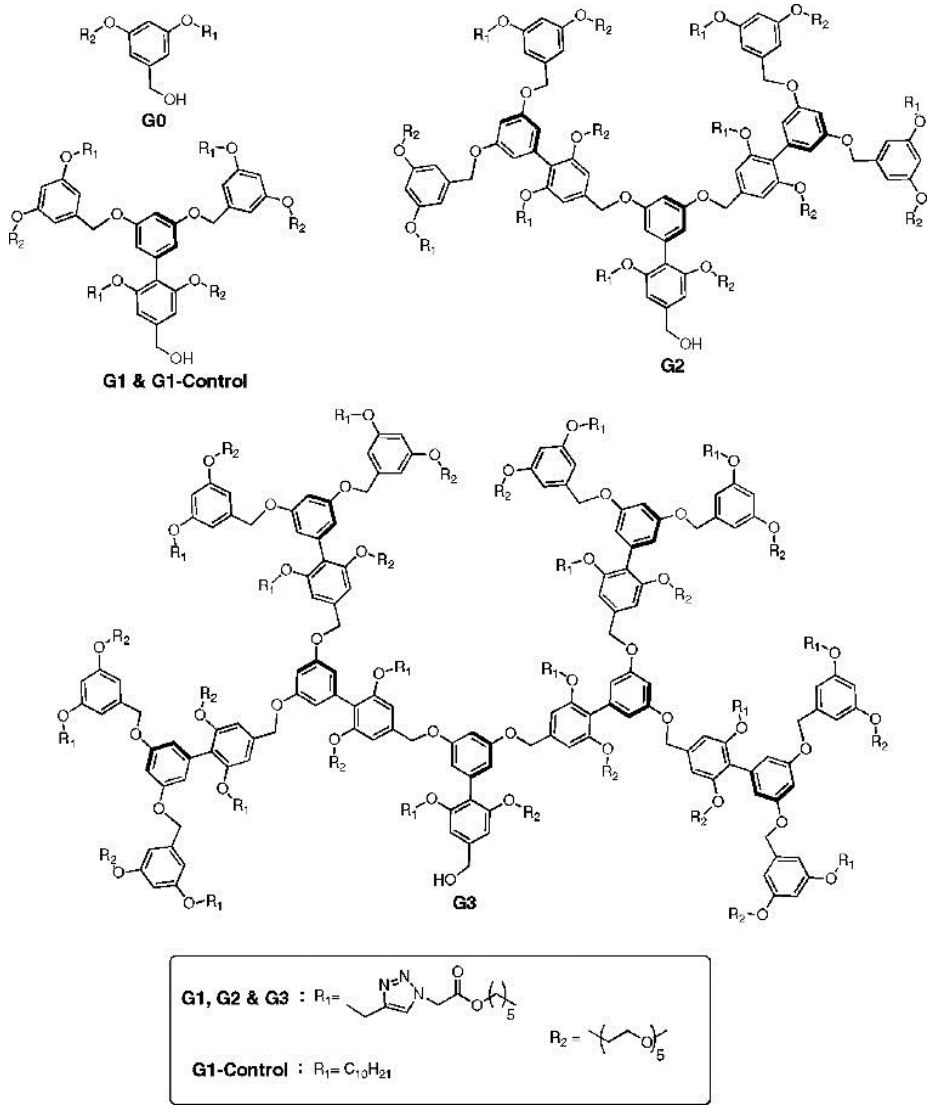

Chart 1.1: Structures of ester-functionalized amphiphilic dendrons.

Supramolecular assemblies derived from amphiphilic dendrimers have also been

extensively studied.[42,43] Dendrimers have the advantage of providing low critical aggregation concentrations, similar to those observed with polymers, but also have the molecular weight control seen in small molecules.[44-47] In addition, dendrimers afford a high degree of tunability over functional group placements within a macromolecule.[48-53] These features make dendrimer a unique class of molecule for fundamental study of interactions between artificial macromolecules and biomolecules. Our group developed a unique class of dendrimer-based amphiphiles, called facially amphiphilic dendrons.[54] In an aqueous solution, these dendrons formed nano-sized micellar assemblies with a water-excluded lipophilic interior capable of sequestering hydrophobic molecules. Because nano-scale (20 nm-200 nm) particles have the propensity to accumulate much more in tumor tissue than they do in normal tissues,[55-58] these facially amphiphilic dendrimers have the great potential to be utilized as stimuli-responsive drug delivery vehicles.

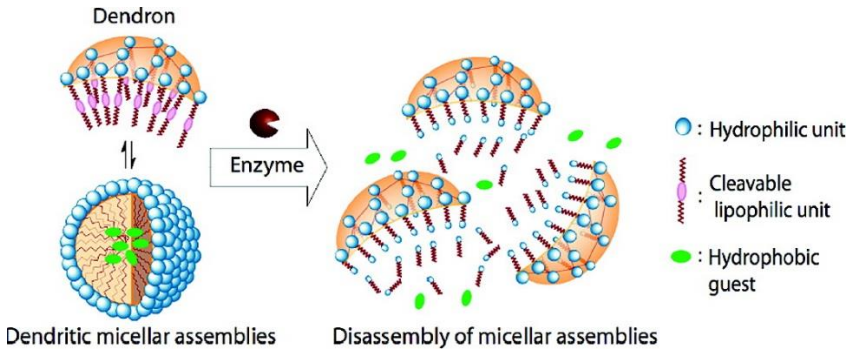

Figure 1.4: Schematic representation of enzyme-induced disassembly of dendritic micellar assemblies and guest release.

First, we designed and synthesized a dendritic amphiphile that is responsive to enzymatic activity. For this purpose, dendrons with orthogonally placed hydrophilic pentaethylene glycol and hydrophobic hexyl ester (enzyme substrate) components were prepared (Chart 1).[47] Upon exposure of these assemblies to the enzyme, porcine liver

esterase (PLE), the enzymatic reaction caused disassembly of nano-assemblies by converting the hydrophobic hexyl ester into a hydrophilic carboxylic acid. Concurrently, the encapsulated lipophilic dye molecules were released due to loss of its container property. This enzyme-induced disassembly was further supported by a control reaction, where PLE did not have any effect on the micelle-like assembly formed from a structurally similar dendron (G1-Control) lacking the enzyme-cleavable ester moiety (Chart 1). Note that in order to cleave the substrates, the enzyme should be accessible to the cleavable functional groups. Considering that the enzymes are rather large and hydrophilic and that substrates are located in the hydrophobic core of the micelles, we envisaged that the dendrons are in equilibrium between the unimeric state and the aggregate state and substrates were cleaved by the target enzyme when they are in the unimeric state (Figure 4).

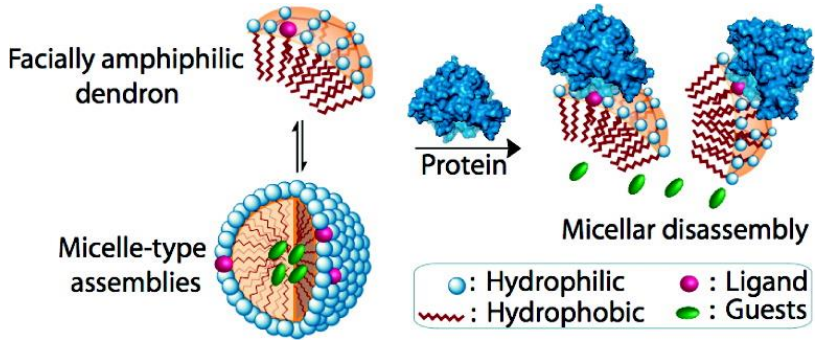

Figure 1.5: Schematic of protein−ligand binding-induced disassembly of dendritic micellar assemblies and resultant guest release.

While the enzyme-sensitive disassembly represents a covalent and irreversible modification of the assemblies, supramolecular disassembly based on noncovalent interactions is also of great interest since a lot of disease-relevant proteins do not have known enzymatic activity. To develop a non-enzymatic protein responsive assembly, we

designed a ligand-bearing amphiphilic dendron that formed stable assemblies but disassembled upon binding the target protein (Figure 5).[59] We conceived that the HLB of a dendron was significantly different from that of the protein−dendron complex, because the protein was rather large and hydrophilic compared to the dendron. The disassembly event was observed with a gradual decrease in assembly size and concurrent release of dye molecules.

1.4 Stimuli Responsive Supramolecular Assemblies Based On Small Molecules

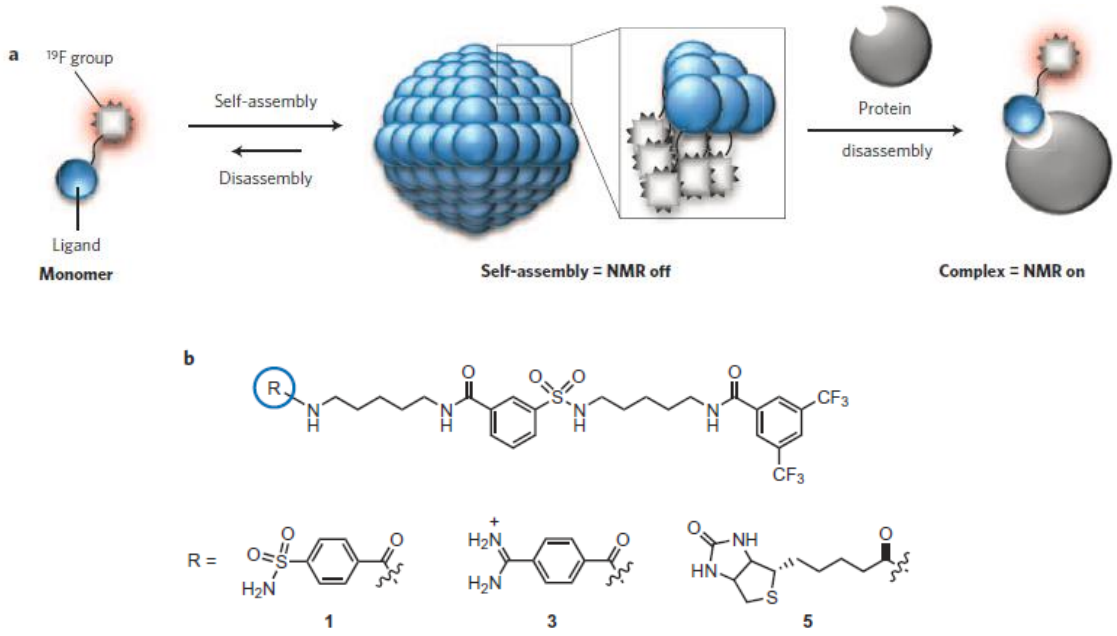

Figure 1.6: (a) Schematic of off/on ^{19}F NMR probes for protein imaging. (b) Chemical structures of probes.

Supramolecular disassembly utilizing HLB change has also been developed for small molecules. Hamachi developed a self-assembling probe that displays off/on ^{19}F magnetic resonance signals for protein detection and imaging.[60] The probe was a surfactant-type molecule composed of a hydrophilic ligand that is capable of binding the target protein and a hydrophobic ^{19}F moiety. The probe self-assembled into micellar

assemblies and the ^{19}F magnetic resonance signal is off. Upon binding to the target enzyme, the micellar assemblies disassembled and gave a sharp and intense ^{19}F signal. Disassembly occurred because binding of protein to the ligand caused a change in the probe's HLB which is essential for the formation of micellar aggregates. Using the same concept, Hamachi and coworkers also designed a fluorescent probe containing a ligand and a self-quenching dye.[61] In the aggregate state, the fluorescence was quenched due to high local dye concentration. Protein binding caused the probes to be separated from one another and the fluorescence to turn on.

1.5 Thesis Overview

This thesis work focuses the design and synthesis of amphiphilic assemblies that have applications in both sensing and drug delivery. In Chapter 2, we developed a simple and versatile nanoparticle platform based on amphiphilic random copolymers. The designed polymer nanoparticles provided the ability to encapsulate hydrophobic guest molecules and surface functionalization with a wide range of functional groups. In addition, we also demonstrated a simple approach to tune the size of the nanoparticles using pH. In Chapter 3, we reported a simple, robust, and general strategy for protein detection based on supramolecular dissociation. The simplicity of the design was exemplified by the fact that the host assemblies can be widely varied and that these assemblies can be achieved from commercially available surfactants. An operating mechanism that was consistent with all the data was also proposed.

In Chapter 4, we described a novel activatable probe for fluorine-19 NMR based on self-assembling amphiphilic dendrons. The dendron probe was designed to be spectroscopically silent due to the formation of large aggregates. Upon exposure to the

specific target enzyme, the aggregates disassembled to give rise to a sharp ^{19}F NMR signal. The probe was capable of detecting enzyme concentrations in the low nanomolar range. Response time of the probe was found to be affected by the hydrophilic-lipophilic balance of dendrons. In Chapter 5, we continued to investigate factors that affect enzyme-induced disassembly in addition the HLB of a molecule. In this chapter, we designed and synthesized a series of amphiphilic oligomers with the same HLB but different molecular weights and compared their rates of enzyme-induced disassembly.

1.6 References

1. Evans, D. F.; Wennerstrom, H. *The Colloidal Domain*, 2nd ed.; Wiley-VCH: New York, 1999.

2. Menger, F. M. The Structure of Micelles. *Acc. Chem. Res.* **1979**, *12*, 111–117.

3. Miyake, M.; Yamada, K.; Oyama, N. Self-Assembling of Guanidine-Type Surfactant. *Langmuir* **2008**, *24*, 8527–8532.

4. Tung, S. H.; Lee, H. Y.; Raghavan, S. R. A Facile Route for Creating "Reverse" Vesicles: Insights into "Reverse" Self-Assembly in Organic Liquids. *J. Am. Chem. Soc.* **2008**, *130*, 8813– 8817.

5. Vauthey, S.; Santoso, S.; Gong, H.; Watson, N.; Zhang, S. Molecular Self-Assembly of Surfactant-like Peptides to Form Nanotubes and Nanovesicles. *Proc. Natl. Acad. Sci. U.S.A.* **2002**, *99*, 5355–5360.

6. Torchilin, V. P. Structure and Design of Polymeric Surfactant-based Drug Delivery Systems. *J. Control. Release* **2001**, *73*, 137−172.

7. Cabral, H.; Nishiyama, N.; Kataoka, K. Supramolecular Nanodevices: From Design Validation to Theranostic Nanomedicine. *Acc. Chem. Res.* **2011**, *44*, 999−1008.

8. Soussan, E.; Cassel, S.; Blanzat, M.; Rico-Lattes, I. Drug Delivery by Soft Matter: Matrix and Vesicular Carriers. *Angew. Chem., Int. Ed.* **2009**, *48*, 274−288.

9. Hartgerink, J. D.; Beniash, E.; Stupp, S. I. Self-Assembly and Mineralization of Peptide-Amphiphile Nanofibers. *Science* **2001**, *294*, 1684−1688.

10. Brunsveld, L.; Folmer, B. J. B.; Meijer, E. W.; Sijbesma, R. P. Supramolecular Polymers. *Chem. Rev.* **2001**, *101*, 4071–4098.

11. Discher, B. M.; Won, Y. Y.; Ege, D. S.; Lee, J. C.-M.; Bates, F. S.; Discher, D. E.; Hammer, D. A. Polymersomes: Tough Vesicles Made from Diblock Copolymers. *Science* **1999**, *284*, 1143–1146.

12. Fuhrhop, J.-H.; Wang, T. Bolaamphiphiles. *Chem. Rev.* **2004**, *104*, 2901–2937.

13. Lee, M.; Cho, B.-K.; Zin, W.-C. Supramolecular Structures from Rod−Coil Block Copolymers. *Chem. Rev.* **2001**, *101*, 3869–3892.

14. Moffitt, M.; Khougaz, K.; Eisenberg, A. Micellization of Ionic Block Copolymers. *Acc. Chem. Res.* **1996**, *29*, 95–102.

15. Neiser, M. W.; Muth, S.; Kolb, U.; Harris, J. R.; Okuda, J.; Schmidt, M. Micelle Formation from Amphiphilic "Cylindrical Brush"–Coil Block Copolymers Prepared by Metallocene Catalysis. *Angew. Chem., Int. Ed.* **2004**, *43*, 3192–3195.

16. Zhang, L.; Yu, K.; Eisenberg, A. Ion-Induced Morphological Changes in "Crew-Cut" Aggregates of Amphiphilic Block Copolymers. *Science* **1996**, *272*, 1777–1779.

17. Okhapkin, I. M.; Makhaeva, E. E.; Khokhlov, A. R. Water Solutions of Amphiphilic Polymers: Nanostructure Formation and Possibilities for Catalysis. *Adv. Polym. Sci.* **2006**, *195*, 177–210.

18. Israelachvili, J. N.; Mitchell, D. J.; Ninham, B. W. Theory of Self-Assembly of Hydrocarbon Amphiphiles into Micelles and Bilayers. *J. Chem. Soc., Faraday Trans II.* **1976**, *72*, 1525−1568.

19. Evans, D. F.; Ninham, B. W. Molecular Forces in the Self-Organization of Amphiphiles. *J. Phys. Chem.* **1986**, *90*, 226−234.

20. Nagarajan, R. Molecular Packing Parameter and Surfactant Self-assembly: The Neglected Role of the Surfactant Tail. *Langmuir* **2002**, *18*, 31−38.

21. Alarcon, C. d. l. H.; Pennadam, S.; Alexander, C. Stimuli Responsive Polymers for Biomedical Applications. *Chem. Soc. Rev.* **2005**, *34*, 276–285.

22. Kwon, I. C.; Bae, Y. H.; Kim, S. W. Electrically Credible Polymer Gel for Controlled Release of Drugs. *Nature* **1991**, *354*, 291–293.

23. Langer, R. New Methods of Drug delivery. *Science* **1990**, *249*, 1527–1533.

24. Meng, F.; Zhong, Z.; Feijen, J. Stimuli-Responsive Polymersomes for Programmed Drug Delivery. *Biomacromolecules* **2009**, *10*, 197–209.

25. Stuart, M. A. C.; Huck, W. T. S.; Genzer, J.; Muller, M.; Ober, C.; Stamm, M.; Sukhorukov, G. B.; Szleifer, I.; Tsukruk, V. V.; Urban, M.; Winnik, F.; Zauscher, S.; Luzinov, I.; Minko, S. Emerging Applications of Stimuli-Responsive Polymer Materials. *Nat. Mater.* **2010**, *9*, 101–113.

26. Juodkazis, S.; Mukai, N.; Wakaki, R.; Yamaguchi, A.; Matsuo, S.; Misawa, H. Reversible Phase Transitions in Polymer Gels Induced by Radiation Forces. *Nature* **2000**, *408*, 178–181.

27. Liu, J.; Lu, Y. Stimuli-Responsive Disassembly of Nanoparticle Aggregates for Light-Up Colorimetric Sensing. *J. Am. Chem. Soc.* **2005**, *127*, 12677–12683.

28. Ikeda, M.; Ochi, R.; Wada, A.; Hamachi, I. Supramolecular Hydrogel Capsule Showing Prostate Specific Antigen-Responsive Function for Sensing and Targeting Prostate Cancer Cells. *Chem. Sci.* **2010**, *1*, 491–498.

29. Yashima, E.; Maeda, K. Chirality-Responsive Helical Polymers. *Macromolecules* **2007**, *41*, 3–12.

30. Kang, Y.; Walish, J. J.; Gorishnyy, T.; Thomas, E. L. Broad-Wavelength-Range Chemically Tunable Block-Copolymer Photonic Gels. *Nat. Mater.* **2007**, *6*, 957–960.

31. Lee, H. C.; Kim, S.-J.; Kim, K.-S.; Shin, H.-C.; Yoon, J.-W. Remission in Models of Type 1 Diabetes by Gene Therapy Using a Single-Chain Insulin Analogue. *Nature* **2000**, *408*, 483–488.

32. Tandon, N.; Cannizzaro, C.; Chao, P.-H. G.; Maidhof, R.; Marsano, A.; Au, H. T. H.; Radisic, M.; Vunjak-Novakovic, G. Electrical Stimulation Systems for Cardiac Tissue Engineering. *Nat. Protoc.* **2009**, *4*, 155–173.

33. Chung, H. J.; Park, T. G. Self-Assembled and Nanostructured Hydrogels for Drug Delivery and Tissue Engineering. *Nano Today* **2009**, *4*, 429–437.

34. Kim, J.; Yoon, J.; Hayward, R. C. Dynamic Display of Biomolecular Patterns Through an Elastic Creasing Instability of Stimuli-Responsive Hydrogels. *Nat Mater.* **2010**, *9*, 159–164.

35. Shchukin, D. G.; Grigoriev, D. O.; Mohwald, H. Application of Smart Organic Nanocontainers in Feedback Active Coatings. Soft Matter **2010**, *6*, 720–725.

36. Diaz Diaz, D.; Kuhbeck, D.; Koopmans, R. J. Stimuli-Responsive Gels as Reaction Vessels and Reusable Catalysts. Chem. Soc. Rev. **2011**, *40*, 427–448.

37. Ge, Z.; Xie, D.; Chen, D.; Jiang, X.; Zhang, Y.; Liu, H.; Liu, S. Stimuli-Responsive Double Hydrophilic Block Copolymer Micelles with Switchable Catalytic Activity. Macromolecules **2007**, *40*, 3538–3546.

38. Kikuchi, A.; Okano, T. Intelligent Thermoresponsive Polymeric Stationary Phases for Aqueous Chromatography of Biological Compounds. Prog. Polym. Sci. **2002**, *27*, 1165–1193.

39. Wahlund, P. O.; Galaev, I. Y.; Kazakov, S. A.; Lozinsky, V. I.; Mattiasson, B. "Protein-Like" Copolymers: Effect of Polymer Architecture on the Performance in Bioseparation Process. *Macromol. Biosci.* **2002**, *2*, 33–42.

40. Zhuang, J.; Gordon, M.; Ventura, J.; Li, L. Thayumanavan, S. Multi-Stimuli Responsive Macromolecules and Their Assemblies. *Chem. Soc. Rev.* **2013**, *42*, 7421–7435.

41. Sandanaraj, B. S.; Demont, R.; Thayumanavan, S. Generating Patterns for Sensing Using a Single Receptor Scaffold. *J. Am. Chem. Soc.* **2007**, *129*, 3506–3507.

42. Bosman, A. W.; Janssen, H. M.; Meijer, E. W. About dendrimers: Structure, Physical Properties, and Applications. *Chem. Rev.* **1999**, *99*, 1665−1688.

43. Dendrimer Assemblies and Supramolecular Aspects. *C.R. Chim.* **2003**, *6*, Issues 8−10, pp 709−817.

44. Newkome, G. R.; Yao, Z.; Baker, G. R.; Gupta, V. K. Micelles. Part 1. Cascade Molecules: a New Approach to Micelles. A [27]-Arborol. *J. Org. Chem.* **1985**, *50*, 2003-2004.

45. Hawker, C. J.; Wooley, K. L.; Fréchet, J. M. J. Unimolecular Micelles and Globular Amphiphiles: Dendritic Macromolecules as Novel Recyclable Solubilization Agents. *J. Chem. Soc., Perkin Trans. 1* **1993**, 1287-1297.

46. Tomalia, D. A.; Baker, H.; Dewald, J.; Hall, M.; Kallos, G.; Martin, S.; Roeck, J.; Ryder, J.; Smith, P. A New Class of Polymers: Starburst-Dendritic Macromolecules. *Polym. J.* **1985**, *17*, 117-132.

47. Azagarsamy, M. A.; Sokkalingam, P.; Thayumanavan, S. Enzyme-Triggered Disassembly of Dendrimer-Based Amphiphilic Nanocontainers. *J. Am. Chem. Soc.* **2009**, *131*, 14184-14185.

48. Bo, Z.; Schäfer, A.; Franke, P.; Schlüter, a. D. A Facile Synthetic Route to a Third-Generation Dendrimer with Generation-Specific Functional Aryl Bromides. *Org. Lett.* **2000**, *2*, 1645-1648.

49. Azagarsamy, M. A.; Krishnamoorthy, K.; Sivanandan, K.; Thayumanavan, S. Site-Specific Installation and Study of Electroactive Units in Every Layer of Dendrons. *J. Org. Chem.* **2009**, *74*, 9475-9485.

50. Sivanandan, K.; Aathimanikandan, S. V.; Arges, C. G.; Bardeen, C. J.; Thayumanavan, S. Probing Every Layer in Dendrons. *J. Am. Chem. Soc.* **2005**, *127*, 2020-2021.

51. Sivanandan, K.; Sandanaraj, B. S.; Thayumanavan, S. Sequences in Dendrons and Dendrimers. *J. Org. Chem.* **2004**, *69*, 2937-2944.

52. Lee, C.; Lo, S.-T.; Lim, J.; da Costa, V. C. P.; Ramezani, S.; Öz, O. K.; Pavan, G. M.; Annunziata, O.; Sun, X.; Simanek, E. E. Design, Synthesis and Biological Assessment of a Triazine Dendrimer with Approximately 16 Paclitaxel Groups and 8 PEG Groups. *Mol. Pharm.* **2013**, *10*, 4452-4461.

53. Woller, E. K.; Cloninger, M. J. Mannose Functionalization of a Sixth Generation Dendrimer. *Biomacromolecules* **2001**, 2, 1052-1054.

54. Bharathi, P.; Zhao, H. D.; Thayumanavan, S. Toward Globular Macromolecules with Functionalized Interiors: Design and Synthesis of Dendrons with an Interesting Twist. *Org. Lett.* **2001**, *3*, 1961−1964.

55. Maeda, H.; Wu, J.; Sawa, T.; Matsumura, Y.; Hori, K. Tumor Vascular Permeability and the EPR Effect in Macromolecular Therapeutics: A Review. *J. Control. Release* **2000**, *65*, 271–284.

56. Brannon-Peppas, L.; Blanchette, J. O. Nanoparticle and Targeted Systems for Cancer Therapy. *Adv. Drug Deliv. Rev.* **2004**, *56*, 1649–1659.

57. Iyer, A. K.; Khaled, G.; Fang, J.; Maeda, H. Exploiting the Enhanced Permeability and Retention Effect for Tumor Targeting. *Drug Discov. Today* **2006**, *11*, 812–818.

58. Maeda, H.; Bharate, G. Y.; Daruwalla, J. Polymeric Drugs for Efficient Tumor-Targeted Drug Delivery based on EPR-Effect. *Eur. J. Pharm. Biopharm.* **2009**, *71*, 409–419.

59. Azagarsamy, M.; Yesilyurt, V.; Thayumanavan, S. Disassembly of Dendritic Micellar Containers due to Protein Binding. *J. Am. Chem. Soc.* **2010**, *132*, 4550–4551.

60. Takaoka, Y.; Sakamoto, T.; Tsukiji, S.; Narazaki, M.; Matsuda, T.; Tochio, H.; Shirakawa, M.; Hamachi, I. Self-Assembling Nanoprobes that Display off/on ^{19}F Nuclear Magnetic Resonance Signals for Protein Detection and Imaging. *Nat. Chem.* 2009, **1**, 557–561.

61. Yoshii, T.; Mizusawa, K.; Takaoka, Y.; Hamachi, I. Intracellular Protein-Responsive Supramolecules: Protein Sensing and In-Cell Construction of Inhibitor Assay System. *J. Am. Chem. Soc.* 2014, **136**, 16635–16642.

CHAPTER 2

SURFACE FUNCTIONALIZABLE POLYMER NANOPARTICLES

2.1 Introduction

Nanoparticles, polymer or otherwise, have had a significant impact on a variety of areas such as utilization in microelectronics, multiphase catalysis, sensing and therapeutics.[1-4] For all of these applications, facile modulation of the nanoparticle surface is critical, in order to obtain appropriate interfacial properties. Similarly, the ability to encapsulate and release guest molecules within the nanoparticle interior is also required for applications such as sensing and therapeutics. A platform that affords both surface functionalization and guest encapsulation in a single nanoscopic scaffold is highly desirable. Nanoscale materials, such as metallic or semiconductor nanoparticles and dendrimers, are excellent scaffolds for displaying surface functional groups.[5-9] For example, monolayer protection of gold nanoparticles is easily achieved with thiol-bearing molecules due to the high affinity of thiol moiety toward gold nanoparticles. However, these scaffolds generally lack features that allow for favorable non-covalent host-guest interactions. On the contrary, amphiphilic molecules readily self-assemble into nanoassemblies, such as micelles and liposomes, which can encapsulate guest molecules within their interior.[10-15] Nevertheless, modifying their surface functional groups are

challenging, because these modifications often result in change in the hydrophilic-lipophilic balance that is necessary for retaining the fidelity of the assembly. An impending intellectual challenge in this area is to capture the essence of surface functionalization capabilities available in dendrimers and metallic nanoparticles and combine them with the host-guest features presented in micelles and vesicles. Amphiphilic block copolymer micelles, which are cross-linked either at the core or at the shell, can potentially satisfy this requirement.[16-18] While these architectures have had an impressive impact, they do require demanding polymer synthesis. Also, these assemblies are often achieved under rigorous processing conditions. We were interested in developing a simple approach for functionalizable polymer nanoparticles, where we stipulated that: (*i*) the precursor polymer is based on a random copolymer, which is synthetically accessible; (*ii*) the polymer self-assembles in a solvent, which can then be converted to nanoparticle in one step without the need for any additional processing; (*iii*) the nanoparticle contains a surface functional group, which can be further manipulated easily; (*iv*) the size of the nanoparticle is tunable; and (*iv*) the interior of the nanoparticle is capable of sequestering guest molecules.

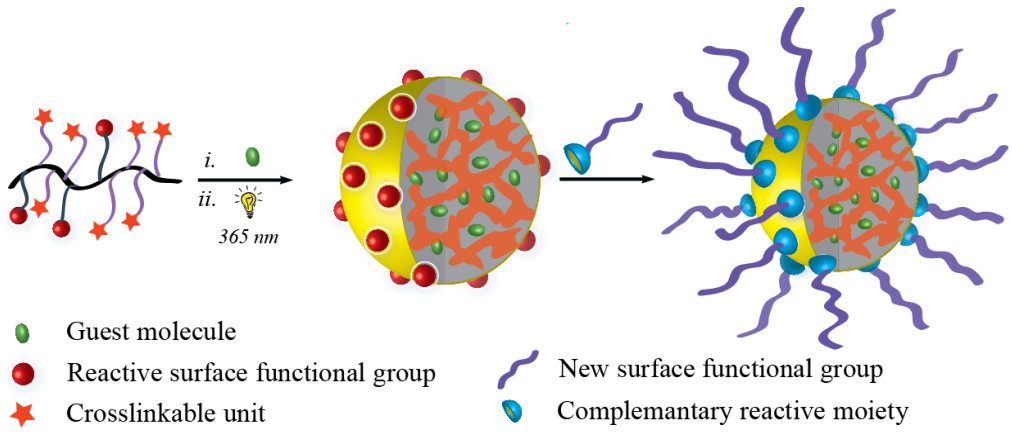

Figure 2.1: Schematic representation of the polymer nanoparticle with surface functionalization and guest binding abilities.

2.2 Results and Discussions

2.2.1 Amine-based Polymer Nanoparticles

2.2.1.1 Design and Synthesis

In this chapter, we report on the design, synthesis, characterization, and further functionalization of amine-functionalized polymeric nanoparticles that satisfy all the above requirements. We targeted primary amines as the surface functional group, because its reactivity complements a wide range of functional groups such as alkyl halides, Michael acceptors, carboxylic acid, acid chlorides, activated esters, epoxides, anhydride and aldehydes. The basic premise behind our molecular design involves self-assembly of amphiphilic random copolymers. In the aqueous phase, the surface functional groups of such an assembly would be dictated by the hydrophilic moiety of the polymer. Therefore, we hypothesized the use of a primary amine based monomer as the hydrophilic moiety, combined with a reactive hydrophobic monomer as the crosslinkable moiety, will lead to a functionalizable polymer nanoparticle. The amphiphilic nature of the assembly should also allow for incorporation of guest molecules within the hydrophobic interior of the assembly prior to crosslinking.

Accordingly, we targeted polymer **1**, a poly(methacrylamide), derived from the co-polymerization of 2-aminoethylmethacylamide and 3-(9-methylcoumarinoxy)propyl-methacrylamide. This co-polymer should self-assemble into an amphiphilic aggregate, where the hydrophilic amino moieties are exposed to the aqueous phase, while the coumarin moieties are tucked in the hydrophobic interior. We will take advantage of the propensity of coumarins to undergo photochemically driven [2+2] cylcoaddition reaction[19-23] to achieve the targeted polymer nanoparticles (Scheme 1).

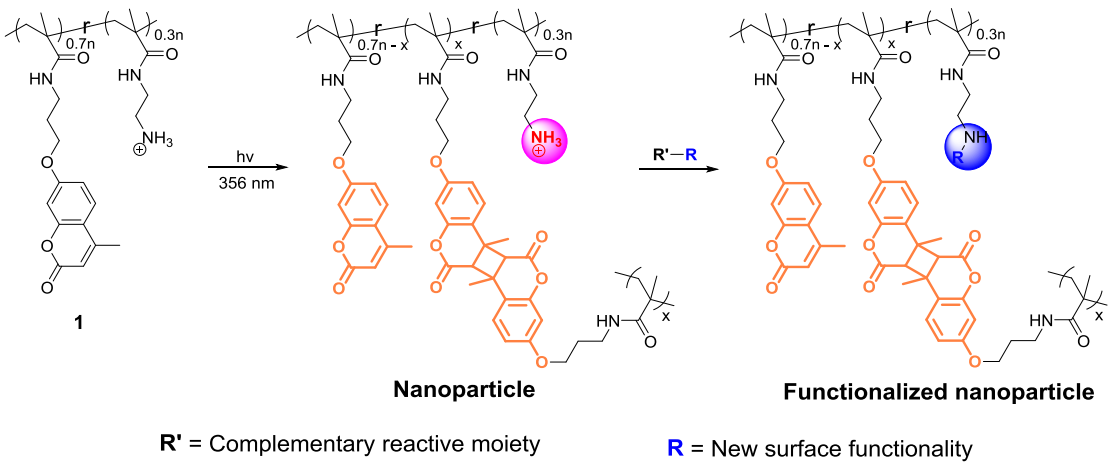

Scheme 2.1: Cross-linking and functionalization of polymer **1**.

To realize the synthesis of the targeted polymer **1**, we first synthesized the precursor random copolymer, which contains 30% of *N*-Boc-aminoethylmethacrylamide and 70% of 3-(9-methylcoumarinoxy)propylmethacrylamide; this polymer was prepared by reversible addition-fragmentation chain transfer (RAFT) polymerization. The Boc group was deprotected using trifluoroacetic acid in dichloromethane to yield the random copolymer **1**. Our design requires that this amphiphilic polymer form a nanoscale aggregate, which can be photochemically trapped to form a surface functionalized nanoparticle. Indeed, this polymer with 70:30 monomer ratio exhibits the right hydrophilic-liphophilic balance required to form the amphiphilic assemblies. An aqueous solution of this polymer forms an aggregate of ~22 nm at 1 mg/mL concentration, as discerned by dynamic light scattering (DLS). This solution was then irradiated at 365 nm for 10 minutes to generate the crosslinked nanoparticle. Several features of this reaction are noteworthy: (*i*) the intensity of the absorption peak centered at 320 nm, which corresponds to the coumarin moiety, reduces within this irradiation time – confirming the photochemical reaction of the coumarin moiety (Figure 2d); (*ii*) the size of the nanoparticle is the same as the aggregate,

suggesting that the coumarin dimerization process is exclusively intra-aggregate – note that inter-aggregate reactions would result higher nanoparticle sizes; (*iii*) there is no discernible nanoaggregate of the uncrosslinked polymer in 10% water in DMSO, while the crosslinked nanoparticle's size is slightly increased in this solvent mixture (Figure 2a & 2b) – this swelling feature further confirms the crosslinked nature of the nanoparticle. The degree of swelling should inversely vary with the degree of crosslinking. It is known that irradiation of coumarin dimers at 250 nm causes it to revert to the monomer.[19-23] This reaction is often not complete because of the photo-stationary state between the monomer and the dimer at this irradiation wavelength. Therefore, this reaction should cause the crosslink density to lower. Accordingly, crosslinked nanoparticle in 10% water in DMSO was irradiataed at 250 nm for 30 minutes. DLS study of this solution indeed showed a further increase in size (Figure 2C).

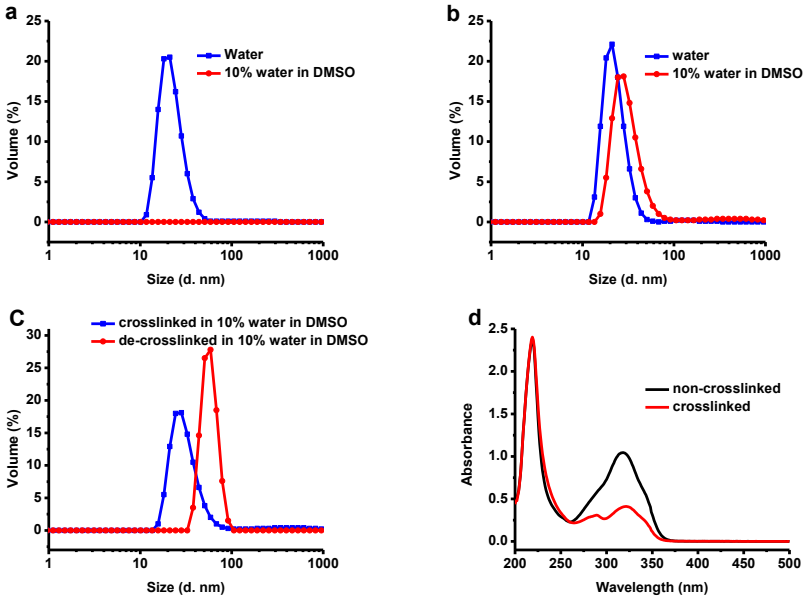

Figure 2.2: Size distributions of (a) non-crosslinked, (b) cross-linked, and (c) de-crosslinked random copolymer **1** by DLS; (d) Absorption spectra of non-crosslinked and cross-linked.

2.2.1.2 Guest Molecule Encapsulation

Since these nanoparticles are formed from amphiphilic assemblies in aqueous solutions, we envisaged the possibility of these nanoparticles being hosts for hydrophobic guest molecules. Indeed, we were able to encapsulate hydrophobic dye molecules, such as 1,1′-dioctadecyl-3,3,3′,3′-tetramethylindocarbocyanine perchlorate (DiI) or 3,3′-dioctadecyloxacarbocyanine perchlorate (DiO) using the polymer aggregates successfully and guest molecules were retained in the interiors of nanoparticles after photo-induced crosslinking (Figure 3).

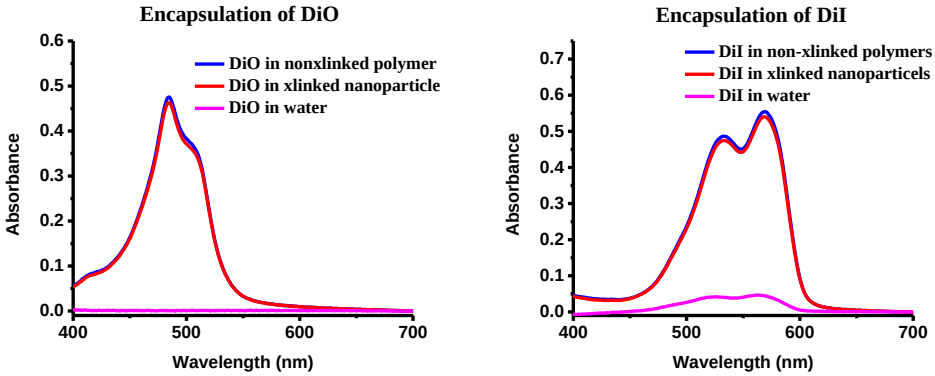

Figure 2.3: Absorption spectra of guest molecules in non-crosslinked and crosslinked random copolymer **1**.

2.2.1.3 Surface Functionalization

To investigate the versatility of the amine functionality as a handle for surface functionalization of the nanoparticles, we tested a wide range of functional groups and characterized these modifications with different techniques. First, we reacted amines with an activated ester and a cyclic anhydride to provide amides with complementary surface characteristics. Reaction of the amine nanoparticles with a peg-2000 NHS ester should convert the positively charged surface of the polymer nanoparticle to a charge neutral surface, while the reaction with succinic anhydride should convert the charge to negative.

Zeta potential measurements of the reactants and the products indeed confirmed such surface charge modification (Figure 4a).

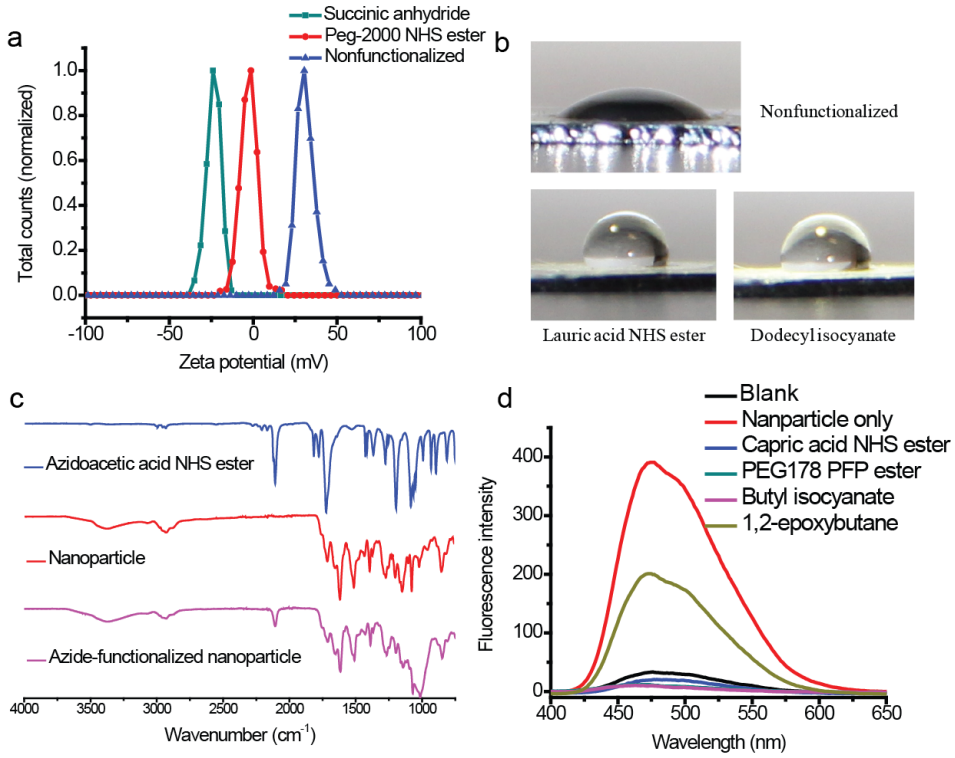

Figure 2.4: (a) Surface charges of nanoparticles by zeta potential (b) Contact angle measurements of unmodified nanoparticles (top) and nanoparticles modified by lauric acid NHS ester (bottom left) and dodecyl isocyanate (bottom right). (c) IR spectra of azidoacetic acid NHS ester (top), unmodified nanoparticles (middle), and nanoparticles functionalized with azidoacetic acid NHS ester (bottom). (d) Fluorescence emission intensity of nanoparticles treated with excess fluorescamine after reacting with different functional groups.

Second, the nanoparticles were modified by a NHS ester (of lauric acid) and an isocyanate (dodecyl). Both modifications would change the surface nanoparticles from hydrophilic to hydrophobic. Evaluation of the nanoparticle surface hydrophobicity by contact angle showed that the unmodified nanoparticles exhibited a contact angle of 33°, while the modified nanoparticles have a contact angle of 103° and 98°, respectively (Figure 4b). To confirm that the contact angle change after modification was due to hydrophobicity

change rather than surface roughness difference, atomic force microscopy (AFM) was used to evaluate the surface roughness of these nanoparticles. AFM images of these nanoparticles showed a similar mean roughness (R_a) value of ~9 nm (Figure 12).

Next, we sought to monitor the surface functionalization by FTIR. To this end, the nanoparticles were reacted with the NHS-ester of azidoacetic acid. The FTIR spectrum of modified nanoparticles showed the appearance of a peak at 2100 cm^{-1}, characteristic of the azido group, with the concurrent disappearance of the NHS ester peaks at 1812 cm^{-1} and 1783 cm^{-1} (Figure 4c).

The techniques outlined above, including the IR, do not directly analyze the conversion of the amino moiety on the nanoparticle surface. Therefore, we used the well-established fluorescamine assay,[24] in which selective reaction of primary amines with fluorescamine provides a fluorescent derivative. The relative fluorescence can then be used to ascertain the extent of surface functionalization. Accordingly, nanoparticles were first reacted with molecules with different amine-reactive functional groups (pentafluorophenol (PFP) ester, NHS ester, epoxide, and isocyanate). The extent of functionalization was analyzed by comparing the fluorescence from the functionalized amine nanoparticles and the unreacted amine nanoparticle. The fluorescence from three of the functionalized nanoparticles (PFP ester, NHS ester, and isocyanate) was found to be similar to that found with the negative control, suggesting that the reaction is quantitative in these cases (Figure 4d). The reason for the inefficiency of the epoxide ring opening reaction is not clear.

2.2.1.4 Particle Size Control

Next, we sought to investigate the possibility of tuning the nanoparticle sizes. While variations such as polymer MW, concentration, and monomer ratio could afford different

aggregate sizes, we were interested in a simpler variation with the same polymer. We envisioned that the pH of the solution and the ensuing variation the hydrophilic-lipophilic balance of the polymer could afford polymer aggregates with different sizes. To test our hypothesis, aqueous solutions of polymer **1** at different pH were prepared. The polymer precipitates out at pH~9, consistent with the pK_a of amine groups. We also observed that the aggregate sizes were not significantly different between pH 3.0 and 6.5. Interestingly, the greatest size differences were observed with subtle pH changes between 7.0 and 8.5, indicating that subtle changes in the degree of protonation of the amines lead to significant size differences. This is presumably due to the difference in hydrophilic lipophilic balance of the polymer at these pHs. We have utilized these differences to systematically tune the size of the nanoparticles by photochemically locking these aggregates, as shown in Figure 5a.

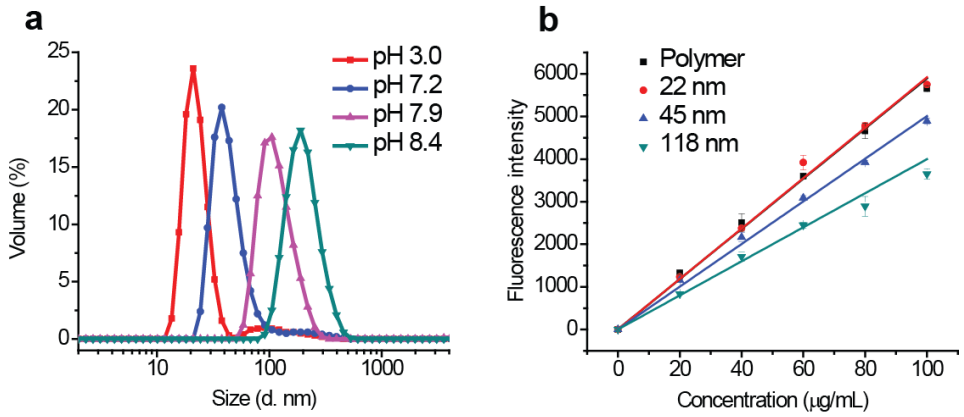

Figure 2.5: (a) Size distribution of nanoparticles cross-linked at different pHs in water. The DLS measurements were all done at pH 3. (b) Percentage of amine available for functionalization on different nanoparticle sizes accessed by fluorescamine assay.

Although the fluorescamine assay showed that all the accessible amines can be utilized for surface decoration, it is important to investigate the percentage of amines in the polymer nanoparticle that are inherently accessible. We hypothesized that smaller

nanoparticles would have higher percentage of accessible amines, since some of these moieties might be buried in the interior of larger particles. To test our hypothesis, fluorescamine assay was carried out in 1:3 water/DMSO mixture, in which no aggregation was observed for the non-crosslinked polymer. Therefore, the fluorescence generated from the uncrosslinked polymer is a true indicator of the amine moieties available in the polymer. Evaluation of nanoparticles of different sizes, using this as the standard, indicated that nearly all the amine moieties seem to be available at a particle size of 22 nm. However, only 85% and 65% of the amine moieties were available for functionalization in 45 nm and 118 nm particles respectively (Figure 5b). This supports the expectation that the smaller surface area of larger nanoparticles will lead to decreased availability of surface functionalities.

2.2.2 Water-Soluble Activated Ester Polymer Nanoparticles

2.2.2.1 Design and Synthesis

To further demonstrate the versatility of our methodology, we were interested in expanding the repertoire of functional groups that could be used to form the surface functionalizable polymer nanoparticles. While our molecular design requires that one of the functional groups to be hydrophilic and the other to be hydrophobic, their chemical reactivity should also be highly specific and independent of each other. Previously, we have shown that a random copolymer composed of an oligoethyleneglycol (OEG) methacrylate and a pyridyldisulfide-derived (PDS) methacrylate (Scheme 2), prepared by reversible addition-fragmentation chain transfer (RAFT) polymerization, was also capable of forming nanoparticles with guest encapsulation and surface functionalization capabilities.[25, 26]

In this system, the role of the OEG unit is to introduce a charge-neutral hydrophilic functional group, which is known to endow biocompatibility. The PDS functionality plays several key roles: (*i*) it is a lipophilic functionality and thus plays a critical role in providing a supramolecular amphiphilic nanoassembly in the aqueous phase. (*ii*) the amphiphilic nature of the assembly and lipophilic environment afforded by the PDS functionality provides the opportunity for lipophilic guest molecules to be sequestered within these nanoassemblies prior to cross-linking. (*iii*) The PDS functionality is reactive, but specific to thiols and thus provides a mild method for disulfide cross-linking to form the nanoparticles. (*iv*) Since the nanoparticles are based on disulfide cross-linkers that can be cleaved by thiol-disulfide exchange reactions, these nanoparticles also provide a pathway to trigger the release of the stably encapsulated guest molecules in response to an external stimulus.

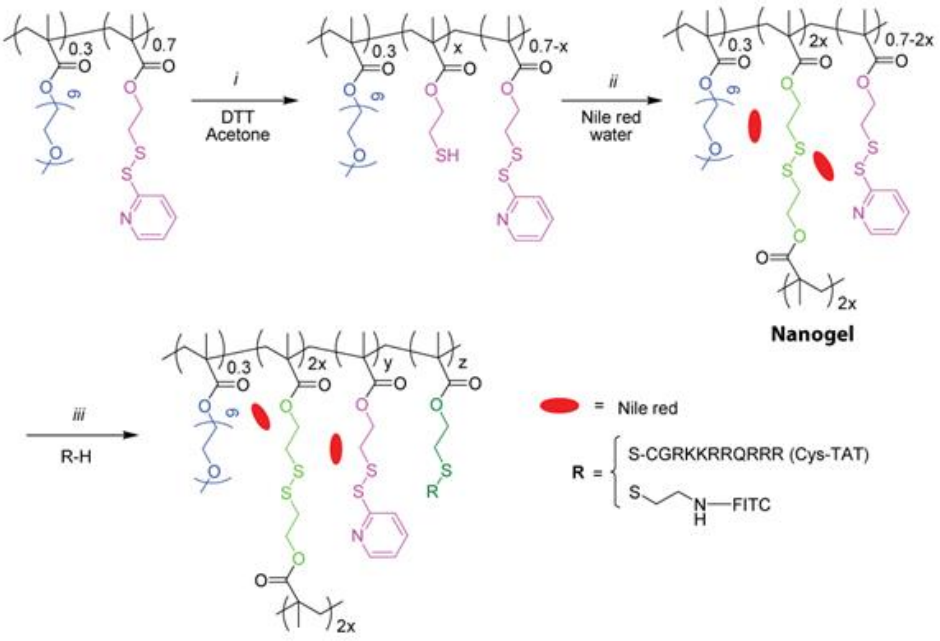

Scheme 2.2: Structures of the OEG/PDS polymer nanoparticles. (*i*) Cleavage of specific amount of PDS groups by DTT. (*ii*) Nanoparticle formation by inter/intrachain cross-linking. (*iii*) Surface modification of nanoparticles with thiol-modified Tat peptide or FITC.

Briefly, the cross-linking of the polymer nanoassemblies was achieved by adding deficient amount of dithiothreitol (DTT) which caused the cleavage of a well-defined percentage of the PDS groups to the corresponding thiol functionalities. These thiol functionalities will then react within the polymeric aggregates with unreacted PDS functionalities. This reaction results in disulfide cross-links within the polymeric aggregates causing the formation of the polymeric nanoparticles. Surface functionalization of these nanoparticles were achieved by thiol-disulfide exchange reactions with the unreacted PDS groups. These residual PDS groups can be reacted with thiol-containing compounds, allowing for post-modification of nanoparticles. Note that the role of OEG unit was simply providing hydrophilicity to the nanoparticles. It didn't involve in either cross-linking or surface modification of the nanoparticles. On the other hand, PDS unit acted as both the cross-linking and surface functionalization functional group. Even though relying both cross-linking and surface functionalization on one single functional group is viable method, it can be problematic sometimes. For example, excessive surface modification would exhaust the hydrophobic portion of nanoparticles. This can cause the nanoparticles to lose its capability to stably retain the guest molecules. To avoid those potential issues, we were interested in developing polymer nanoparticles in which cross-linking reaction and surface functionalization rely on different functional groups.

Specifically, we targeted hydrophilic activated ester as the surface functional group, because its reactivity towards primary amine is highly efficient and specific. Primary amine is a very common functional group present in a wide range of compounds including many biomolecules, such as amino acids, peptides, and proteins. Nanoparticles having activated ester present on its surface would allow facile surface modification with any primary

amine-containing compounds. To provide the hydrophilicity necessary for the self-assembly of amphiphilic random copolymers and its presence on the surface, we chose charged activated ester to be the hydrophilic and surface functionalizable group. Accordingly, we targeted polymer **4**, a poly(methacrylate), derived from the co-polymerization of 4-sulfo-2-nitrophenyl methacrylate (Sulfo-NP) and 3-(9-methylcoumarinoxy)propyl-methacrylate. This co-polymer should self-assemble into an amphiphilic aggregate, where the hydrophilic activated ester moieties are exposed to the aqueous phase, while the coumarin moieties are tucked in the hydrophobic interior. The sulfonate group of Sulfo-NP endows the hydrophilicity to the polymer, while the nitrophenyl moiety provides reactivity towards primary amines. We will again take advantage of the photochemically driven [2+2] cylcoaddition reaction of coumarins to cross-link the polymeric micelles (Scheme 3).

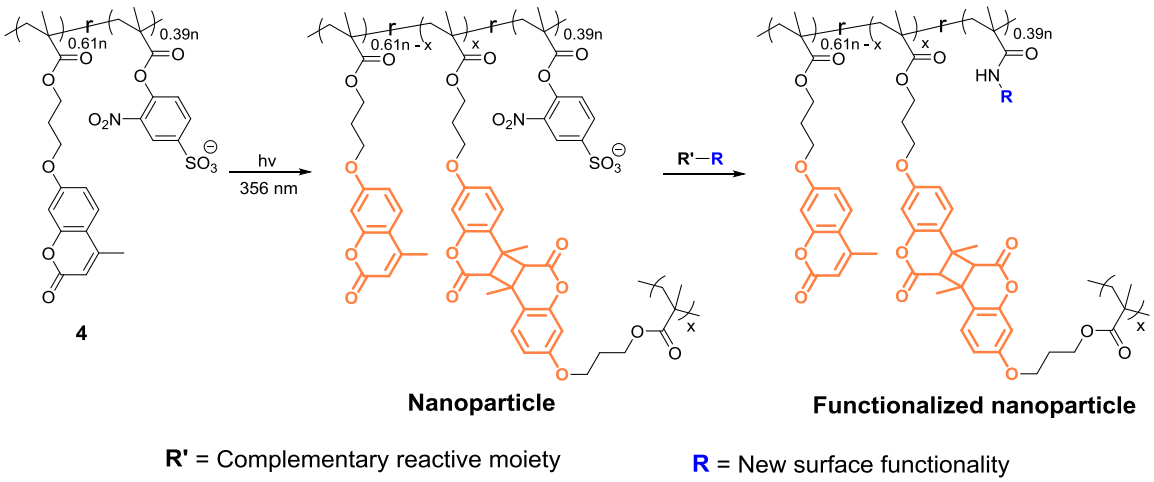

Scheme 2.3: Cross-linking and functionalization of polymer **4**.

To realize the synthesis of the targeted polymer **4**, we first synthesized the two methacrylate monomers, respectively. Briefly, 4-hydroxybenzenesulfonate was treated with fuming nitric acid to generate 4-sulfo-2-nitrophenol, followed by DCC coupling with

methacrylic acid to obtain the Sulfo-NP monomer. 4-Methylumbelliferone was first alkylated with 3-bromo-1-propanol, followed by acylation with methacryloyl chloride to obtain the coumarin monomer. Polymer **4** was then prepared by reversible addition-fragmentation chain transfer (RAFT) polymerization. Our design requires that this amphiphilic polymer form a nanoscale aggregate, which can be photochemically trapped to form a surface functionalized nanoparticle. Indeed, this polymer with 39% Sulfo-NP to 61% coumarin monomer ratio exhibits the right hydrophilic-lipophilic balance required to form the amphiphilic assemblies. An aqueous solution of this polymer forms an aggregate of ~5 nm at 1 mg/mL concentration, as discerned by dynamic light scattering (Figure 6). This solution was then irradiated at 365 nm for 10 minutes to generate the crosslinked nanoparticle.

2.2.2.2 Particle Size Control

To investigate the possibility of tuning the nanoparticle sizes, we first tried to vary the monomer ratio. However, variations on monomer ratio did not seem to have an effect on the polymer aggregate size (Figure 6). Size tuning based on pH of the solution would not work for this polymer as well because the hydrophilicity of sulfonate group is not pH dependent. In addition, high pH could potentially cause hydrolysis of the Sulfo-NP. While there are other possible ways of controlling particle size, such as polymer MW and concentration, we were interested in a simpler variation with the same polymer.

We envisioned that the nature and concentration of the salt ions in the polymer solution and the ensuing variation of the hydrophilic-lipophilic balance of the polymer could afford polymer aggregates with different sizes. This hypothesis was based on Hofmeister effect phenomenon, which originally states that inorganic salts have the ability

to enhance solubilization or precipitate proteins in an aqueous solution.[27-29] Besides proteins, the Hofmeister effect has also been extended to other non-biological systems, such as polymers and nanoparticles.[30-36]

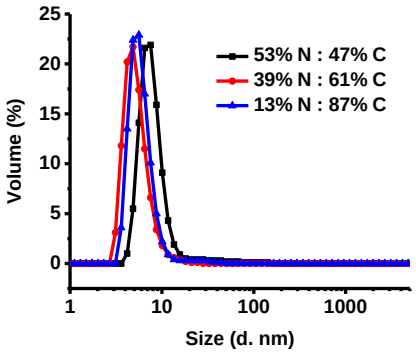

Figure 2.6: Size distributions of polymer nanoparticles with different monomer ratios by DLS. (N stands for Sulfo-NP monomer; C stands for coumarin monomer.)

To test our hypothesis, aqueous solutions of polymer **4** with different salt types and concentrations were prepared. The nanoparticle size increased from ~5 nm to ~80 nm with increasing concentration of NaCl range from 0 to 240 mM. Polymer aggregates precipitate out above 240 mM NaCl. The effect of Na_2SO_4 on polymer aggregate size followed a similar trend, yet was more profound than NaCl. While 240 mM NaCl was required to increase the particle size to ~80 nm, only 100 mM Na_2SO_4 was needed to achieve the same size. This difference is consistent with the Hofmeister series effect, as Na_2SO_4 is a stronger kosmotrope than NaCl. Interestingly, a similar trend was also observed with much lower $CaCl_2$ concentrations, ranging from 0 to 1.2 mM. This is a concentration range outside the functional concentration of Hofmeister salts, indicating that a different mechanism is dictating the size differences. This is presumably due to the divalent cation, Ca^{+2}, causing the aggregation of polymer aggregates through electronic interaction with the negative charge of Sulfo-NP. We also observed that the aggregate sizes were not significantly varied

at different concentrations of NaSCN, a chaotropic agent, consistent with our previous findings.[36]

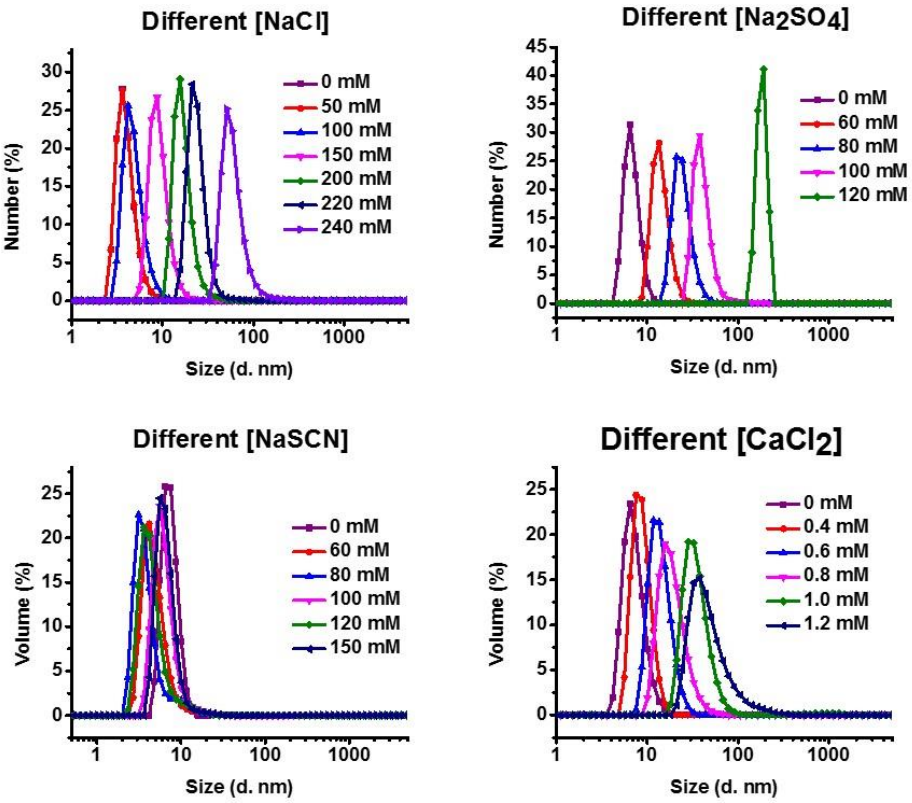

Figure 2.7: Size distributions of polymer nanoparticles with different salts by DLS.

2.2.2.3 Surface Functionalization

To investigate the versatility of the 4-sulfo-2-nitrophenyl activated ester as a handle for surface functionalization of the nanoparticles, we tested many primary amine compounds and characterized these modifications with different techniques. First, we reacted the activated esters with a primary amine-containing boron-dipyrromethene (BODIPY) dye to provide fluorescent nanoparticles. As a control experiment, we also reacted the activated esters with the same BODIPY dye which lacked the primary amine functionality. After removing the excess unreacted dyes by dialysis, the nanoparticle

solution modified with amine-containing BODIPY dye showed intense absorbance around 470 nm which is characteristic of the BODIPY dye, indicating the nanoparticles were successfully modified with the dye molecules. In contrast, the nanoparticle solution reacted with the amine-deficient dye molecule did not show any BODIPY absorbance. Next, we sought to monitor the surface functionalization by FTIR. To this end, the nanoparticles were reacted with the 6-azido hexylamine. After dialyzing off the excess unreacted azido compound, the FTIR spectrum of modified nanoparticles showed the appearance of a peak at 2100 cm^{-1}, characteristic of the azido group (Figure 8). We also tried to modify the nanoparticles with (2-Aminoethyl)trimethylammonium chloride and 2-(2-Aminoethoxy)ethanol to provide nanoparticles with a positive charge and a neutral surface. However, characterizations of these modifications with zeta potential measurements were not successful with our first attempt. They will be repeated in the future.

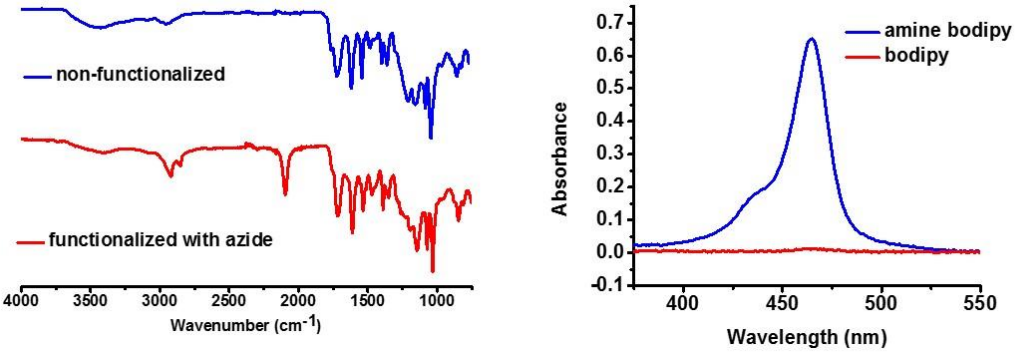

Figure 2.8: IR spectra of unmodified nanoparticles and nanoparticles functionalized with 6-azido hexylamine (left). UV-Vis absorption spectra of nanoparticles treated with an amine-containing or an amine-deficient BODIPY dye.

The techniques outlined above do not directly analyze the conversion of the sulfo-NP on the nanoparticle surface. To find a universal method to quantify the degree of surface modification, we were interested in monitoring the release of the amidation by-product, 4-

sulfo-2-nitrophenol which has UV absorbance maximum around 400 nm. Comparison of UV absorbance after reaction with a calibration curve would allow us to quantify the degree of functionalization. To avoid making any quantification errors, we should be aware of several key features of 4-sulfo-2-nitrophenol. Firstly, UV absorbance of 4-sulfo-2-nitrophenol is pH dependent (Figure 9). At same concentration of 4-sulfo-2-nitrophenol, the maximum absorbance at pH 9 was larger than the absorbance at pH 7. Whereas, the absorbance maximum blue shifted and its absorbance was much lower at acidic pH. Secondly, hydrolysis of sulfo-NP also causes the release of 4-sulfo-2-nitrophenol. Therefore, an additional calibration curve should be performed to account for the release of 4-sulfo-2-nitrophenol caused by hydrolysis reaction.

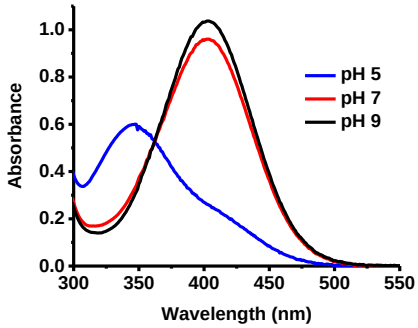

Figure 2.9: UV-Vis absorption spectra of 4-sulfo-2nitrophenol solutions at different pH.

2.2.2.4 Hydrolysis Rate

Since hydrolysis rates are also pH dependent, hydrolysis of both the uncross-linked and cross-linked polymer nanoparticles were performed at 3 different pH (Figure 10). As expected, both polymer nanoparticles hydrolyzed faster at higher pH. However, we also observed several peculiar hydrolysis activities. Firstly, the total amount of 4-sulfo-2-nitrophenol released by cross-linked nanoparticles after 11 days is higher than that released

by uncross-linked nanoparticles. Secondly, the concentration of 4-sulfo-2-nitrophenol increased a lot after UV irradiation of the polymer nanoparticles. Lastly, the initial hydrolysis rates of cross-linked polymer nanoparticles are faster than those of uncross-linked nanoparticles over all pH range (Table 1). Two hypothesis were proposed to account for these unexpected hydrolysis results. i) Can temperature increased during UV irradiation cause faster hydrolysis of the polymer nanoparticles? ii) Does the coumarin [2+2] photocycloaddition play a role in the increased hydrolysis rate?

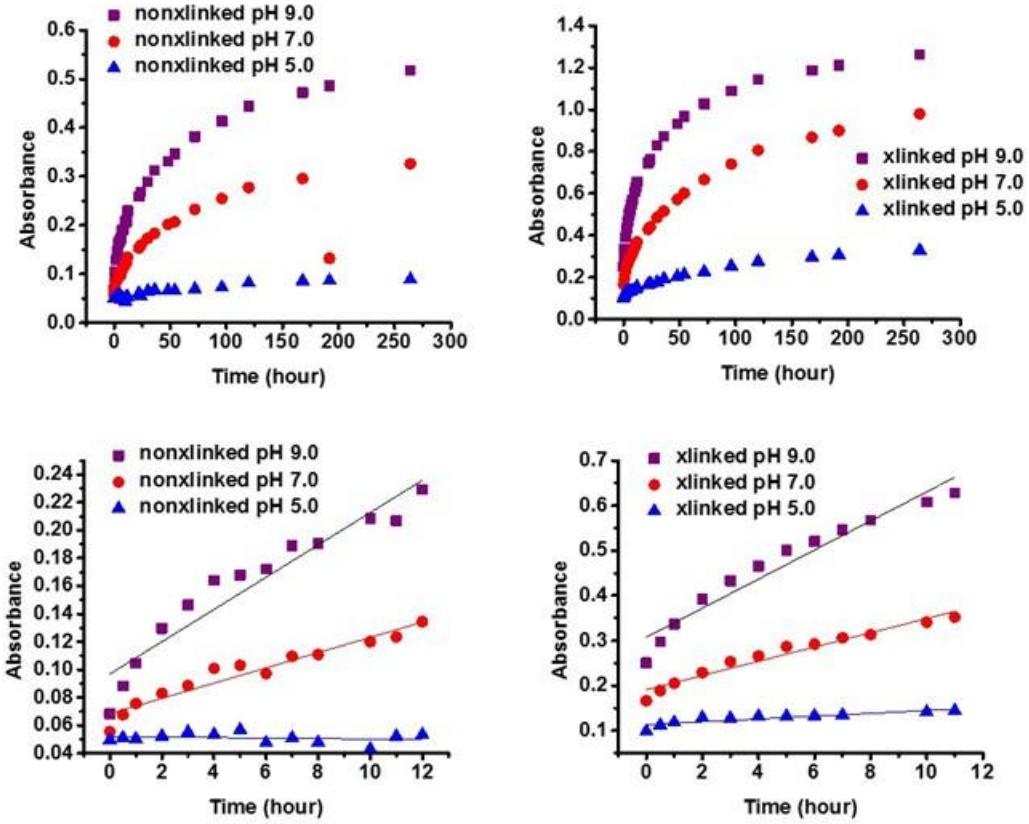

Figure 2.10: UV-Vis absorption spectra of cross-linked and uncross-linked polymer nanoparticles at different pH over 11 days (top); over 12 hours (bottom).

To test our first hypothesis, both the nanoparticle solutions were kept at 0^{o}C during the course of UV irradiation. However, the results were negative (data not shown). Cross-

linked nanoparticle still hydrolyzed at a faster rate. To test the role of coumarin, we simply UV irradiated the Sulfo-NP monomer itself for 10 min. In comparison with the un-irradiated monomer solution, we found that the absorbance of 4-sulfo-2-nitrophenol increased simply after irradiation. After careful literature search, we believed it was the consequence of the so called Photo-Fried reaction.[37, 38] It states that aromatic esters undergo rearrangement under UV light. If UV irradiation indeed causes spontaneous 4-sulfo-2-nitrophenol release or Sulfo-NP rearrangement, we will need to modify our molecular design. This violates our initial design principle that the reactivity of the two functional groups should be orthogonal to each other. To address this issue, an alternative design should be proposed. The new molecular designs will be discussed in the Summary and Future Directions chapter.

	Initial slopes	
	Cross-linked	Uncross-linked
pH 9.0	0.0323	0.0116
pH 7.0	0.0158	0.00547
pH 5.0	0.00312	~ 0

Table 2.1: Initial hydrolysis slopes of cross-linked and uncross-linked polymer nanoparticles at different pH.

2.3 Summary

In summary, we have designed and characterized a versatile polymer nanoparticle platform that: (*i*) displays a versatile functional group on its surface, which can be further manipulated with a variety of complementary reactive moieties; (*ii*) is capable of non-covalently binding hydrophobic guest molecules; (*iii*) afford size tunability by simply altering the salt types and concentrations of the solution or the pH at which the nanoparticle is synthesized; (*iv*) has a very high percentage of the accessible surface moieties at smaller

sizes. Overall, the simplicity and versatility of the surface functionalizable soft nanoparticles with host-guest capabilities will have implications in a variety of applications from materials to biology. Incorporating stimuli-responsive characteristics and expanding this method to a broader range of functional groups are among the current foci in our laboratory.

2.4 Experimental

2.4.1 Materials and Methods

All chemicals and reagents were purchased from commercial sources and were used as received, unless otherwise mentioned. ^{1}H-NMR spectra were recorded on a 400 MHz Bruker NMR spectrometer using the residual proton resonance of the solvent as the internal standard. ^{13}C-NMR spectra were recorded on a 400MHz Bruker NMR spectrometer using carbon signal of the deuterated solvent as the internal standard. ^{19}F-NMR spectra were collected on a 300 MHz Bruker NMR spectrometer. Molecular weights of the polymers were estimated by gel permeation chromatography (GPC) using PMMA standard with a refractive index detector. Dynamic light scattering (DLS) and zeta potential were determined by Nano-ZS (Malvern Instrument) Zetasizer. The fluorescence spectra were obtained from a JASCO FP-6500 spectrofluorimeter. UV-visible absorption spectra were collected using a Cary 100 spectrophotometer. FTIR spectra were recorded on a Perkin Elmer spectrometer. Contact angles of water were examined on a Ramé-Hart telescopic goniometer. Transmission electron microscopy (TEM) images were taken from JEOL 100CX at 100 KV. Atomic force microscopy (AFM) images were collected on a Digital Instruments 3000 Nanoscope IV in tapping mode under ambient conditions by use of silicon cantilievers (spring constant 0.58 N/m).

2.4.2 Synthetic Schemes and Procedures

Synthetic schemes for monomers and random copolymer 1:

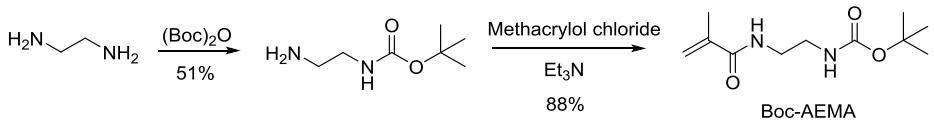

Scheme 2.4: Synthesis of N-2-[(tert-butoxycarbonyl)amino] ethyl methacrylamide (Boc-AEMA).

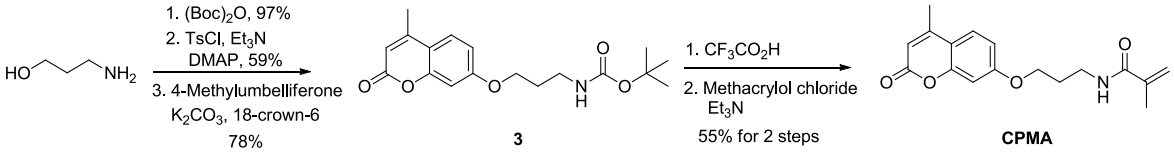

Scheme 2.5: Synthesis of 4-methylcoumarin-7-oxypropyl methacrylamide (CPMA).

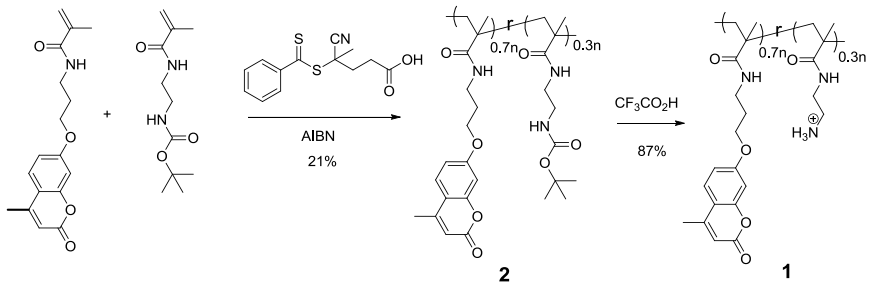

Scheme 2.6: Synthesis of amphiphilic random copolymer **1**.

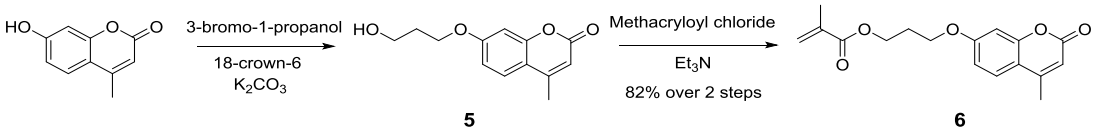

Scheme 2.7: Synthesis of 4-methylcoumarin-7-oxypropyl methacrylate (**6**).

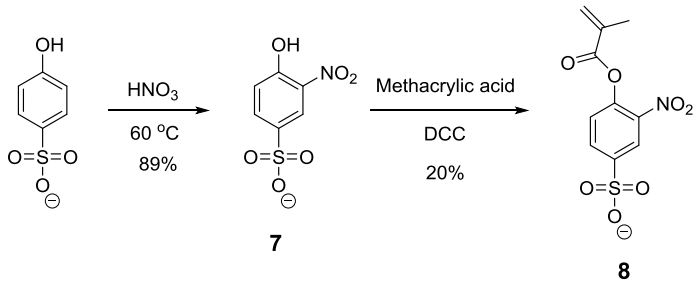

Scheme 2.8: Synthesis of sulfo-NP monomer (**8**).

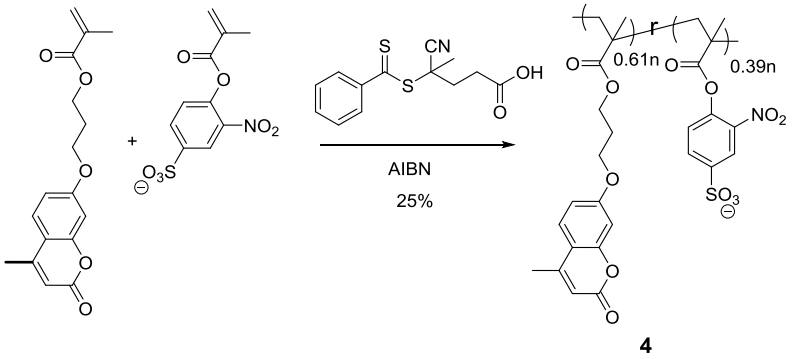

Scheme 2.9: Synthesis of amphiphilic random copolymer **4**.

Synthesis of *N*-Boc-ethylenediamine:

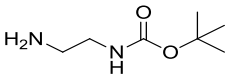

Di-*tert*-butyl dicarbonate (8.0 g, 36.7 mmol) was dissolved in chloroform (50 mL) and added dropwise to a solution of ethylenediamine (13.2g, 220 mmol) in chloroform (250 mL) at 0 °C. The mixture was allowed to warm to room temperature. After stirring for 12 hours, the reaction crude was filtered and washed with chloroform. The filtrates were collected and the solvent was evaporated. The crude was re-dissolved in ethyl acetate and washed with brine (3×100 mL) and water (100 mL). The organic solution was dried over anhydrous Na_2SO_4, filtered and concentrated under reduced pressure to afford *N*-Boc ethylenediamine (2.97 g, 51%) as a colorless oil. ^{1}H NMR (400MHz, $CDCl_3$) δ: 4.95 (bs,

1H), 3.20 (q, 2H), 2.82 (t, 2H), 1.99 (s, 2H).[39]

Synthesis of N-2-[(tert-butoxycarbonyl)amino] ethyl methacrylamide (Boc-AEMA):

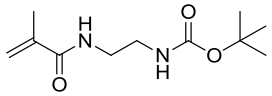

To a solution of N-Boc-ethylenediame (2.0 g, 12.5 mmol) in 20 mL of dry dichloromethane was added 1.5 g (15.0 mmol) of triethylamine and the mixture was cooled in an ice-bath. To this cold mixture, a solution of methacryloyl chloride (1.3 g, 12.5 mmol) in 10 mL dichloromethane was added dropwise with continuous stirring. After the addition, the reaction mixture was stirred at room temperature for 6 h. The stirring was stopped and the reaction mixture was washed with 3x30 mL distilled water and then with 30 mL of brine. The organic layer was collected, dried over anhydrous Na_2SO_4 and concentrated to get the crude product as a white solid. It was purified by column chromatography using silica gel as stationary phase and mixture of ethyl acetate/hexane as eluent. Yield: 2.52 g (88%). ^{1}H NMR (400MHz, $CDCl_3$) δ: 6.70 (bs, 1H), 5.75 (s, 1H), 5.33 (s, 1H), 4.92 (bs, 1H), 3.41 (q, 2H) 3.33 (q, 2H), 1.96 (s, 3H), 1.44 (s, 9H).[40]

Synthesis of Compound 3a:

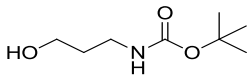

To a solution of 3-aminopropanol (2.0 g, 26.6 mmol) in chloroform (50 mL) was added di-*tert*-butyl dicarbonate (7.0 g, 31.9mmol) at 0 ^{o}C and stirred for 6h at room temperature. Chloroform was evaporated and the residue was re-dissolved in ethyl acetate and washed with saturated $NaHCO_3$ aqueous solution (100 mL) and brine (2 ×100 mL) The organic solution was dried over anhydrous Na_2SO_4, filtered and concentrated in vacuo to afford N-boc-3-aminopropanol (4.5 g, 97 % yield). ^{1}H NMR (400MHz, $CDCl_3$) δ: 3.66

(t, 2H), 3.29 (t, 2H), 1.66 (p, 2H), 1.44 (s, 9H).[41]

Synthesis of compound 3b:

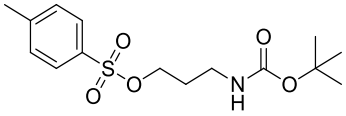

N-boc-3-aminopropanol (4.0g, 22.8 mmol) was dissolved in 100 mL of dry dichloromethane and 2.7g (27.4 mmol) of triethylamine was added to it. To this mixture, a solution of p-toluenesulfonyl chloride (5.2 g, 27.4 mmol) and 4-dimethylaminopyridine (catalytic amount) in 20 mL dry dicholoromethane was added. The reaction mixture was allowed to stir at room temperature overnight. Solvent was evaporated to get the crude product, which was purified by flash column chromatography using silica gel as stationary phase and mixture of ethyl acetate/hexane as eluent. Yield: 4.46 g (59 %). ^{1}H NMR (400MHz, $CDCl_3$) δ: 7.80 (d, 2H), 7.36 (d, 2H), 4.10 (t, 2H), 3.16 (t, 2H), 2.45 (s, 3H), 1.84 (p, 2H), 1.42 (s, 9H).[42]

Synthesis of compound 3:

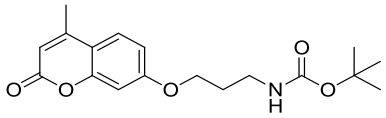

In a two-neck round bottom flask, compound **3b** (3.0 g, 9.1 mmol) was mixed with 4-methylumbelliferone (1.76 g, 10.0 mmol), K_2CO_3 (1.38 g, 10.0 mmol), and 18-crown-6 (0.48 g, 1.82 mmol) in acetone (300 mL) under argon atmosphere. The reaction mixture was refluxed for 12 hours. Then, the crude reaction mixture was filtered and washed with acetone. The filtrates were collected and the solvent was evaporated. The crude was then poured into water and extracted with ethyl acetate (3 x 100 mL). The organic layers were dried over anhydrous Na_2SO_4, filtered, and concentrated in vacuo. The crude product was

purified by flash column chromatography using silica gel as stationary phase and mixture of ethyl acetate/hexane as eluent. Yield: 2.36 g (78 % yield). ^{1}H NMR (400MHz, $CDCl_3$) δ: 7.48 (d, 1H), 6.84 (dd, 1H), 6.80 (d, 1H), 6.13 (s, 1H), 4.73 (bs, 1H), 4.07 (t, 2H), 3.34 (q, 2H), 2.39 (s, 3H), 2.01 (p, 2H), 1.44(s, 9H). ^{13}C NMR (400MHz, $CDCl_3$) δ: 162.0, 161.5, 156.1, 155.4, 152.7, 125.7, 113.8, 112.7, 112.2, 101.58, 79.8, 66.3, 38.0, 29.7, 28.5, 18.8.

Synthesis of 4-Methylcoumarin-7-oxypropyl methacrylamide (CPMA):

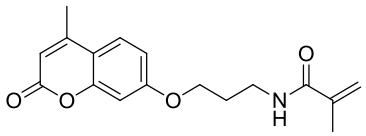

To deprotect the N-boc amine functionality, compound **3** (2.36 g, 7.1 mmol) was dissolved in 10 mL of 1:1 v/v dichloromethane/trifluoroacetic acid mixture. After stirring at room temperature for 2 h, solvent mixture was removed by evaporation, and the oil residue was rinsed two times with diethyl ether (20 mL). The resultant precipitate was collected and dried in vacuo. To a solution of the dried precipitate in 50 mL of dry dichloromethane was added 2.15 g (21.3 mmol) of triethylamine and the mixture was cooled in an ice-bath. To this cold mixture, a solution of methacryloyl chloride (0.82 g, 7.8 mmol) in 10 mL dichloromethane was added drop-wise with continuous stirring. After the addition, the reaction mixture was stirred at room temperature for 6 h. The reaction mixture was then washed with 3x30 mL distilled water and then with 30 mL of brine. The organic layer was collected, dried over anhydrous Na_2SO_4 and concentrated to get the crude product as a yellow solid. It was purified by column chromatography using silica gel as stationary phase and mixture of ethyl acetate/hexane as eluent. Yield: 1.18 g (55 %). ^{1}H NMR (400MHz, $CDCl_3$) δ: 7.50 (d, 1H), 6.84 (dd, 1H), 6.80 (d, 1H), 6.19 (bs, 1H), 6.14

(s, 1H), 5.71 (s, 1H), 5.34 (s, 1H), 4.12 (t, 2H), 3.55 (q, 2H), 2.39 (s, 3H), 2.10 (p, 2H), 1.97 (s, 3H); ^{13}C NMR (400MHz, $CDCl_3$) δ: 168.7, 161.8, 161.4, 155.3, 152.7, 140.0, 125.7, 119.8, 113.8, 112.4, 112.1, 101.6, 67.0, 37.5, 28.9, 18.8.

Synthesis of 4-Methylcoumarin-7-oxypropyl methacrylate (6):

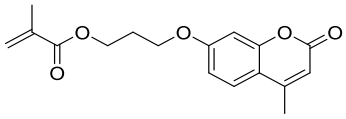

In a two-neck round bottom flask, 3-bromo-1-propanol (1.5 equivalent) was mixed with 4-methylumbelliferone (1.0 equivalent), K_2CO_3 (1.2 equivalent), and 18-crown-6 (0.2 equivalent) in acetone under argon atmosphere. The reaction mixture was refluxed for 12 hours. Then, the crude reaction mixture was filtered and washed with acetone. The filtrates were collected and the solvent was evaporated. The crude was then poured into water and extracted with ethyl acetate (3 x 100 mL). The organic layers were dried over anhydrous Na_2SO_4, filtered, and concentrated in vacuo. The crude product was directly taken to next step without further purification. To a solution of the crude product (1.0 equivalent) in dry dichloromethane was added 2.0 equivalents of triethylamine and the mixture was cooled in an ice-bath. To this cold mixture, a solution of methacryloyl chloride (1.5 equivalent) in dichloromethane was added dropwise with continuous stirring. After the addition, the reaction mixture was stirred at room temperature for overnight. The stirring was stopped and the reaction mixture was washed with distilled water and then with brine. The organic layer was collected, dried over anhydrous Na_2SO_4 and concentrated to get the crude product as a white solid. It was purified by column chromatography using silica gel as stationary phase and mixture of ethyl acetate/hexane as eluent. Yield: 80%. ^{1}H NMR (400MHz, $CDCl_3$) δ: 7.50 (d, 1H), 6.84 (dd, 1H), 6.80 (d, 1H), 6.13 (s, 1H), 6.11 (s, 1H),

5.59 (s, 1H), 4.34 (t, 2H), 4.12 (t, 2H), 2.39 (s, 3H), 2.20 (m, 2H), 1.97 (s, 3H).

Synthesis of compound 7:

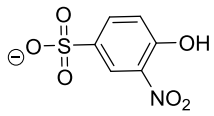

Sodium 4-hydroxybenzenesulfonate (1.0 equivalent) was dissolved in water and heated to 60 ^{o}C, followed by addition of nitric acid (2.3 equivalents) slowly. The reaction mixture was stirred at 60 ^{o}C for 20 min. The mixture was then cooled to room temperature and then cooled in ice to allow precipitation of the product. The mixture was filtered and washed with little amount of cold water. The solids were collected and dried under vaccum to yield the product as a yellow solid. Yield: 60 %. ^{1}H NMR (400MHz, MeOD) δ: 8.49 (d, 1H), 8.0 (dd, 1H), 7.21 (d, 1H).

Synthesis of compound 8:

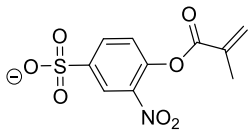

To a solution of compound **7** (1 equivalent) and methacrylic acid (1.2 equivalent) in dry DMF was added N,N'-Dicyclohexylcarbodiimide (1.5 equivalent) at 0 °C. The reaction mixture was stirred for 6 h at room temperature. The reaction mixture was precipitated in excess amount of diethyl ether to get rid of DMF. The precipitates were packed with silica gel and purified by column chromatography using mixture of chloroform/methanol as eluent. Yield: 15%. 1H NMR (400MHz, MeOH) δ: 8.50 (d, 1H), 8.17 (dd, 1H), 7.49 (d, 1H), 6.38 (s, 1H), 5.91 (s, 1H), 2.10 (s, 3H).

Synthesis of random copolymer 1:

A mixture of 4-cyano-4-(phenylcarbonothioylthio)pentanoic acid (7.8 mg, 0.028

mmol), Boc-AEMA (194 mg, 0.85 mmol), CPMA (600 mg, 1.99 mmol) and AIBN (0.92 mg, 0.0019 mmol) was dissolved in DMF (10 ml) and degassed by performing three freeze-pump-thaw cycles. The reaction mixture was sealed and then heated with a pre-heated oil bath at 75 °C for 12 h. The resultant mixture was precipitated in ethyl acetate (200 mL) to remove unreacted monomers. The precipitate was further dissolved in dichloromethane (5 mL) and re-precipitated in ethyl acetate (200 mL) to yield purified random copolymer as a yellow solid. Yield: 21%. ^{1}H NMR (400MHz, $CDCl_3$/MeOD) δ: 6.8-7.4, 6.5-6.8, 5.8-6.0, 3.8-4.1, 3.0-3.4, 2.1-2.4, 1.5-2.0, 1.2-1.4, 0.7-1.2. GPC (THF) M_n: 3000 Da. PDI: 1.3. The molar ratio between two blocks was determined by integrating the Boc group protons in Boc-AEMA and an aromatic proton in the coumarin and found to be 3:7 (Boc-AEMA:CPMA). To remove the Boc groups, the resulting random copolymer was dissolved in 10 mL of 1:1 v/v trifluoroacetic acid/dichloromethane mixture and stirred overnight at room temperature. Solvent mixture was then removed by evaporation, and the oil residue was rinsed three times with diethyl ether. The resultant precipitate was collected and dried overnight in vacuum to afford random copolymer **1**. Yield: 87%. ^{1}H NMR (400MHz, DMSO-d6) δ: 7.3-8.2, 6.7-7.1, 6.0-6.2, 3.9-4.2, 3.0-3.3, 2.7-2.9, 2.2-2.4, 1.5-2.1, 0.7-1.2.Complete disappearance of the methyl proton signal of the Boc group at 1.2-1.4 ppm confirmed that all the Boc groups have been removed.

Synthesis of random copolymer 4:

A mixture of 4-cyano-4-(phenylcarbonothioylthio)pentanoic acid (1 equivalent), monomer **6** (25 equivalent), monomer **8** (25 equivalent) and AIBN (0.2 equivalent) was dissolved in DMF and degassed by performing three freeze-pump-thaw cycles. The reaction mixture was sealed and then heated with a pre-heated oil bath at 75 °C for 12 h.

The resultant mixture was precipitated in ethyl acetate and methanol to remove unreacted monomers, respectively, to yield the purified random copolymer. Yield: 40%. ^{1}H NMR (400MHz, DMSO-d6) δ: 8.1-8.2, 7.2-7.6, 6.6-6.9, 5.9-6.2, 3.9-4.3, 1.6-2.4, 0.6-1.5.

Synthesis of azidoacetic acid:

To a solution of sodium azide (2.3 g, 36 mmol) in water (50 mL) was added bromoacetic acid (1.0 g, 7.2 mmol) slowly. The reaction mixture was stirred overnight at room temperature. The reaction was quenched with 1 M of HCl aqueous solution. The crude material was mixed with water (50 mL) and extracted with ethyl acetate (3 x 100 mL). The organic solution was dried over anhydrous Na_2SO_4, filtered and concentrated under reduced pressure to afford azidoacetic acid (0.39 g, 54% yield). ^{1}H NMR (400MHz, $CDCl_3$) δ: 10.62 (bs, 1H), 3.98 (s, 2H).[43]

Synthesis of [2-(2-methoxyethoxy)ethoxy]acetic acid pentafluorophenyl ester (Peg178 PFP ester):

To a solution of [2-(2-methoxyethoxy)ethoxy]acetic acid (1 equivalent) and pentafluorophenol (1.2 equivalent) in dry dichloromethane was added 1-(3-dimethylaminopropyl)-3-ethylcarbodiimide hydrochloride (1.2 equivalent) and catalytic amount of 4-dimethylaminopyridine at 0 °C. The reaction mixture was stirred for 6 h at room temperature. The reaction mixture was washed with saturated $NaHCO_3$ aqueous solution and then with brine. The organic solution was dried over anhydrous Na_2SO_4, filtered and concentrated under reduced pressure to afford the crude product. It was purified by column chromatography using silica gel as the stationary phase and mixture of ethyl acetate/hexane as eluent. Yield: 50%. 1H NMR (400MHz, CDCl3) δ: 4.54 (s, 2H), 3.83 (m, 2H), 3.74 (m, 2H), 3.65 (m, 2H), 3.57 (m, 2H), 3.38 (s, 3H). 19F NMR (300 MHz,

CDCl3) δ: -152.5 (2F), -157.3 (1F), -161.9 (2F).

General procedure for the synthesis of N-hydroxysuccinimide (NHS) ester:

To a solution of carboxylic acid (1 equivalent) and N-hydroxysuccinimide (1.2 equivalent) in dry dichloromethane was added 1-(3-Dimethylaminopropyl)-3-ethylcarbodiimide hydrochloride (1.2 equivalent) at 0 °C and stirred for 12 hours at room temperature. The stirring was stopped and the reaction mixture was washed with saturated $NaHCO_3$ aqueous solution and then with brine. The organic solution was dried over anhydrous Na_2SO_4, filtered and concentrated under reduced pressure to afford the N-hydroxysuccinimide ester.

Methoxypolyethylene glycol 2,000 acetic acid NHS ester (PEG2000 NHS ester):

Synthesis of PEG2000 NHS ester was done in dry DMF and the crude reaction mixture was directly taken to next step without any purification.

Azidoacetic acid NHS ester:

Yield: 61%. ^{1}H NMR (400MHz, $CDCl_3$) δ: 4.24 (s, 2H), 2.88 (s, 4H).[43]

Lauric acid NHS ester:

Yield: 71%. ^{1}H NMR (400MHz, $CDCl_3$) δ: 2.84 (s, 4H), 2.60 (t, 2H), 1.74 (p, 2H), 1.40 (p, 2H), 1.20-1.35 (m, 14H), 0.88 (t, 3H).[44]

Capric acid NHS ester:

^{1}H NMR (400MHz, $CDCl_3$) δ: 2.84 (s, 4H), 2.60 (t, 2H), 1.74 (p, 2H), 1.17-1.48 (m, 12H), 0.88 (t, 3H).[45]

2.4.3 Nanoparticle Preparation

To a solution of random copolymer **1** (20 mg) dissolved in 200 uL of DMSO was added 19.8 mL of milliQ water. After sonicating for 2 h, the solution was filtered through

a filter with a pore size of 0.22 μm. The polymer solution was adjusted to pH 3 in a scintillation vial and irradiated under a XX-15LW Bench Lamp (UVP) with UV light (365 nm) for 10 min. Crosslinking was monitored by the reduction of absorbance at 320 nm. In order to show that the synthesized nanoparticles are stable cross-linked networks, rather than the simple aggregation of the polymer, nanoparticles were redispersed in 1:9 H_2O/DMSO mixture in which DLS data shows a size of ~32 nm. The increase in size is likely due to the swelling of nanoparticles caused by DMSO. In contrast, DLS studies reveal no aggregates for the redispersion of non-crosslinked polymers in 1:9 H_2O/DMSO.

2.4.4 Encapsulation of Guest Molecules

50 μL of 1mg/mL DiO/DiI (in acetone) was added to a vial, followed by evaporating the acetone with mild blow of air. To this was added 2 mL of nanoparticle solution (1 mg/mL) and sonicated at room temperature for 2 h. The resultant mixture was then passed through 0.22 μm filter to remove the non-encapsulated DIO/DiI, followed by stirring the solution at room temperature overnight to remove any residual acetone present in the solution. This stock solution was accordingly diluted with milliQ water (pH 3) to achieve required concentration of the nanoparticles.

2.4.5 General Procedures for Surface Charge, Contact Angle, AFM and FTIR Measurements

To 1 mL of nanoparticle stock solution (1 mg/mL) at basic pH was added the functionalization agents (10 equivalents) dissolved in DMF. After stirring overnight at room temperature, the excess functional group reagents were removed by dialysis. For the functionalization with succinic anhydride, the reaction was done in 0.1 M NaCl solution to minimize the aggregation of opposite charge nanoparticles that could prevent the reaction

from going to completion.

Surface charge measurements:

The reaction mixtures were first dialyzed in acetone to remove excess reagents and then were switched to aqueous medium. Solutions after dialysis were accordingly diluted with milliQ water to achieve a final concentration of 0.35mg/mL. All solutions were adjusted to pH 7.1 and then filtered through a 0.22 μm filter before performing surface charge measurements.

Contact angle and AFM measurements:

To prepare samples for contact angle and AFM measurements, stock solution of nanoparticles dissolved in water and dodecyl-functionalized nanoparticles dissolved in dichloromethane were dropped onto a silicon slides and dried at room temperature overnight.

2.4.6 Functionalization of Nanoparticles for Emission Spectrum Measurements

Emission spectra were recorded on a JASCO (FP-6500) spectrofluorimeter using quartz cuvettes. To 100 μL of nanoparticle (1 equivalent) stock solution at basic pH, functional groups (3 equivalents) dissolved in DMSO (800 μL) were added and stirred overnight at room temperature. Fluorescamine (10 equivalents) dissolved in DMSO (100 μL) was then added and stirred for another 2 h at room temperature. All solutions were directly taken to the spectrofluorimeter for measurement without further purification. The emission spectra for fluorescamine-amine adduct were recorded by exciting at 390 nm, with both excitation and emission bandwidths set at 3 nm.

2.4.7 Quantifying the Amounts of Amine Available for Functionalization

Different aliquots of nanoparticle (200 μg/mL) were pipetted into a 96 well

microplate in triplicates. Different volumes of water and DMSO were added to adjust the final water/DMSO (1:2, v:v) volume to 150 µL. The microplate was placed on a microplate shaker and 50 µl of 3.6 mM (1 mg/mL) fluorescamine dissolved in DMSO was added to each well. Following the addition of fluorescamine the plate was shaken for one minute and then allowed to stand at room temperature for 2 h. The fluorescence was then determined using a SpectraMax M5 plate reader with a 400 nm excitation filter and a 460 nm emission filter. The sensitivity setting was at 6 and the data collected from the top.

2.4.8 Different Percentage of Amines on the Nanoparticles can be Functionalized

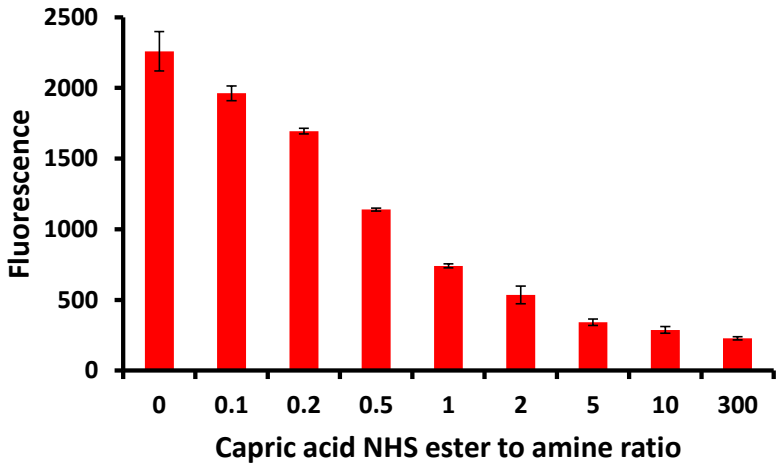

Figure 2.11: Nanoparticles reacted with different concentrations of capric acid NHS ester monitored by fluorescamine.

100 µL aliquots of nanoparticle (200 µg/mL) were pipetted into a 96 well microplate in triplicates, followed by addition of different equivalents of capric acid NHS ester dissolved in DMSO to each well. Different volumes of water and DMSO were added accordingly to adjust the final water/DMSO (1:2, v:v) volume to 150 µL. The microplate was allowed to stay at room temperature for 6 hours during which it was shaken on a microplate shaker for the frequency of one minute per hour.

2.4.9 Size Control

2 mL polymer solutions (1 mg/mL) in scintillation vials were adjusted to the required pH using NaOH and HCl aqueous solution. After sonicating for 2 min, all solutions were irradiated under UV light (365nm) for 10 min to crosslink the polymers. The nanoparticle solutions were dialyzed in milliQ water to remove residual DMSO. All nanoparticle solutions were adjusted to pH 3 and then filtered through a 0.22 μm filter before performing dynamic light scattering measurements.

2.4.10 AFM Images

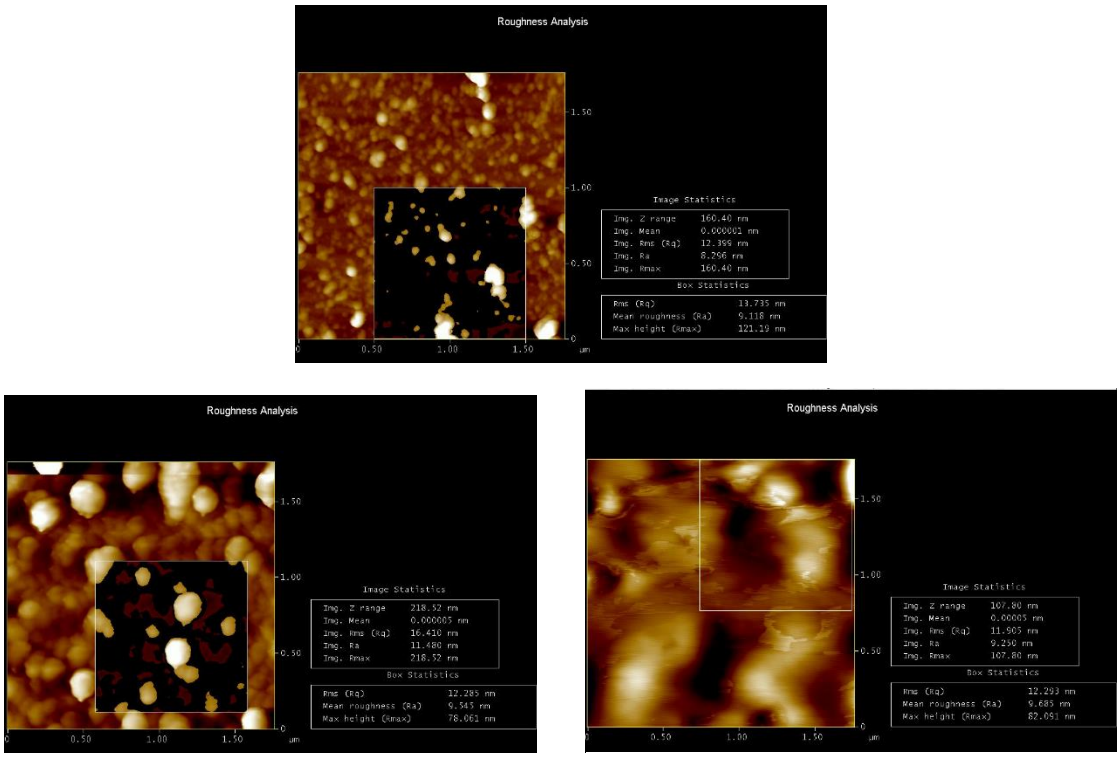

Figure 2.12: AFM images of unmodified nanoparticles (top) and nanoparticles modified by lauric acid NHS ester (bottom left) and dodecyl isocyanate (bottom right).

2.4.11 TEM Image

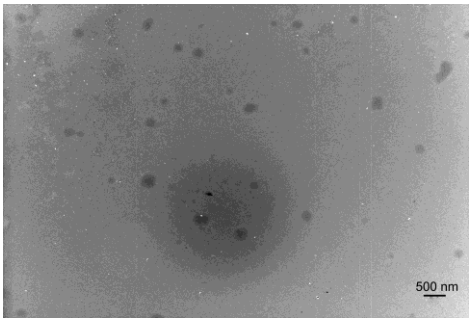

Figure 2.13: Size distribution of nanoparticles functionalized with capric acid NHS ester by TEM.

2.5 References

1. *Nanoparticles: From Theory to Application*; Schmid, G., Ed.; Wiley-VCH: Essen, 2004.

2. Zhang, J.; Wang, Z.-l.; Liu, J.; Chen, S.; Liu, G.-y. *Self-Assembled Nanostructures*; Nanostructure Science and Technology Series; Springer: 2002.

3. *Nanoparticles: Building Blocks for Nanotechnology*; Rotello, V. M., Ed.; Springer: 2003.

4. Daniel, M. -C.; Astruc, D. Gold Nanoparticles: Assembly, Supramolecular Chemistry, Quantum-Size-Related Properties, and Applications toward Biology, Catalysis, and Nanotechnology. *Chem. Rev.* **2004,** *104*, 293–346.

5. Giljohann, D. A.; Seferos, D. S.; Daniel, W. L.; Massich, M. D.; Patel, P. C.; Mirkin, C. A. Gold Nanoparticles for Biology and Medicine. *Angew. Chem. Int. Ed.* **2010,** *49*, 3280–3294.

6. Saha, K.; Agasti, S. S.; Kim, C.; Li, X.; Rotello, V. M. Gold Nanoparticles in Chemical and Biological Sensing. *Chem. Rev.* **2012,** *112*, 2739–2779.

7. Khandare, J.; Calderon, M.; Dagi, N. M.; Haag, R. Multifunctional Dendritic Polymers in Nanomedicine: Opportunities and Challenges. *Chem. Soc. Rev.* **2012,** *41*, 2824–2848.

8. Grayson, S. M.; Fréchet, J. M. J. Convergent Dendrons and Dendrimers: from Synthesis to Applications. *Chem. Rev.* **2001,** *101*, 3819–3868.

9. Arima, H.; Motoyama, K.; Higashi, T. Polyamidoamine Dendrimer Conjugates with Cyclodextrins as Novel Carriers for DNA, shRNA and siRNA. *Pharmaceutics* **2012,** *4*, 130–148.

10. Harada, A.; Kataoka, K. Supramolecular Assemblies of Block Copolymers in Aqueous Media as Nanocontainers Relevant to Biological Applications. *Progress in Poly. Sci.* **2006,** *31*, 949–982.

11. O'Reilly, R. K.; Hawker, C. J.; Wooley, K. L. Cross-Linked Block Copolymer Micelles: Functional Nanostructures of Great Potential and Versatility. *Chem. Soc. Rev.* **2006,** *35*, 1068–1083.

12. Zhu, Z.; Sukhishvili, S. A. Layer-by-Layer Films of Stimuli-Responsive Block Copolymer Micelles. *J. Mat. Chem.* **2012,** *22*, 7667–7671.

13. Owen, S. C.; Chan, D. P. Y.; Shoichet, M. S. Polymeric Micelle Stability. *Nano Today* **2012,** *7*, 53–65.

14. Sawant, R. R.; Torchilin, V. P. Liposomes as 'Smart' Pharmaceutical Nanocarriers. *Soft Matter* **2010,** *6*, 4026–4044.

15. Micheli, M.-Rita; Bova, R.; Magini, A.; Polidoro, M.; Emiliani, C. Lipid-Based Nanocarriers for CNS-Targeted Drug Delivery. *Recent Pat. CNS Drug Discov.* **2012,** *7*, 71–86.

16. Van Nostrum, C. F. Covalently Cross-Linked Amphiphilic Block Copolymer Micelles. *Soft Matter* **2011,** *7*, 3246–3259.

17. Elsabahy, M.; Wooley, K. L. Design of Polymeric Nanoparticles for Biomedical Delivery Applications. *Chem. Soc. Rev.* **2012,** *41*, 2545–2561.

18. Bell, C. A.; Smith, S. V; Whittaker, M. R.; Whittaker, A. K.; Gahan, L. R.; Monteiro, M. J. Surface-Functionalized Polymer Nanoparticles for Selective Sequestering of Heavy Metals. *Adv. Mater.* **2006,** *18*, 582–586.

19. Muthuramu, K.; Ramamurthy, V. Photodimerization of Coumarin in Aqueous and Micellar Media. *J. Org. Chem.* **1982,** *47*, 3976–3979.

20. Gnanaguru, K.; Ramasubbu, N.; Venkatesan, K.; Ramamurthy, V. A Study on the Photochemical Dimerization of Coumarins in the Solid State. *J. Org. Chem.* **1985,** *50*, 2337–2346.

21. He, J.; Tremblay, L.; Lacelle, S.; Zhao, Y. Preparation of Polymer Single Chain Nanoparticles Using Intramolecular Photodimerization of Coumarin. *Soft Matter* **2011,** *7*, 2380–2386.

22. Trenor, S. R.; Shultz, A. R.; Love, B. J.; Long, T. E. Coumarins in Polymers: From Light Harvesting to Photo-Cross-Linkable Tissue Scaffolds. *Chem. Rev.* **2004,** *104*, 3059–3078.

23. Raghupathi, K. R.; Azagarsamy, M. A.; Thayumanavan, S. Guest-Release Control in Enzyme-Sensitive, Amphiphilic-Dendrimer-Based Nanoparticles through Photochemical Crosslinking. *Chem. Eur. J.* **2011,** *17*, 11752–11760.

24. Udenfriend, S.; Stein, S.; Böhlen, P.; Dairman, W.; Leimgruber, W.; Weigele, M. Fluorescamine: A Reagent for Assay of Amino Acids, Peptides, Proteins, and Primary Amines in the Picomole Range. *Science* **1972,** 178, 871–872.

25. Ryu, J.-H.; Jiwpanich, S.; Chacko, R.; Bickerton, S.; Thayumanavan, S. Surface-Functionalizable Polymer Nanogels with Facile Hydrophobic Guest Encapsulation Capabilities. *J. Am. Chem. Soc.* **2010**, *132*, 8246–8247.

26. Ryu, J.-H.; Chacko, R.; Jiwpanich, S.; Bickerton, S.; Babu, R. P.; Thayumanavan, S. Self-Crosslinked Polymer Nanogels: a Versatile Nanoscopic Drug Delivery Platform. *J. Am. Chem. Soc.* **2010**, *132*, 17227–17235.

27. Hofmeister, F. On the Understanding of the Effects of Salts, Second report. On Irregularities in The Precipitating Effect of Salts and Their Relationship to Their Physical Behavior. *Arch. Exp. Pathol. Pharmocol.* **1888**, *24*, 247–260.

28. Von Hippel, P. H.; Wong., K. Y. Neutral Salts: The Generality of Their Effects on the Stability of Macromolecular Conformations. *Science* **1964**, *145*, 577–580.

29. Baldwin, R. L. How Hofmeister Ion Interactions Affect Protein Stability. *Biophys. J.* **1996**, *71*, 2056–2063.

30. Zhang, Y. J.; Furyk, S.; Bergbreiter, D. E.; Cremer, P. S. Specific Ion Effects on the Water Solubility of Macromolecules: PNIPAM and the Hofmeister Series. *J. Am. Chem. Soc.* **2005**, *127*, 14505–14510.

31. Magnusson, J. P.; Khan, A.; Pasparakis, G.; Saeed, A. O.; Wang, W. X.; Alexander, C. Ion-sensitive "Isothermal" Responsive Polymers Prepared in Water. *J. Am. Chem. Soc.* **2008**, *130*, 10852–10853.

32. Suwa, K.; Yamamoto, K.; Akashi, M.; Takano, K.; Tanaka, N.; Kunugi, S. Effects of Salt on the Temperature and Pressure Responsive Properties of Poly(N-vinylisobutyramide) Aqueous Solutions. *Colloid Polym. Sci.* **1998**, *276*, 529–533.

33. Zhang, Y.; Furyk, S.; Sagle, L. B.; Cho, Y.; Bergbreiter, D. E.; Cremer, P. S. Effects of Hofmeister Anions on the LCST of PNIPAM as a Function of Molecular Weight. *J. Phys. Chem. C* **2007**, *111*, 8916–8924.

34. He, Y.; Shao, Q.; Chen, S. F.; Jiang, S. Y. Water Mobility: A Bridge between the Hofmeister Series of Ions and the Friction of Zwitterionic Surfaces in Aqueous Environments. *J. Phys. Chem. C* **2011**, *115*, 15525–15531.

35. Swann, J. M. G.; Bras, W.; Topham, P. D.; Howse, J. R.; Ryan, A. J. Effect of the Hofmeister Anions Upon the Swelling of a Self-Assembled pH-Responsive Hydrogel. *Langmuir* **2010**, *26*, 10191–10197.

36. Li, L.; Ryu, J.; Thayumanavan, S. Effect of Hofmeister Ions on the Size and Encapsulation Stability in Polymer Nanogels. *Langmuir*, **2013**, *29*, 50–55.

37. Bellus, D. *Advances in Photochemistry*; John Wiley & Sons: Chichester, 1971; Vol. 8, pp. 109-159.

38. Searle N. *Environmental Effects on Polymeric Materials*; Plastics and the Environment; Andrade, A., Ed.; Wiley: 2003; pp. 313-358.

39. Roy, D.; Sumerlin, B. S. Glucose-Sensitivity of Boronic Acid Block Copolymers at Physiological pH. *ACS Macro Lett.* **2012,** *1,* 529–532.

40. Sun, W.; Bandmann, H.; Schrader, T. A Fluorescent Polymeric Heparin Sensor. *Chem. Eur. J.* **2007,** *13,* 7701–7707.

41. Mehlich, J.; Ravoo, B. J. Click Chemistry by Microcontact Printing on Self-Assembled Monolayers: A Structure–Reactivity Study by Fluorescence Microscopy. *Org. Biomol. Chem.* **2011,** *9,* 4108–4115.

42. Simoni, E.; Daniele, S.; Bottegoni G.; Pizzirani D.; Trincavelli, M. L.; Goldoni, L.; Tarozzo, G.; Reggiani, A.; Martini, C.; Piomelli, D.; Melchiorre, C.; Rosini, M.; Cavall, A. Combining Galantamine and Memantine in Multitargeted, New Chemical Entities Potentially Useful in Alzheimer's Disease. *J. Med. Chem.* **2012,** *55*, 9708–9721.

43. Ghosh, P. S.; Hamilton, A. D. Supramolecular Dendrimers: Convenient Synthesis by Programmed Self-Assembly and Tunable Thermoresponsivity. *Chem. Eur. J.* **2012,** *18*, 2361–2365.

44. Kapdi, A. R.; Fairlamb, I. J. S. Synthesis of Macrocyclic Ketones Exploiting Palladium-Catalyzed Activation of Carboxylic Acids as an Enabling Step. *New J. Chem.* **2013,** *37*, 961–964.

45. Schulze, A.; Giannis, A. IBX-Mediated Conversion of Primary Alcohols and Aldehydes to N-Hydroxysuccinimide Esters. *Adv. Synth. Catal.* **2004,** *346*, 252–256.

CHAPTER 3

A SUPRAMOLECULAR DISSOCIATION STRATEGY FOR PROTEIN SENSING

Adapted with permission from Wang, H.; Zhuang, J.; Raghupathi, K. R.; Thayumanavan, S. A Supramolecular Dissociation Strategy for Protein Sensing. *Chem. Commun.* **2015**, *51*, 17265–17268.

3.1 Introduction

Development of new biosensors for recognizing biological analytes and reporting their presence is important due to the implications in proteomics, medical diagnostics, and pathogen detection. Approaches to developing new sensors can be broadly classified into two categories, both of which are inspired by nature: (*i*) array-based sensing, where several less-specific receptors are used to develop a response pattern for each analyte;[1-7] and (*ii*) sensing based on 'lock-and-key' design, where specific receptors are needed to selectively bind the analytes of interest.[8-12] The former method has the advantage of being simple as the receptor design is less intense and provides convenient opportunities to transduce the analyte recognition. In contrast, the latter approach has the promise of being specific to the target analyte even when the analyte mixture becomes complex. An approach that captures the simplicity of the former and the specificity of the latter would certainly be desirable for ultimately implementing these strategies in practical systems. Here, we disclose a simple supramolecular dissociation approach to protein sensing based on specific ligand-analyte interactions.

3.2 Results and Discussions

3.2.1 Design and Synthesis

A sensor system requires two important elements, *viz.* specific recognition of the target analyte and generation of a signal that transduces the recognition event. Enabled by the efforts in drug discovery to impact pharma, specific ligands have been developed for many important proteins.[13, 14] However, methods that utilize these ligand discoveries to develop protein sensors are scarce, as these are hampered by strategies that transduce these binding events. Prior approaches that utilize these ligands require a supramolecular disassembly event to occur in response to a specific ligand-protein binding event.[15-18] This strategy therefore requires a design strategy that requires the lignad-containing molecule to assemble in the absence of the protein, but disassemble in its presence.

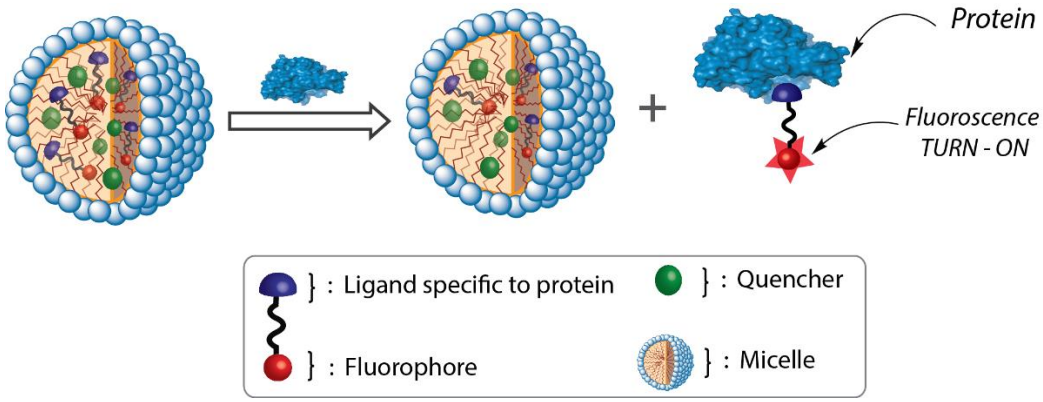

Figure 3.1: Schematic illustration of the supramolecular dissociation based protein sensor. The difference in the equilibrium concentrations (between the interior of the micelle and the bulk aqueous phase) of the pristine fluorescent probe and the probe-protein complex affords a simple, turn-on fluorescent sensor.

We envisaged a simple supramolecular dissociation strategy that obviates this rigorous design requirement (Figure 1). Briefly, in this approach, a probe is generated by simply tethering the protein-specific ligand moiety to a hydrophobic fluorophore, which is

non-covalently incorporated into a micelle along with a corresponding hydrophobic fluorescence quencher. The micelle itself is chosen such that it is known to exhibit good guest exchange dynamics with the bulk solvent, *i.e.* the aqueous phase.[19] Here, since the probe molecule is hydrophobic, its thermodynamic distribution coefficient will dictate that most of it is present inside the micelle, where the fluorescence is quenched due to its co-confinement with the quencher. We hypothesized that in the presence of the analyte protein, the binding event between the ligand moiety in the probe and the protein should cause the complex to decidedly favor the bulk solvent. This anticipation is because, in contrast to the probe by itself, the probe-protein complex should not have the hydrophobic driving force to re-bind to the interior of the micellar host. This specific protein-driven dissociation of the probe from the micelle also drastically decreases the proximity of the fluorophore and the quencher, which can be conveniently read as fluorescence increase, as schematically illustrated in Figure 1. The extent of this dissociation should also be dependent on the concentration of analyte protein.

To test our design hypothesis, we chose human carbonic anhydrase I (hCAI) as the target analyte because of its disease relevance.[20, 21] This protein also has several well-established ligand moieties.[20-23] Brij 35, a commercially available surfactant, is used as the micelle-forming macromolecule because its non-ionic head group, composed of polyethylene glycol unit, helps reduce nonspecific interactions. Benzenesulfonamide, which is used as a specific ligand to bind hCAI,[20-23] is tethered to pyrene as the fluorophore using a simple hydrophobic linker to obtain the fluorescent probe **1** (Figure 2a).

3.2.2 Encapsulation of Probe in Micellar Assemblies

For the design to be functional, it's pivotal that probe **1** is incorporated into the

micellar assemblies. To test this, probe **1** was dissolved in a buffer solution (pH 7.4) in the presence and absence of Brij 35 in the solution. Absorption spectra of the solutions indicated that while the solution without Brij 35 has negligible absorbance at 340 nm, the solution with Brij 35 exhibits strong absorption peaks that correspond to pyrene (Figure 6a). This indicates micellar assemblies help solubilize the hydrophobic probe **1**, which otherwise has limited solubility in aqueous solution. Thus, this observation also provides the support that the majority of the probe in the solution will be present inside the Brij 35 micelle, compared to the bulk solvent. To achieve a fluorescence "OFF" state, a known photoinduced electron transfer quencher (benzophenone (BP))[24] was co-encapsulated in the micelle. This co-encapsulation indeed causes the pyrene fluorescence to be predominantly quenched (Figure 7a).

3.2.3 Protein Detection

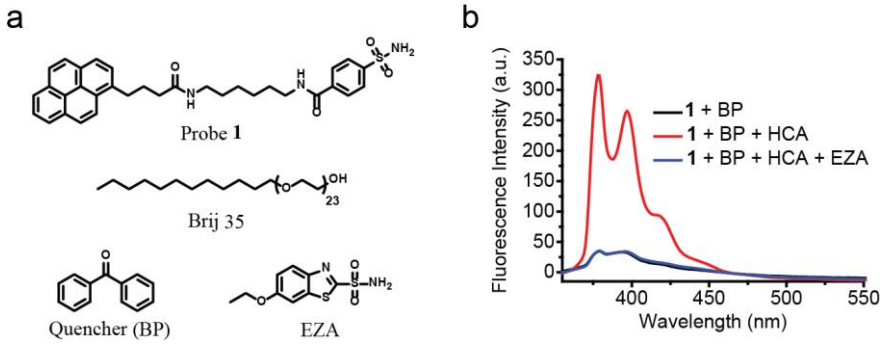

Figure 3.2: (a) Chemical structures of probe **1**, quencher and micelle. (b) Fluorescence spectra of probe **1** (1 μM) and benzophenone (5 mM) in Brij 35 (1 mM) Tris buffer solution (25 mM, pH 7.4) treated without or with HCA (5 μM) or with HCA (5 μM) and EZA (100 μM). All spectra were taken after 3-hour HCA incubation at room temperature.

Next, we examined the possibility of utilizing this assembly to sense the presence of the analyte protein. Accordingly, hCAI was added to the Brij 35 micellar assembly containing probe **1** and BP. Indeed, upon addition of the protein, the fluorescence of pyrene

increased dramatically, as shown in Figure 2b. To check if this fluorescence enhancement is indeed due to the ligand-protein binding mechanism illustrated in Figure 1, we added a competitive ligand to hCAI. The presence of the competitive ligand should displace the fluorescent probe from the protein. Since the probe is hydrophobic, it should be re-encapsulated into the micelle upon release from the protein to cause the fluorescence to be quenched again. As shown in Figure 2b, addition of 6-Ethoxy-2-benzothiazolesulfonamide (EZA), a strong competitive inhibitor of hCAI,[25] caused the fluorescence to go back to the original fluorescence level, *i.e.* significantly quenched. In addition to supporting the design hypothesis outlined in Figure 1, this observation also suggests that the micellar assembly itself is intact and that the BP quencher stays encapsulated in this assembly to cause the re-encapsulated fluorophore to be quenched.

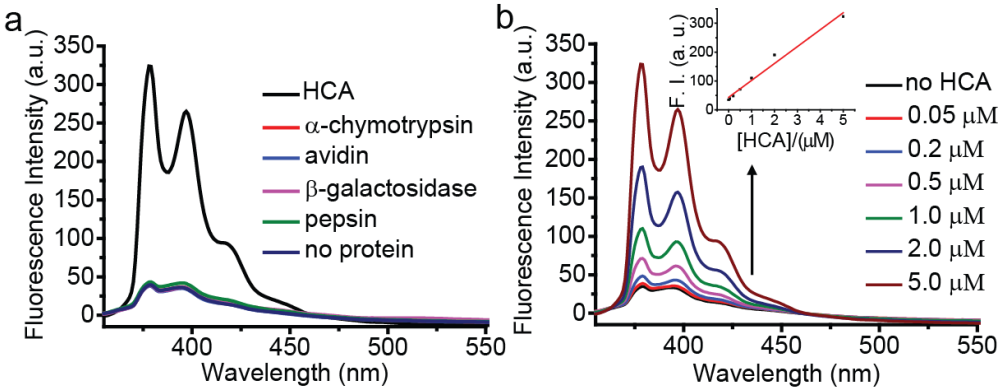

Figure 3.3: Fluorescence spectra of probe **1** (1 μM) and benzophenone (5 mM) in Brij 35 (1 mM) Tris buffer solution (25 mM, pH 7.4) treated with (a) 5 μM of proteins; (b) different concentrations of HCA. The inset shows fluorescence intensity at λ_{em} = 379 nm. All spectra were taken after 3-hour protein incubation at room temperature.

To further confirm that the fluorescence enhancement was indeed caused by the specific protein-ligand interaction, an unmodified pyrene fluorophore, which lacks the sulfonamide ligand moiety, was encapsulated along with benzophenone in Brij 35 micelle

assemblies. Upon exposure to hCAI, no fluorescence enhancement was observed (Figure 8). Similarly, to test whether the probe design is specific to hCAI, solutions of BP quenched probe **1** in Brij 35 micelles were exposed to four different proteins with different isoelectric points (α-chymotrypsin, avidin, β-galactosidase, and pepsin) that have no known binding affinity toward benzenesulfonamide. As shown in Figure 3a, none of these proteins caused a significant change in pyrene fluorescence. In addition, we also found that the hCAI-induced fluorescence enhancement occurred in a 50% fetal bovine serum solution (Figure 9b), which suggests that this sensing strategy has the potential to be translated to a complex milieu containing many biological macromolecules.

3.2.4 Detection Limit

We were also interested in investigating the sensitivity of this sensing strategy. If our mechanistic hypothesis is correct, then we should have a linear increase in fluorescence with increase in concentration of the protein. This is because, the inherent preference for the probe is to be within the micellar assembly and therefore exhibit fluorescence quenching. However, the bound probes have the opposite preference, *i.e.* to stay in the bulk aqueous phase where there is no fluorescent quenching. Since increasing concentrations of protein should afford higher amounts of bound probes, the fluorescence increase should be linear. Indeed, we found that the fluorescence increased linearly with increasing hCAI concentrations (Figure 3b). We found that a reproducible change in the fluorescence can be achieved even at 50 nM concentration of the protein and an appreciable change starts occurring in the protein above 200 nM hCAI. Overall, the sensitivity of this surfactant-probe-quencher combination is in the high nM range.

3.2.5 Effect of Surfactant Concentration on Probe Sensitivity

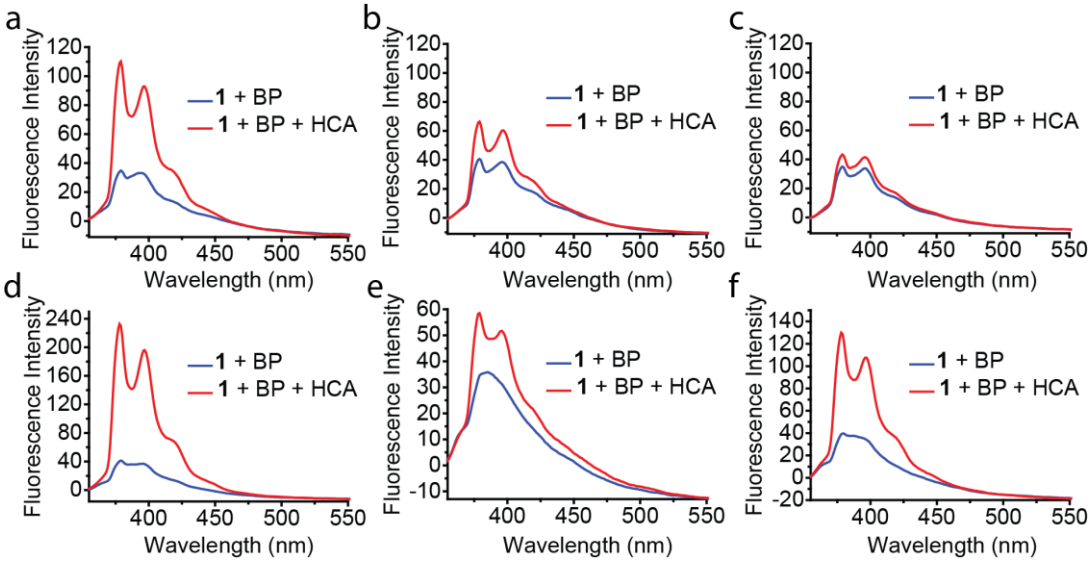

Figure 3.4: Fluorescence spectra of probe **1** (1 μM) and benzophenone (5 mM) treated without or with 1 μM HCA in different surfactant solutions: (a) 1 mM Brij 35; (b) 5 mM Brij 35; (c) 20 mM Brij 35; (d) 4 mM Triton X-100; (e) 1 mM Tween 20; (f) 1 mg/mL PEG-dodecyl random copolymer. All experiments were carried out in Tris buffer solution (25 mM, pH 7.4). All spectra were taken after 3-hour protein incubation at room temperature.

While investigating the factors that could affect the sensitivity of this method, we found that the sensitivity of the probe was affected by the concentration of the surfactant. As indicated in Figure 4a-c, fluorescence enhancement becomes less obvious as the concentration of Brij 35 increases. In these cases, the probe and quencher concentrations were kept constant. These observations seem to be consistent with our mechanistic hypothesis that the probe binds to the protein in the bulk solvent, as it has some propensity to partition to the bulk solvent. It is reasonable to suggest that the probe partitions between the micellar core and bulk solvent with the equilibrium largely favoring the micelle core. Increasing the surfactant concentration increases the effective micelle concentration, which should shift the equilibrium even further toward the micellar core. This should render the

availability of the probe for protein binding even lesser and therefore the sensitivity of the probe becomes lesser.

3.2.6 Surfactant Type and Protein Ligand Variations

Next, we were interested in testing the broad utility of this approach. From the perspective of varying the fluorophore and the quencher, it is perhaps obvious that other combinations can be utilized for this purpose. However, we were interested in testing the versatility of this approach by investigating whether it will accommodate variations in the micellar assembly and the target protein. Instead of Brij 35, we investigated other charge neutral micelles generated from Triton X-100, Tween 20 and an amphiphilic random copolymer based on PEG-acrylate and dodecyl-acrylate. First of all, we were gratified to find that in all these cases the protein-induced fluorescence change can be observed (Figure 4d-f). Next, we also tested whether the sensitivity to the concentration of the surfactants would be different in each of these cases. All surfactants exhibited the same trend in that the sensitivity decreased with increasing surfactant concentration (Figure 11), suggesting similar operating mechanism. It is however interesting that the relative sensitivity itself was different at concentrations above their respective critical micelle concentration. Triton X-100 was found to provide the most sensitive sensing system and Tween 20 was found to be the least sensitive system. Although we do not understand the reasons for these differences at this time, this observation suggests that a systematic structure-property relationship study in the future could provide an even more sensitive system.

Finally, to test whether this design principle can be applied to detect other proteins, we synthesized a structurally similar probe to target avidin (probe **2**, Figure 5a). Biotin, which has extraordinary binding affinity toward avidin, was linked to the pyrene

fluorophore in the place of benzenesulfonamide. Similar to that observed with probe **1** and hCAI, the fluorescence intensity was very weak when probe **2** and benzophenone were co-encapsulated in Brij 35. On the other hand, the fluorescence was dramatically enhanced upon the addition of avidin (Figure 5b). As biotin binds strongly and irreversibly to avidin, the displacement method using a competitive inhibitor for probe **1** would not be viable for probe **2**.

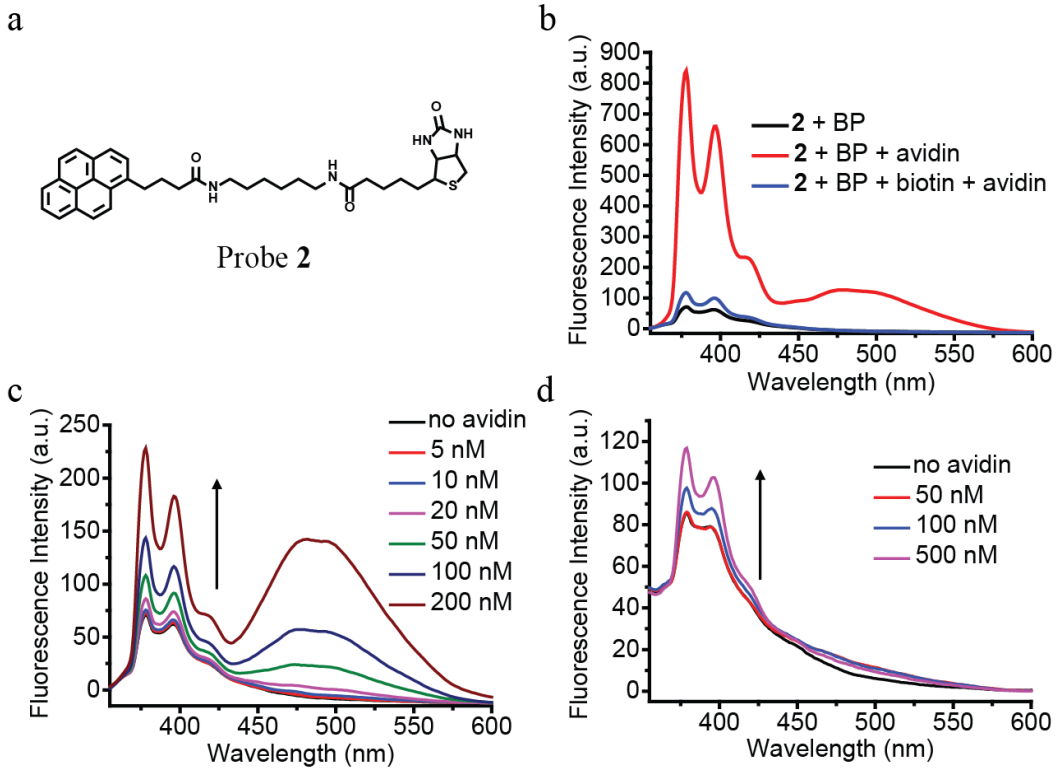

Figure 3.5: (a) Chemical structure of probe **2**. (b) Fluorescence spectra of probe **2** (1 μM) and benzophenone (5 mM) in Brij 35 (1 mM) solution treated without or with avidin (1 μM) or with avidin (1 μM) and biotin (20 μM). Fluorescence spectra of probe **2** (1 μM) and benzophenone (5 mM) treated with different concentrations of avidin in (c) Brij 35 (1 mM) solution; (d) PEG-dodecyl random copolymer (1 mg/mL) solution. All experiments were done in Tris buffer solution (25 mM, pH 7.4). All spectra were taken after 3-hour protein incubation at room temperature.

Therefore, to test the recognition-driven dissociation mechanism, a solution of BP-quenched probe **2** in Brij 35 micelles was pre-incubated with 20-fold excess biotin, which

can compete with probe **2** to bind to the protein. As expected, upon exposure to avidin, very little fluorescence enhancement was observed for above solution compared to the one without the free biotin ligand (Figure 5b). Interestingly, in addition to the increase in the monomeric pyrene emission peak, a new peak appears around 485 nm, which correspond to the pyrene excimer emission. Since high fluorophore concentration is required for excimer formation, we attribute this to the tetravalent binding sites of avidin and possible hydrophobic association. Probe **2** is capable of detecting avidin concentration even at 5 nM concentrations (Figure 5c), likely due to the high binding affinity of biotin avidin interaction. To further demonstrate the generality of this sensing strategy, we also showed that probe **2** can also be used to detect avidin using the random copolymer micelles (Figure 5d).

3.3 Summary

In summary, we have developed a new supramolecular dissociation based sensing strategy to detect specific proteins with turn-on fluorescence signals. The sensing approach is based on non-covalent encapsulation of ligand-tethered fluorophore/ quencher pair in the micellar assemblies, where the fluorescence is in the 'off' state. Protein-binding induced dissociation of the ligand-fluorophore combination away from micelle turns the fluorescence to the 'on' state, since its proximity with the quencher is compromised. The versatility of this approach lies in its simplicity: (*i*) well-established and commercially available surfactants can be used; (*ii*) other than being hydrophobic, the fluorophore-ligand combination does not have to exhibit inherent self-assembly features and therefore does not require extensive molecular design; (*iii*) the strategy is conveniently extendable to any fluorophore-quencher combinations to modulate the colour of detection; and (*iv*) the

approach is potentially extendable to most target protein analytes. Overall, we anticipate that the design principle has the potential to open up fundamentally new avenues in supramolecular chemistry for generation of fluorescent signal or even other spectroscopic signals in response to specific protein-ligand recognition events.

3.4 Experimental

3.4.1 Materials and Methods

All chemicals and reagents were purchased from commercial sources and were used as received, unless otherwise mentioned. ^{1}H NMR spectra were recorded on a 400 MHz Bruker NMR spectrometer using the residual proton resonance of the solvent as the internal standard. Chemical shifts are reported in parts per million (ppm). ^{13}C NMR spectra were proton decoupled and recorded on a 100 MHz NMR spectrometer using the carbon signal of the deuterated solvent as the internal standard. Molecular weights of the polymers were estimated by gel permeation chromatography (GPC) using PMMA standard with a refractive index detector. Fluorescence spectra were obtained from a JASCO FP-6500 spectrofluorometer. UV-visible absorption spectra were collected using a Cary 100 spectrophotometer.

3.4.2 Synthetic Schemes and Procedures

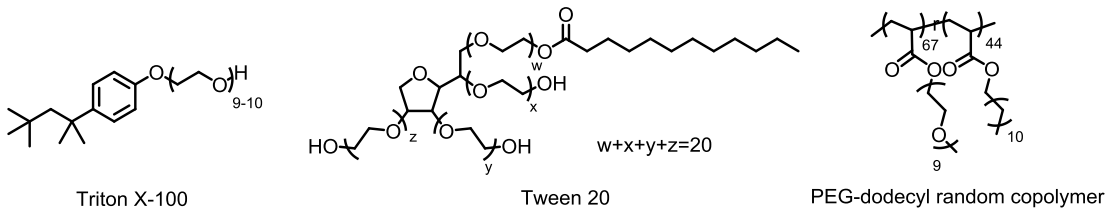

Triton X-100 Tween 20 PEG-dodecyl random copolymer

Chart 3.1: Structure of surfactants and amphiphilic polymer used to form micelles.

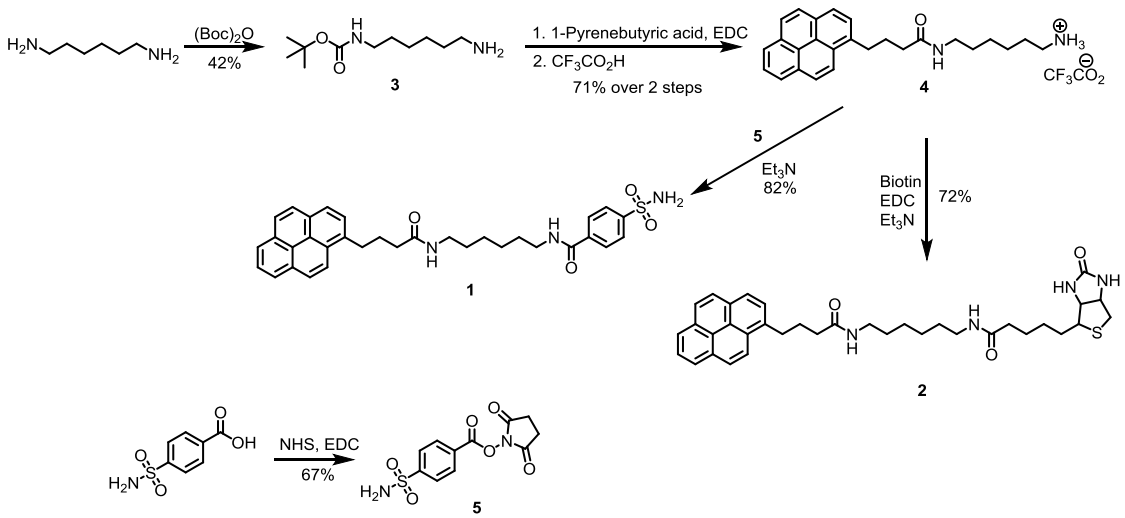

Scheme 3.1: Synthesis of Probe **1** and **2**.

Synthesis of *N*-Boc-hexamethylenediamine (3)

Di-*tert*-butyl dicarbonate (4.0 g, 18.4 mmol) was dissolved in chloroform and added drop-wise to a solution of hexamethylenediamine (10.6 g, 91.6 mmol) in chloroform at 0 °C. The mixture was allowed to warm to room temperature. After stirring for 12 hours, the reaction crude was filtered and washed with chloroform. The filtrates were collected and solvent was evaporated. The residue was re-dissolved in ethyl acetate and washed with water and then brine. The organic solution was dried over anhydrous Na_2SO_4, filtered and concentrated under reduced pressure to afford 1.68 g (42%) *N*-Boc-hexamethylenediamine. ^{1}H NMR (400MHz, $CDCl_3$) δ: 4.52 (bs, 1H), 3.10 (q, *J* = 6.6 Hz, 2H), 2.68 (t, *J* = 7.0 Hz, 2H), 1.49-1.30 (m, 17H), 1.25 (t, *J* = 7.2 Hz, 2H); ^{13}C NMR (100 MHz, $CDCl_3$) δ: 156.1, 79.1, 42.2, 40.5, 33.8, 30.2, 28.4, 26.7, 26.6.

Synthesis of compound 4

To a solution of 1-pyrenebutyric acid (1.0 g, 3.5 mmol) in dry tetrahydrofuran was added N-(3-dimethylaminopropyl)-N'-ethylcarbodiimide hydrochloride (EDC) (0.80 g,

4.2 mmol) at ice bath temperature. The mixture was allowed to stir for 30 min, then *N*-Boc-hexamethylenediamine (0.90 g, 4.2 mmol) was added at the same temperature. The reaction mixture was stirred for 12 hours at room temperature. Tetrahydrofuran was evaporated and the residue was re-dissolved in ethyl acetate and washed with 1M HCl aqueous solution and then brine. The organic layer was dried over anhydrous Na_2SO_4 and evaporated to dryness. The crude product was purified by silica gel column chromatography using mixture of dichloromethane/methanol as eluent to yield the N-boc protected pyrene. To deprotect the N-boc amine functionality, the purified compound was dissolved in 10 mL 1:1 v/v dichloromethane/trifluoroacetic acid mixture. After stirring at room temperature for 2 h, solvent mixture was removed by evaporation, and the residue was rinsed two times with diethyl ether. The resultant precipitate was collected and dried in vacuo to yield 1.2 g (71%) of compound **4**. ^{1}H NMR (400MHz, CD_3OD) δ: 8.35-7.88 (m, 9H), 3.37 (t, *J* = 7.7 Hz, 2H), 3.18 (t, *J* = 7.0 Hz, 2H), 2.87 (t, *J* = 7.6 Hz, 2H), 2.35 (t, *J* = 7.3 Hz, 2H), 2.16 (quin, *J* = 7.6 Hz, 2H), 1.61 (quin, *J* = 7.5 Hz, 2H), 1.51 (quin, *J* = 6.7 Hz, 2H), 1.38-1.37 (m, 4H); ^{13}C NMR (100 MHz, CD_3OD) δ: 175.8, 137.2, 132.7, 132.2, 131.3, 129.8, 128.5, 128.4, 128.3, 127.6, 126.9, 126.2, 126.0, 125.9,125.9, 125.8, 124.3, 40.5, 40.1, 36.8, 33.8, 30.1, 29.1, 28.4, 27.3, 26.9.

Synthesis of 4-sulfamoylbenzoic acid-NHS (5)

To a solution of 4-sulfamoylbenzoic acid (1.0 g, 5.0 mmol) in dry tetrahydrofuran was added N-hydroxysuccinimide (0.69 g, 6.0 mmol) and cooled to ice bath temperature. Then EDC (1.15 g, 6.0 mmol) was added at the same temperature. The reaction mixture was stirred for 12 hours at room temperature. Tetrahydrofuran was evaporated and the residue was re-dissolved in ethyl acetate and washed with saturated $NaHCO_3$ aqueous

solution and then brine. The organic solution was dried over anhydrous Na_2SO_4, filtered and concentrated in vacuo to yield 1.0 g (67%) of 4-sulfamoylbenzoic acid-NHS. ^{1}H NMR (400MHz, Acetone-d_6) δ: 8.32-8.29 (m, 2H), 8.15-8.12 (m, 2H), 6.91 (bs, 2H), 2.99-2.98 (m, 4H); ^{13}C NMR (100 MHz, Acetone-d_6) δ: 170.4, 161.9, 150.6, 131.7, 129.0, 127.7, 26.3.

Synthesis of probe 1

To a solution of compound **4** (0.31 g, 0.75 mmol) in dry tetrahydrofuran was added 4-sulfamoylbenzoic acid-NHS (0.25 g, 0.83 mmol) and triethylamine (0.23 g, 2.3 mmol). The reaction mixture was heated for 6 h at 50 ^{o}C. Products precipitated out during the course of reaction. The reaction mixture was concentrated in vacuo and the crude product was purified by silica gel column chromatography using mixture of dichloromethane/methanol as eluent to yield 0.35 g (82%) of probe **1**. ^{1}H NMR (400MHz, DMSO-d_6) δ: 8.61 (t, J = 5.4 Hz, 1H), 8.38-7.86 (m, 13H), 7.81 (t, J = 5.5 Hz, 1H), 7.46 (s, 2H), 3.31 (t, J = 8.3 Hz, 2H), 3.27-3.22 (m, 2H), 3.08-3.04 (m, 2H), 2.22 (t, J = 7.1 Hz, 2H), 2.01 (quin, J = 7.5 Hz, 2H), 1.51 (quin, J = 7.2 Hz, 2H), 1.41 (quin, J = 6.2 Hz, 2H), 1.31-1.29 (m, 4H); ^{13}C NMR (100 MHz, DMSO-d_6) δ: 172.5, 165.6, 146.3, 137.9, 136.8, 131.2, 130.7, 129.6, 128.4, 128.1, 127.8, 127.8, 127.6, 126.8, 126.5, 125.9, 125.9, 125.3, 125.1, 124.5, 124.4, 123.7, 38.7, 35.4, 32.4, 29.3, 29.2, 27.9, 26.4; HRMS (ESI) calculated for $C_{33}H_{35}N_3O_4S$ 569.23, found 592.23 (M+Na).

Synthesis of probe 2

Biotin (0.083 g, 0.34 mmol) was dissolved in dry dimethylformamide heated at 50 ^{o}C and then allowed to cool to RT. To the above-obtained biotin solution was added EDC (0.098 g, 0.51 mmol) and stirred at RT for 1h. To this mixture was added solution of

compound **4** (0.17 g, 0.34 mmol) and triethylamine (0.069 g, 0.68 mmol) in dry dimethylformamide and stirred for 12h. The crude product was precipitated by pouring the reaction mixture into a large volume of diethyl ether. The precipitates were collected and purified by silica gel column chromatography using mixture of dichloromethane/methanol as eluent to yield 0.15 g (72%) of probe **2**. ^{1}H NMR (400MHz, DMSO-d_6) δ: 8.39-7.93 (m, 9H), 7.81 (t, J = 5.6 Hz, 1H), 7.72 (t, J = 5.7 Hz, 1H), 6.41 (s, 1H), 6.35 (s, 1H), 4.28-4.25 (m, 1H), 4.09-4.07 (m, 1H), 3.31 (t, J = 8.3 Hz, 2H), 3.07-2.97 (m, 5H), 2.78 (dd, J_1 = 5.1 Hz, J_2 = 12.4 Hz, 1H), 2.56 (d, J = 12.4 Hz, 1H), 2.22 (t, J = 7.1 Hz, 2H), 2.04-1.97 (m, 4H), 1.62-1.23 (m, 14H); ^{13}C NMR (100 MHz, DMSO-d_6) δ: 172.1, 171.9, 162.9, 136.7, 131.0, 130.5, 129.4, 128.3, 127.7, 127.6, 127.4, 126.6, 126.3, 125.1, 124.9, 124.3, 124.3, 123.6, 61.2, 59.3, 55.6, 55.1, 38.5, 38.4, 35.3, 35.2, 32.4, 29.2, 29.2, 28.3, 28.1, 27.7, 26.3, 26.3, 25.5; HRMS (FAB+) calculated for $C_{36}H_{44}N_4O_3S$ 612.31, found 613.31 (M+H).

Synthesis of PEG-dodecyl random copolymer

A mixture of cyanomethyl dodecyl trithiocarbonate (6.6 mg, 0.021 mmol), lauryl acrylate (200 mg, 0.83 mmol), poly(ethylene glycol) methyl ether acrylate (M_n = 480) (600 mg, 1.25 mmol) and AIBN (0.68 mg, 0.0042 mmol) was dissolved in toluene (1.5 mL) and degassed by performing three freeze-pump-thaw cycles. The reaction mixture was sealed and then heated with a pre-heated oil bath at 65 °C for 48 h. The resultant mixture was precipitated twice in diethyl ether to remove unreacted monomers and initiators. ^{1}H NMR (400MHz, $CDCl_3$) δ: 4.27-4.07, 4.07-3.85, 3.62-3.55, 3.37, 2.45-2.01, 1.94-1.78, 1.70-1.52, 1.34-1.18; GPC (THF) M_n: 42800 Da. PDI: 1.3.

3.4.3 Encapsulation of Probe/Quencher in Micellar Solutions

To a 970 μL solution of surfactants or polymer in Tris buffer (25 mM, pH = 7.4)

was slowly added 10 µL (100 µM) solution of probe in dimethyl sulfoxide (DMSO), followed by 10 µL (500 µM) solution of benzophenone (BP) in DMSO under vigorously stirring. The mixture was allowed to stir for 30 min at room temperature and then filtered through a filter with a pore size of 0.22 µm to remove excess BP that was not encapsulated. Excess BP was needed to minimize the background signal.

3.4.4 Protein Detection Procedures

To a 990 µL solution of probe/BP or pyrene/BP encapsulated micelles in Tris buffer (25 mM, pH = 7.4) was added 10 µL (0 – 500 µM) solution of proteins in Tris buffer (25 mM, pH = 7.4). The mixture was incubated for 3 hours at room temperature before the emission spectrum of pyrene was recorded (λ_{ex} = 345 nm, the excitation and emission band widths were set to 3 and 3 nm respectively and the scanning speed was 500 nm/min).

3.4.5 Supporting Figures

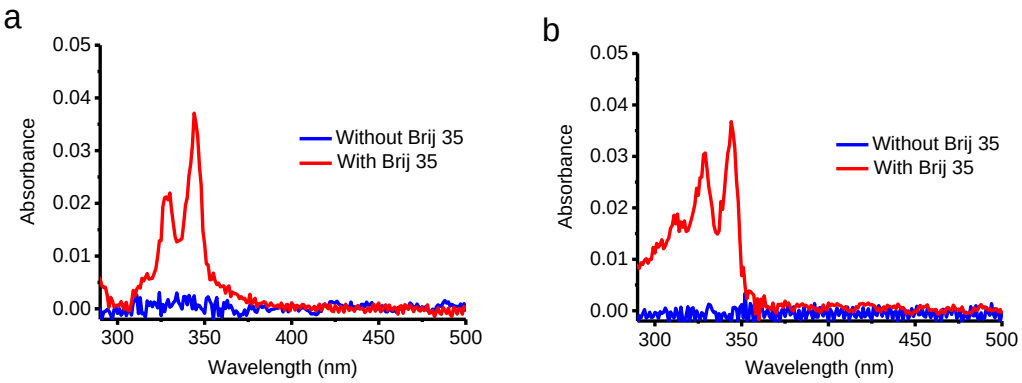

Figure 3.6: Absorption spectra of probes (1 µM) in Tris buffer solutions with or without Brij 35 (1 mM): (a) probe **1**; (b) probe **2**.

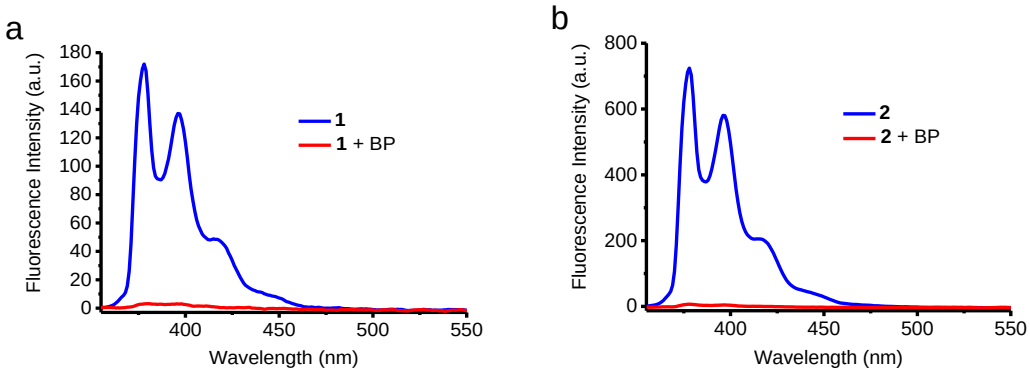

Figure 3.7: Fluorescence spectra of probes (1 μM) and Brij 35 (1 mM) in Tris buffer with or without BP (5 mM): (a) probe **1**; (b) probe **2**. (λ_{ex} = 345 nm, the excitation and emission band width were 1 and 3 nm respectively and the scanning speed was 500 nm/min).

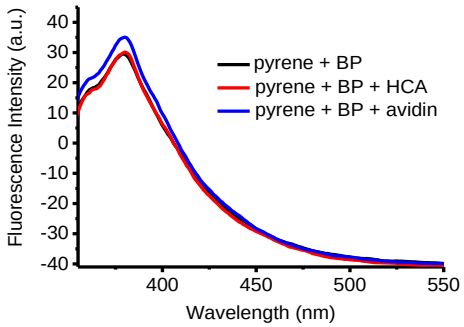

Figure 3.8: Fluorescence spectra of pyrene (1 μM), BP (5 mM), and Brij 35 (1 mM) in Tris buffer (25 mM, pH 7.4) treated with HCA (5 μM) or avidin (1 μM) (λ_{ex} = 335 nm for pyrene).

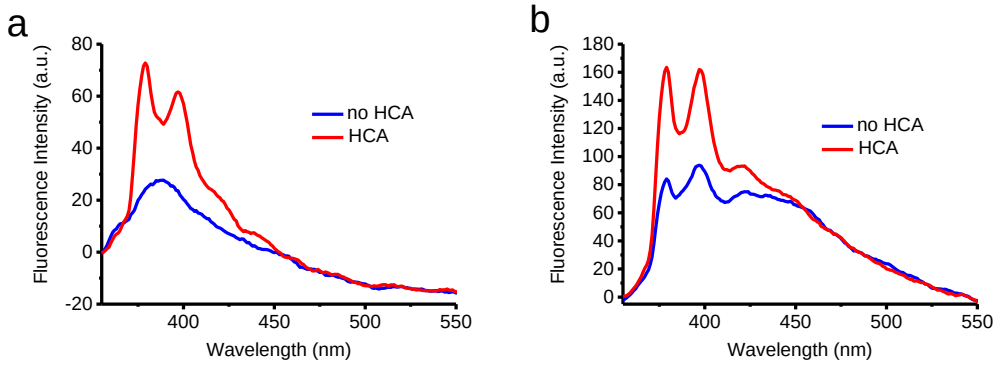

Figure 3.9: Fluorescence spectra of probe **1** (1 μM), BP (5 mM), and Brij 35 (1 mM) treated with or without HCA (1 μM): (a) in Tris buffer solution; (b) in 50% fetal bovine serum in Tris buffer solution.

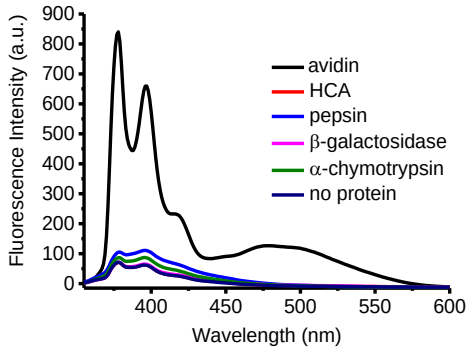

Figure 3.10: Fluorescence spectra of probe **2** (1 μM), BP (5 mM), and Brij 35 (1 mM) in Tris buffer treated with different proteins (1 μM).

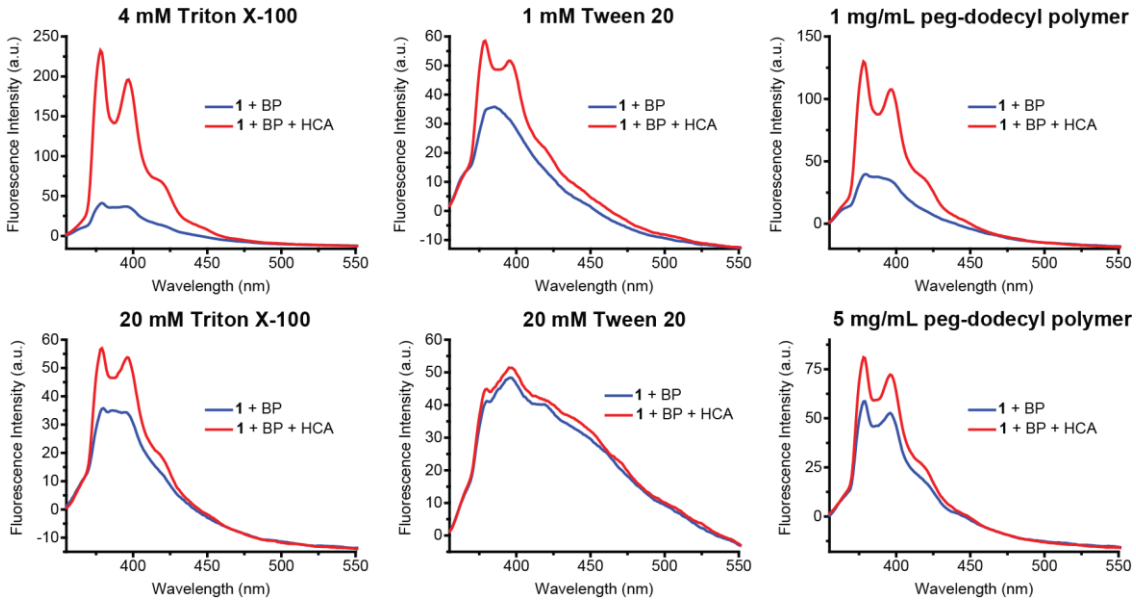

Figure 3.11: Fluorescence spectra of probe **1** (1 μM) and BP (5 mM) without or with 5 μM HCA in different concentrations of surfactants or amphiphilic polymer.

3.5 References

1. Albert, K. J.; Lewis, N. S.; Schauer, C. L.; Sotzing, G. A.; Stitzel, S. E.; Vaid, T. P.; Walt, D. R. Cross-Reactive Chemical Sensor Arrays. *Chem. Rev.* **2000**, *100*, 2595–2626.

2. Adams, M.; Joyce, L.; Anslyn, E. V. *Supramolecular Chemistry: From Molecules to Nanomaterials*; Gale, P. A.; Steed, J. W., Eds.; Wiley: Chichester, 2012, Vol. 2, pp.709–732.

3. Gutiérrez, J.; Horrillo, M. C. Advances in Artificial Olfaction: Sensors and Applications. *Talanta* **2014**, *124*, 95–105.

4. You, L.; Zha, D.; Anslyn, E. V. Recent Advances in Supramolecular Analytical Chemistry Using Optical Sensing. *Chem. Rev.* **2015**, *115*, 7840–7892.

5. You, C.-C.; Miranda, O. R.; Gider, B.; Ghosh, P. S.; Kim, I.-B.; Erdogan, B.; Krovi, S. A.; Bunz, U. H. F.; Rotello, V. M. Detection and Identification of Proteins Using Nanoparticle–Fluorescent Polymer 'Chemical Nose' Sensors. *Nat. Nanotechnol.* **2007**, *2*, 318–323.

6. Sandanaraj, B. S.; Demont, R.; Thayumanavan, S. Generating Patterns for Sensing Using a Single Receptor Scaffold. *J. Am. Chem. Soc.* **2007**, *129*, 3506–3507.

7. Goodwin, S.; Gade, A. M.; Byrom, M.; Herrera, B.; Spears, C.; Anslyn, E. V.; Ellington, A. D. Next-Generation Sequencing as Input for Chemometrics in Differential Sensing Routines. *Angew. Chem. Int. Ed.* **2015**, *54*, 6339–6342.

8. Behr, J. -P. *The Lock-and-Key Principle*; The State of the Art – 100 Years On; John Wiley & Sons: Chichester, U.K., 2008.

9. Ma, X.; Zhao, Y. Biomedical Applications of Supramolecular Systems Based on Host–Guest Interactions. *Chem. Rev.* **2015**, *115*, 7794–7839.

10. Elghanian, R.; Storhoff, J. J.; Mucic, R. C.; Letsinger, R. L.; Mirkin, C. A. Selective Colorimetric Detection of Polynucleotides Based on the Distance-Dependent Optical Properties of Gold Nanoparticles. *Science* **1997**, *277*, 1078–1081.

11. Oh, K. J.; Cash, K. J.; Plaxco, K. W. Excimer-Based Peptide Beacons: A Convenient Experimental Approach for Monitoring Polypeptide−Protein and Polypeptide−Oligonucleotide Interactions *J. Am. Chem. Soc.* **2006**, *128*, 14018–14019.

12. Thurley, S.; Röglin, L.; Seitz, O. Hairpin Peptide Beacon: Dual-Labeled PNA-Peptide-Hybrids for Protein Detection. *J. Am. Chem. Soc.* **2007**, *129*, 12693–12695.

13. Stockwell, B. R. Exploring Biology with Small Organic Molecules. *Nature* **2004**, *432*, 846–854.

14. Kodadek, T.; Reddy, M. M.; Olivos, H. J.; Bachhawat-Sikder, K.; Alluri, P. G. Synthetic Molecules as Antibody Replacements. *Acc. Chem. Res.* **2004**, *37*, 711–718.

15. Takaoka, Y.; Sakamoto, T.; Tsukiji, S.; Narazaki, M.; Matsuda, T.; Tochio, H.; Shirakawa, M.; Hamachi, I. Self-Assembling Nanoprobes that Display Off/On ^{19}F Nuclear Magnetic Resonance Signals for Protein Detection and Imaging. *Nat. Chem.* **2009**, *1*, 557–561.

16. Yoshii, T.; Mizusawa, K.; Takaoka, Y.; Hamachi, I. Intracellular Protein-Responsive Supramolecules: Protein Sensing and In-Cell Construction of Inhibitor Assay System. *J. Am. Chem. Soc.* **2014**, *136*, 16635–16642.

17. Azagarsamy, M.; Yesilyurt, V.; Thayumanavan, S. Disassembly of Dendritic Micellar Containers Due to Protein Binding. *J. Am. Chem. Soc.* **2010**, *132*, 4550–4551.

18. Amado Torres, D.; Garzoni, M.; Subrahmanyam, A.; Pavan, G. M.; Thayumanavan, S. Protein–Triggered Supramolecular Disassembly: Insights Based on Variations in Ligand Location in Amphiphilic Dendrons. *J. Am. Chem. Soc.* **2014**, *136*, 5385–5399.

19. Jiwpanich, S.; Ryu, J. H.; Bickerton, S.; Thayumanavan, S. Noncovalent Encapsulation Stabilities in Supramolecular Nanoassemblies. *J. Am. Chem. Soc.* **2010**, *132*, 10683–10685.

20. Krishnamurthy, V. M.; Kaufman, G. K.; Urbach, A. R.; Gitlin, I.; Gudiksen, K. L.; Weibel, D. B.; Whitesides, G. M. Carbonic Anhydrase as a Model for Biophysical and Physical-Organic Studies of Proteins and Protein-Ligand Binding. *Chem. Rev.* **2008**, *108*, 946–1051.

21. Alterio, V.; Di Fiore, A.; D'Ambrosio, K.; Supuran, C. T.; De Simone, G. Multiple Binding Modes of Inhibitors to Carbonic Anhydrases: How to Design Specific Drugs Targeting 15 Different Isoforms? *Chem. Rev.* **2012**, *112*, 4421–4468.

22. Taylor, P. W.; King, R. W.; Burgen, A. S. V. Kinetics of Complex Formation between Human Carbonic Anhydrases and Aromatic Sulfonamides. *Biochemistry* **1970**, *9*, 2638–2645.

23. Matulis, D.; Kranz, J. K.; Salemme, F. R.; Todd, M. J. Thermodynamic Stability of Carbonic Anhydrase: Measurements of Binding Affinity and Stoichiometry using ThermoFluor. *Biochemistry* **2005**, *44*, 5258–5266.

24. Bandyopadhyay, P.; Ghosh, A. K. Reversible Fluorescence Quenching by Micelle Selective Benzophenone-Induced Interactions between Brij Micelles and Polyacrylic Acids: Implications for Chemical Sensors. *J. Phys. Chem. B* **2010**, *114*, 11462–11467.

25. Krishnamurthy, V. M.; Semetey, V.; Bracher, P. J.; Shen, N.; Whitesides, G. M. Dependence of Effective Molarity on Linker Length for an Intramolecular Protein−Ligand System. *J. Am. Chem. Soc.* **2007**, *129*, 1312–1320.

CHAPTER 4

ACTIVATABLE DENDRITIC ^{19}F PROBES FOR ENZYME DETECTION

4.1 Introduction

Detection and imaging of enzyme activity is of great importance in drug discovery research and medical diagnostics.[1-3] Activatable probes, which induce a signal change in response to a specific stimulus, are promising for imaging enzymatic activity, because they provide high sensitivity and selectivity.[4-5] Most of the activatable probes developed so far are based on fluorescence.[6-11] Low penetration depth, caused by scattering, impose some limitations for fluorescence-based *in vivo* imaging. On the other hand, activatable probes based on NMR spectroscopy are gaining interest, as this is the first indicator that a probe could be viable for magnetic resonance imaging (MRI) based deep-tissue visualization.[12-14] There have been efforts to develop activatable probes for enzymes using gadolinium-based reagents, where the enzyme activity changes the coordination sphere of Gd(III).[13, 15-17] This causes changes in the ^{1}H relaxation times of the bound water molecules providing a magnetic resonance signal. Although several Gd-based reagents are in the clinic, recent concerns over these as causative agents for nephrogenic systemic fibrosis[18, 19] have triggered search for alternate imaging modalities. Fluorine-19 has emerged as a promising NMR-active nucleus for this purpose,[20-24] because of its high isotopic abundance (100%)

and also because fluorine is not naturally found in detectible amounts in physiological fluids. The negligible presence of endogenous ^{19}F endows this strategy with the possibility of high contrast, a critical feature for imaging. Despite its great potential, ^{19}F NMR strategies for specifically detecting enzymatic activities are very limited.[25, 26] In this chapter, we introduce a novel ^{19}F NMR strategy for detecting enzyme activity based on self-assembled facially-amphiphilic dendrons and identify the key structural features that control enzyme-induced signal generation.

4.2 Results and Discussions

4.2.1 Design and Synthesis

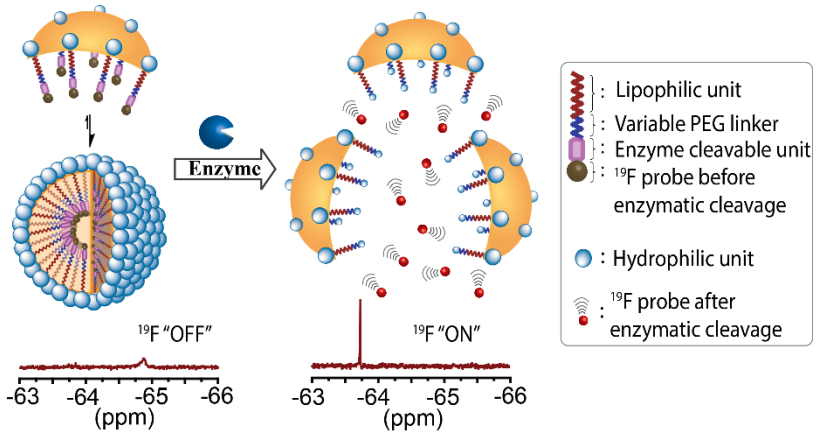

Figure 4.1: Schematic representation of assemblies formed from enzyme cleavable dendrons and the release of 19F reporter upon enzyme exposure.

Our approach is schematically shown in Figure 1, which is based on self-assembling facially amphiphilic dendrons.[27-32] In this study, these dendrons are designed such that the fluorine-bearing hydrophobic functionalities are buried within the interior of the amphiphilic aggregate. However, the ability of these dendrons to aggregate would be compromised, when an enzymatic reaction alters the hydrophilic-lipophilic balance of the dendron. We hypothesize that this transformation will provide a significant change in the

magnetic resonance behavior of the fluorine nuclei, since the transverse (T_2) relaxation in NMR is very sensitive to molecular weight.[33] The formation of a large molecular assembly from the facially amphiphilic dendron would then cause severe broadening and attenuation of the ^{19}F signal. As shown in Figure 1, the dendrons are designed such that the specific enzymatic reaction would release a small molecule that gives rise to a sharp and intense signal.

Binding-induced deaggregation strategies have been previously attempted for sensing and imaging.[24, 30] However, reactivity based strategies targeted here provide an additional challenge. The key functional groups that are responsible for signal generation, *i.e.* the substrate functionalities for the enzyme, are buried in the interior of a large aggregate.[29, 34] It is critical that enzymes have access to these substrates, yet it is also important that the molecules exist mostly in the aggregate form in order to provide a fully turned-off signal, prior to encountering the enzyme. We chose dendritic scaffolds, because they provide a unique opportunity to address this challenge.[35-41] Dendrimers have the advantage of providing low critical aggregation concentrations, similar to those observed with polymers, but provide the molecular weight control seen in small molecules.[42-45] In addition, dendrimers also afford a high degree of control over functional group placements within a macromolecule.[46-51] These features allow for understanding the fundamental structural dependencies in sensitive signal generation, induced by specific enzymatic triggers.

To test our design hypothesis, we synthesized dendron **1** containing three 3,5-bis(trifluoromethyl)phenyl moieties as a hydrophobic side chain in the dendron (Figure 2). Each of these functional groups carries six magnetically equivalent ^{19}F nuclei.

Pentaethylene glycol unit was used as the hydrophilic unit, as these charge-neutral functionalities do not exhibit non-specific interactions with proteins and enzymes. An ester functionality was installed as the enzyme-cleavable substrate. In the absence of target enzyme, dendron **1** self-assembles into a large aggregate, which results in very weak and broad ^{19}F signal. Upon exposure to porcine liver esterase (PLE), the enzymatic reaction should cleave the ester bond to liberate 3,5-bis(trifluoromethyl)benzoic acid. Indeed, when **1** (25 μM) was dissolved in a buffer solution, a weak and broad ^{19}F NMR signal was observed initially (Figure 2b). However, a sharp signal appeared at -63.7 ppm upon addition of PLE (1 μM). This sharp and strong ^{19}F signal, obtained in the reaction mixture, is indicative of the formation of the small molecule.

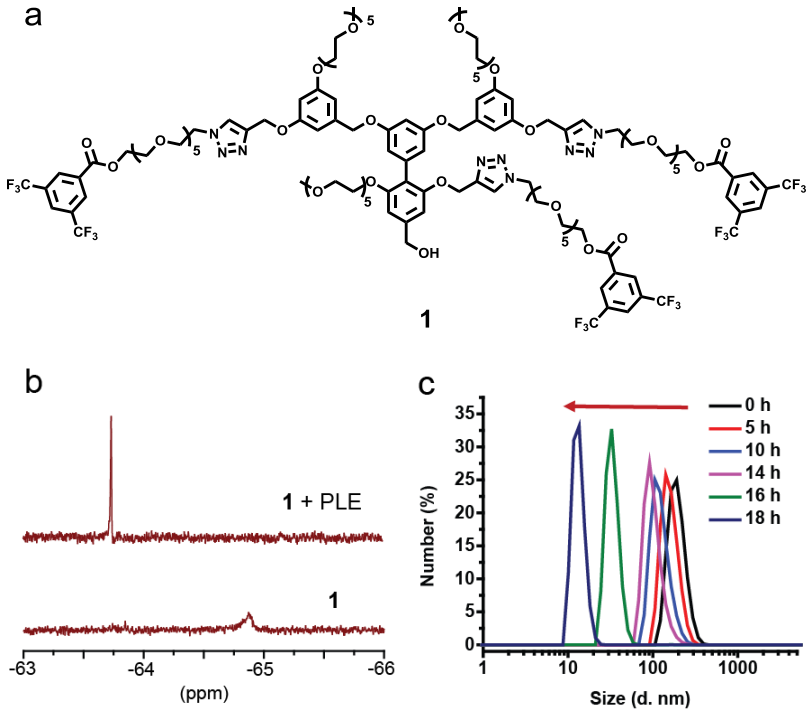

Figure 4.2: (a) Chemical structure of enzyme cleavable dendron **1**. (b) ^{19}F NMR spectra of **1** (25 μM) in the presence or absence of PLE (1 μM) (TFA as an internal standard for chemical shift). (c) Size evolution of **1** (25 μM) in the presence of PLE (1 μM) using DLS.

To further validate the potential of this specific enzyme-responsive signal

enhancement in the context of its ultimate use in MRI applications, we attempted to measure t_2 relaxation time of the sharp signal and found a value of 1.3 sec, which is typical for small molecules. This underlines the extent of signal generation in the presence of enzyme and very low background signal in the absence of the enzyme. Furthermore, we also determined that the ^{19}F signal intensity is proportional to PLE concentration and that the detection limit is 1 nM PLE (Figure 3b). In addition to the generation of the fluorine-containing small molecule, the enzymatic reaction also cleaves the most hydrophobic part of the amphiphilic dendron. This modification changes the hydrophilic-lipophilic balance of the dendron and converts it to a much more hydrophilic one. This should cause the size of the assembly to change significantly. We used dynamic light scattering to measure the size change of the dendron before and after enzyme incubation. The assembly size of **1** (25 μM) alone was ~200 nm (Figure 4). However, the size decreases systematically over time upon addition of PLE (1 μM) (Figure 2c), validating the enzyme-induced disassembly of the aggregates.

4.2.2 Dendron without an Enzyme Substrate

To further confirm that ^{19}F signal and the disassembly were indeed caused by the enzymatic hydrolysis of ester functionalities, we synthesized a structurally similar dendron (Chart 1), **2**, in which ester moieties were replaced by amides. Since PLE should not be able to cleave an amide bond, we anticipated that neither the ^{19}F signal nor the assembly size of dendron **2** would be affected by PLE. Indeed, no new ^{19}F signal appeared and the assembly size stayed the same after dendron **2** (25 μM) was incubated with PLE (1 μM) (Figure 5). Similarly, to determine whether the signal generation is specific to PLE, we exposed dendron **1** (25 μM) to four additional proteins (1 μM) with varying pI values, *viz.*

myoglobin (pI 7.2), hemoglobin (pI 6.8), avidin (pI 10.5), and pepsin (pI 1.0). As expected, none of these proteins showed any ^{19}F signal generation (Figure 6), underlining the specificity of this dendron probe to only the target enzyme.

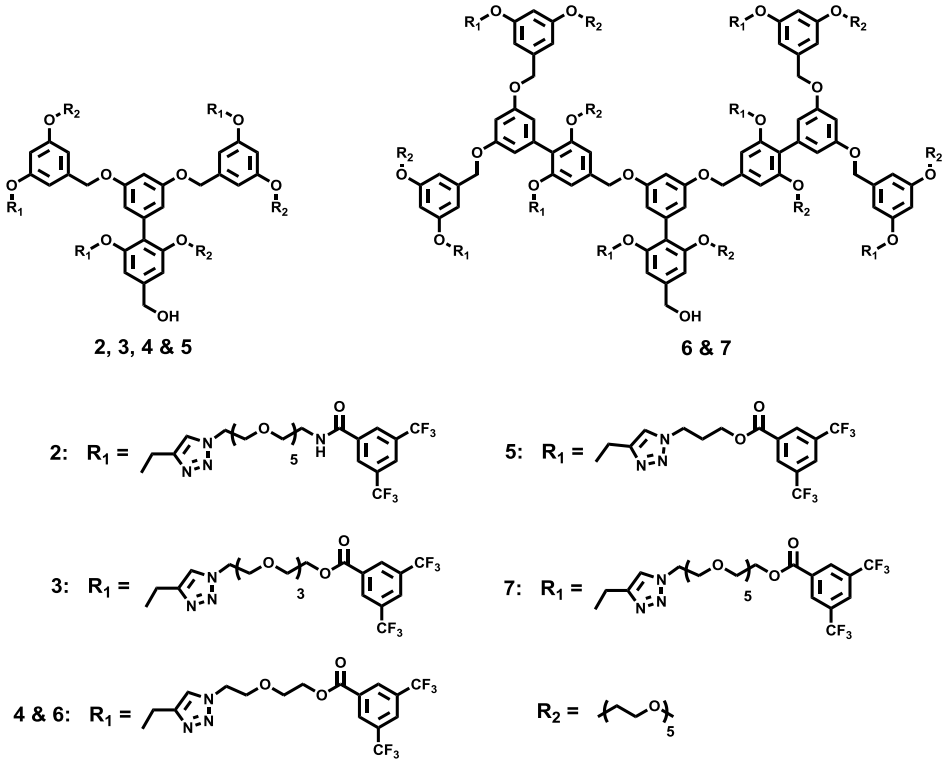

Chart 4.1: Structures of ^{19}F-containing amphiphilic dendrons.

4.2.3 Effect of Dendron HLB on Probe Response Time

If the enzyme-induced deaggregation were correct, then it is critical that the enzyme has access to the ester moiety that is buried in the hydrophobic interior of the aggregate. We hypothesize that it is the unimer-aggregate equilibrium that provides the pathway for the enzymatic access to the substrate moiety and the ensuing deaggregation. To test this hypothesis and thus provide the molecular design guidelines for optimal sensitivity, we evaluated the effect of modulating the hydrophilic-lipophilic balance of the dendron upon the response time in signal generation. Dendrons **3-7** were synthesized to test these

possibilities (Chart 1). First of all, note that dendron **1** contains oligoethyleneglycol moiety on both faces of the dendron with the presence of the bis(trifluoromethyl)phenyl moiety as the key difference between the more hydrophilic and hydrophobic faces of the dendron. When we utilized the more classical hydrophobic linker, as shown in **5**, no signal was generated even after 8 hours. A signal was indeed observed after incubation of the enzyme for 4 days (Figure 7), which suggests that the esterase induced signal generation is indeed possible, but is very slow. This observation is likely due to the increased hydrophobicity of the dendron, which makes the unimer state of the dendron less available. This is consistent with our mechanistic hypothesis.

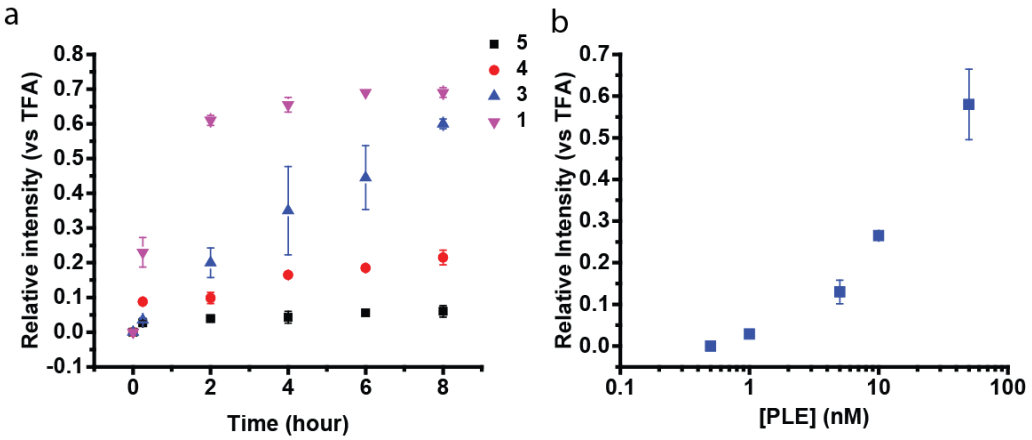

Figure 4.3: (a) Temporal evolution of ^{19}F NMR intensity (-63.7 ppm) of G1 dendrons (25 μM) treated with PLE (1 μM) over the first 8 hours. (b) Dependence of the ^{19}F NMR intensity (-63.7 ppm) on PLE concentration for dendron **1** (25 μM) (Measurements taken after 24 hour PLE incubation). All experiments were performed in 25 mM Tris buffer (pH 7.4, 0.2 mM TFA as an internal standard for peak intensity and chemical shift, 10% D_2O (v/v)) at 25 ºC.

To further test this, we studied dendrons **3** and **4**, where the length of oligoethylene glycol unit side chain was systematically changed compared to that in **1**. These dendrons were incubated with PLE and the temporal evolution of the ^{19}F NMR signal was monitored. As expected, the dendron **1** has the fastest signal evolution, where the signal was saturated

in just 6 hours. Signal evolution from dendron **3** was slower than that from **1**, but faster than that from **4** (Figure 3a). The size evolution of each of these dendrons was also monitored by DLS (Figure 8). Upon incubation with PLE, the assembly size of **3** reduced from ~200 nm to ~30 nm after 17 hours. The size reduction of **4** was slower compared to that of **3** and **1**; it took ~26 hours to reach 30 nm. As anticipated, the aggregate size of dendron **5** reduced only slightly even after 96 hours. All these results are consistent with our mechanistic hypothesis that the signal generation relies on the hydrophilic lipophilic balance of the dendron, which likely affects the unimer-aggregate equilibrium based activation.

4.2.4 Effect of Dendron Generation on Probe Response Time

Finally, we investigated generation-dependence upon the probe response time. G2 dendrons are potentially more sensitive than G1 dendrons as the number of ^{19}F nuclides per dendron unit is more than twice the amount in G1 dendrons. However, similar to increased hydrophobicity causing the equilibrium concentration of the unimer to be smaller, we also anticipated that the unimer equilibrium concentration in G2 dendrons are smaller than that of G1 dendrons. This expectation is based on previous observations that higher generation dendrons exhibit longer residence time in an aggregate, compared to lower generation dendrons.[52] Accordingly, we tested G2 dendrons **6** and **7**. No signal generation was observed for these dendrons, even after PLE incubation for 4 days (Figure 7).

4.3 Summary

In summary, we have shown that: (*i*) by incorporating fluorine-containing hydrophobic units within amphiphilic aggregates of facially amphiphilic dendrons, the ^{19}F-

NMR signal can be made weak and broad; (*ii*) enzyme-induced cleavage of the fluorinated moiety results in the spontaneous generation of a strong and sharp signal; (*iii*) the signal generation is specific to the enzyme for which the linker is engineered; (*iv*) the equilibrium concentration of the unimer in the unimer-aggregate equilibrium plays a key role in the kinetics of signal generation; (*v*) the dendron probe is capable of detecting enzyme concentrations in the nanomolar range. The activatable probe described here and the structural factors that control the signal generation are sufficiently general that this method can be conveniently elaborated to other enzymes. With the increasing potential for the development of ^{19}F MRI for clinical applications, activity-based imaging would play an important future role. Our findings here constitute a promising step for such imaging applications. In combination with the fact that these dendrons are capable of sequestering other guest molecules, these molecules can also be expanded to theranostic applications.

4.4 Experimental

4.4.1 Materials and Methods

^{1}H-NMR spectra were recorded on a 400 MHz Bruker NMR spectrometer using the residual proton resonance of the solvent as the internal standard. Chemical shifts are reported in parts per million (ppm). ^{13}C NMR spectra were proton decoupled and recorded on a 100 MHz NMR spectrometer using the carbon signal of the deuterated solvent as the internal standard. ^{19}F-NMR spectra were collected on a 300 MHz Bruker NMR spectrometer using the fluorine signal of trifluoroacetic acid as the internal standard. MALDI mass spectra data were obtained at the University of Massachusetts mass spectrometry center. Dynamic light scattering (DLS) were determined by Nano-ZS (Malvern Instrument) Zetasizer. Transmission electron microscopy (TEM) images were

taken from JEOL JEM-2000FX. All chemicals and reagents were purchased from commercial sources and were used as received, unless otherwise mentioned. Compounds **13-14** were prepared according to previously reported procedures.[45]

4.4.2 Synthetic Schemes and Procedures

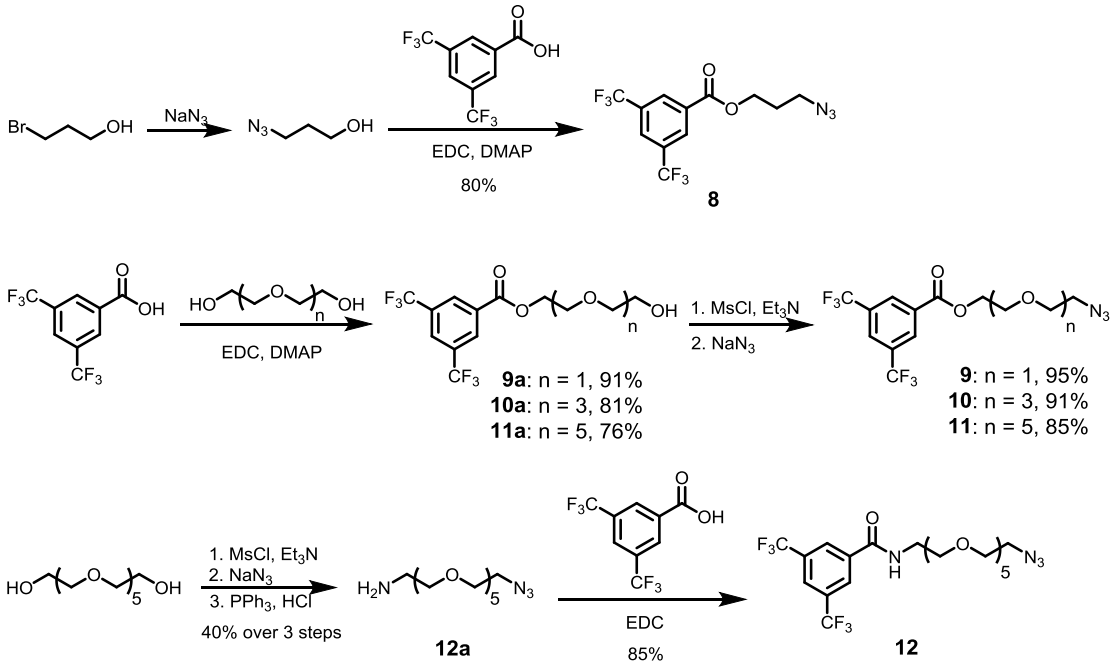

Scheme 4.1: Synthesis of azido compounds (**8-12**).

Synthesis of compound 8:

To a solution of 3-bromo-1-propanol (1.0 g, 7.2 mmol) in water was added sodium azide (1.5 g, 21.6 mmol) at room temperature and stirred for 24 hours at 80 ^{o}C. The reaction mixture was cooled to room temperature and extracted twice with dichloromethane. Combined organic extracts were dried over anhydrous Na_2SO_4 and evaporated to dryness. The crude product **8a** was taken for next step without further purification.

To a solution of 3,5-bis(trifluoromethyl)benzoic acid (0.59 g, 2.3 mmol) in dry

dichloromethane was added **8a** (0.23 g, 2.3 mmol) and cooled to ice bath temperature. Then N-(3-dimethylaminopropyl)-N'-ethylcarbodiimide hydrochloride (0.65 g, 3.4 mmol) and 4-(dimethylamino)pyridine (0.028 g, 0.23 mmol) were added at the same temperature. The reaction mixture was stirred for 2 hours at room temperature. Distilled water was added to the reaction mixture and extracted twice with dichloromethane. Combined organic layers were dried over anhydrous Na_2SO_4 and evaporated to dryness. The crude product was purified by silica gel column chromatography using mixture of ethyl acetate/hexane as eluent to yield 0.62g (80%) of compound **8**. ^{1}H NMR (400MHz, $CDCl_3$) δ: 8.48 (s, 2H), 8.08 (s, 1H), 4.51 (t, J = 6.3 Hz, 2H), 3.50 (t, J = 6.6 Hz, 2H), 2.13-2.07 (m, 2H); ^{13}C NMR (100 MHz, $CDCl_3$) δ: 163.9, 132.4 (q, J_{C-F} = 33.9 Hz), 132.3, 129.9, 129.8, 126.7-126.6 (m), 123.0 (q, J_{C-F} = 271.4 Hz), 63.3, 48.3, 28.2.

Synthesis of compound 9a, 10a and 11a:

To a solution of 3,5-bis(trifluoromethyl)benzoic acid (1.0 g, 3.9 mmol) in dry dichloromethane was added 5 equivalents of oligoethylene glycol (di, tetra, hexa) and cooled to ice bath temperature. Then N-(3-dimethylaminopropyl)-N'-ethylcarbodiimide hydrochloride (1.1 g, 5.8 mmol) and 4-(dimethylamino)pyridine (0.047 g, 0.39 mmol) were added at the same temperature. The reaction was complete in 2 hours, monitored by TLC. Dichloromethane was added to the reaction mixture and washed with distilled water. The organic layer was dried over anhydrous Na_2SO_4 and evaporated to dryness. The crude product was purified by silica gel column chromatography using mixture of dichloromethane/methanol as eluent.

*Compound **9a***, 91%. ^{1}H NMR (400MHz, $CDCl_3$) δ: 8.50 (s, 2H), 8.07 (s, 1H), 4.59-4.57 (m, 2H), 3.89-3.86 (m, 2H), 3.77 (t, J = 4.8 Hz, 2H), 3.67-3.65 (m, 2H), 2.00 (bs, 1H). ^{13}C

NMR (100 MHz, $CDCl_3$) δ: 164.1, 132.4 (q, J_{C-F} = 33.9 Hz), 132.3, 130.0, 130.0, 126.6-126.5 (m), 123.0 (q, J_{C-F} = 271.3 Hz), 72.6, 69.0, 65.2, 61.9.

*Compound **10a***, 81%. ^{1}H NMR (400MHz, $CDCl_3$) δ: 8.50 (s, 2H), 8.05 (s, 1H), 4.57-4.54 (m, 2H), 3.87-3.84 (m, 2H), 3.72-3.62 (m, 10H), 3.59-3.56 (m, 2H), 2.53 (s, 1H); ^{13}C NMR (100 MHz, $CDCl_3$) δ: 164.1, 132.4, 132.2 (q, J_{C-F} = 33.9 Hz), 130.0, 130.0, 126.5-126.4 (m), 123.0 (q, J_{C-F} = 271.0 Hz), 72.6, 70.7, 70.6, 70.3, 69.0, 65.1, 61.7.

*Compound **11a***, 76%. ^{1}H NMR (400MHz, $CDCl_3$) δ: 8.50 (s, 2H), 8.07 (s, 1H), 4.57-4.54 (m, 2H), 3.88-3.85 (m, 2H), 3.73-3.59 (m, 20H), 2.37 (bs, 1H). ^{13}C NMR (100 MHz, $CDCl_3$) δ: 164.0, 132.4, 132.2 (q, J_{C-F} = 33.8 Hz), 130.0, 130.0, 126.5-126.3 (m), 122.9 (q, J_{C-F} = 271.2 Hz), 72.7, 70.7, 70.7, 70.4, 69.1, 65.3, 61.2.

Synthesis of compound 9, 10 and 11:

To a solution of oligoethylene glycol mono(3,5-bis(trifluoromethyl)benzoate) (**9a**, **10a**, **11a**) in dry dichloromethane was added triethylamine (1.2 equivalent) and methanesulfonyl chloride (1.2 equivalent) slowly at ice bath temperature. After stirring for 1 hour at room temperature, the reaction mixture was washed with distilled water and then brine. The organic extract was concentrated and re-dissolved in 10 mL DMF. Sodium azide (2 equivalent) was dissolved in 3 mL distilled water and added to the above solution. The reaction mixture was heated for 12 hours at 80 ^{o}C. Dichloromethane (200 mL) was added to the reaction mixture after it was cooled to room temperature. The reaction mixture was then washed with distilled water (3 x 200mL) and brine (200 mL). The organic layer was dried over anhydrous Na_2SO_4 and evaporated to dryness to obtain pure products.

*Compound **9***, 95%. ^{1}H NMR (400MHz, $CDCl_3$) δ: 8.51 (s, 2H), 8.07 (s, 1H), 4.59-4.56 (m, 2H), 3.89-3.86 (m, 2H), 3.74 (t, J = 4.8 Hz, 2H), 3.40 (t, J = 4.8 Hz, 2H); ^{13}C NMR (100

MHz, $CDCl_3$) δ: 164.1, 132.3, 132.3 (q, J_{C-F} = 33.8 Hz), 130.1, 130.0, 126.6-126.5 (m), 123.0 (q, J_{C-F} = 271.1 Hz), 70.4, 69.0, 65.0, 50.7.

*Compound **10***, 91%. ^{1}H NMR (400MHz, $CDCl_3$) δ: 8.48 (s, 2H), 8.04 (s, 1H), 4.55-4.52 (m, 2H), 3.86-3.83 (m, 2H), 3.71-3.60 (m, 10H), 3.35 (t, *J* = 6.5 Hz, 2H). ^{13}C NMR (100 MHz, $CDCl_3$) δ: 163.9, 132.3, 132.1 (q, J_{C-F} = 33.8 Hz), 129.8, 129.8, 126.4-126.2 (m), 122.9 (q, J_{C-F} = 271.2 Hz), 70.6, 70.0, 68.9, 65.1, 50.6.

*Compound **11***, 85%. ^{1}H NMR (400MHz, $CDCl_3$) δ: 8.50 (s, 2H), 8.07 (s, 1H), 4.57-4.54 (m, 2H), 3.87-3.85 (m, 2H), 3.71-3.61 (m, 18H), 3.38 (t, *J* = 4.9 Hz, 2H); ^{13}C NMR (100 MHz, $CDCl_3$) δ: 163.7, 132.2, 131.9 (q, J_{C-F} = 33.8 Hz), 129.7, 129.7, 126.3-126.1 (m), 122.8 (q, J_{C-F} = 271.1 Hz), 70.5, 70.4, 70.4, 69.9, 68.8, 65.0, 50.5.

Synthesis of compound 12a:

To a solution of hexaethylene glycol (2 g, 7.1 mmol) in dry dichloromethane was added triethylamine (1.7 g, 17.0 mmol) and methanesulfonyl chloride (1.9 g, 17.0 mmol) slowly at ice bath temperature. After stirring for 1 hour at room temperature, the reaction mixture was washed with distilled water and then brine. The organic extract was concentrated and re-dissolved in 50 mL distilled water. Sodium azide (1.8 g, 28.4 mmol) was then added to the solution and heated to reflux for 12 hours. The reaction mixture was cooled to room temperature and extracted with dichloromethane (2 x 50 mL). The combined organic extracts were concentrated and re-dissolved in 60 mL of Et_2O/THF/1M HCl (v/v/v, 5/1/5). A solution of triphenylphosphine (1.1 g, 7.1 mmol) in diethyl ether (50 mL) was added dropwise to the above mixture over a period of 3 hours. After the addition was completed, the reaction mixture was allowed to stir for 20 h at room temperature. The organic layer was discarded. The aqueous layer was washed with diethyl ether (2 x 30 mL).

pH of the aqueous solution was adjusted to 14 using NaOH. The basic aqueous solution was then extracted with dichloromethane (2 x 30 mL). Combined organic layers were dried over anhydrous Na_2SO_4 and evaporated to dryness to yield 0.87 g (40%) of compound **12a**. ^{1}H NMR (400MHz, $CDCl_3$) δ: 3.71-3.58 (m, 18H), 3.52 (t, *J* = 5.2 Hz, 2H), 3.39 (t, *J* = 4.9 Hz, 2H), 2.88-2.85 (m, 2H), 1.73 (bs, 2H). ^{13}C NMR (100 MHz, $CDCl_3$) δ: 72.5, 70.1, 70.0, 70.0, 69.7, 69.5, 50.1, 41.1.

Synthesis of compound 12:

To a solution of 3,5-bis(trifluoromethyl)benzoic acid (0.5 g, 1.9 mmol) in dry dichloromethane was added N-(3-dimethylaminopropyl)-N'-ethylcarbodiimide hydro-chloride (0.48 g, 2.5 mmol) at ice bath temperature and stirred for 20 minutes at the same temperature. **12a** (0.77 g, 2.5 mmol) was dissolved in dichloromethane and added to the above mixture. The reaction mixture was stirred for 2 hours at room temperature. 1M HCl was added to the reaction mixture and extracted twice with dichloromethane. Combined organic layers were dried over anhydrous Na_2SO_4 and evaporated to dryness. The crude product was purified by silica gel column chromatography using mixture of dichloromethane/methanol as eluent to yield 0.88 g (85%) of compound **12**. ^{1}H NMR (400MHz, $CDCl_3$) δ: 8.37 (s, 2H), 7.98 (s, 1H), 7.59 (bs, 1H), 3.73-3.57 (m, 22H), 3.34 (t, *J* = 4.9 Hz, 2H). ^{13}C NMR (100 MHz, $CDCl_3$) δ: 164.6, 136.7, 131.6 (q, J_{C-F} = 33.8 Hz), 127.9, 127.9, 124.5-124.4 (m), 123.0 (q, J_{C-F} = 271.0 Hz), 70.4, 70.4, 70.3, 70.3, 70.0, 69.8, 69.5, 50.5, 40.2.

General procedure for incorporation of azido compound using "click" chemistry:

The mixture of dendritic acetylene compound (1.0 equiv), azido compound (5 equiv for G1-dendrons and 10 equiv for G2-dendrons), $CuSO_4.5H_2O$ (0.5 equiv.) and sodium

ascorbate (0.5 equiv.) in THF/H_2O (1:1) solvent mixture was heated at 50 ^oC for 24-48 h (24h for G1-dendrons and 48h for G2-dendrons). The progress of the reaction was monitored by TLC. After completion of the reaction, saturated aqueous NaCl solution was added to the reaction mixture. The aqueous layer was extracted twice with ethyl acetate and the combined organic layer was dried over Na_2SO_4 and evaporated to dryness. The crude product was purified by silica gel column chromatography using mixture of dichloromethane/methanol as eluent.

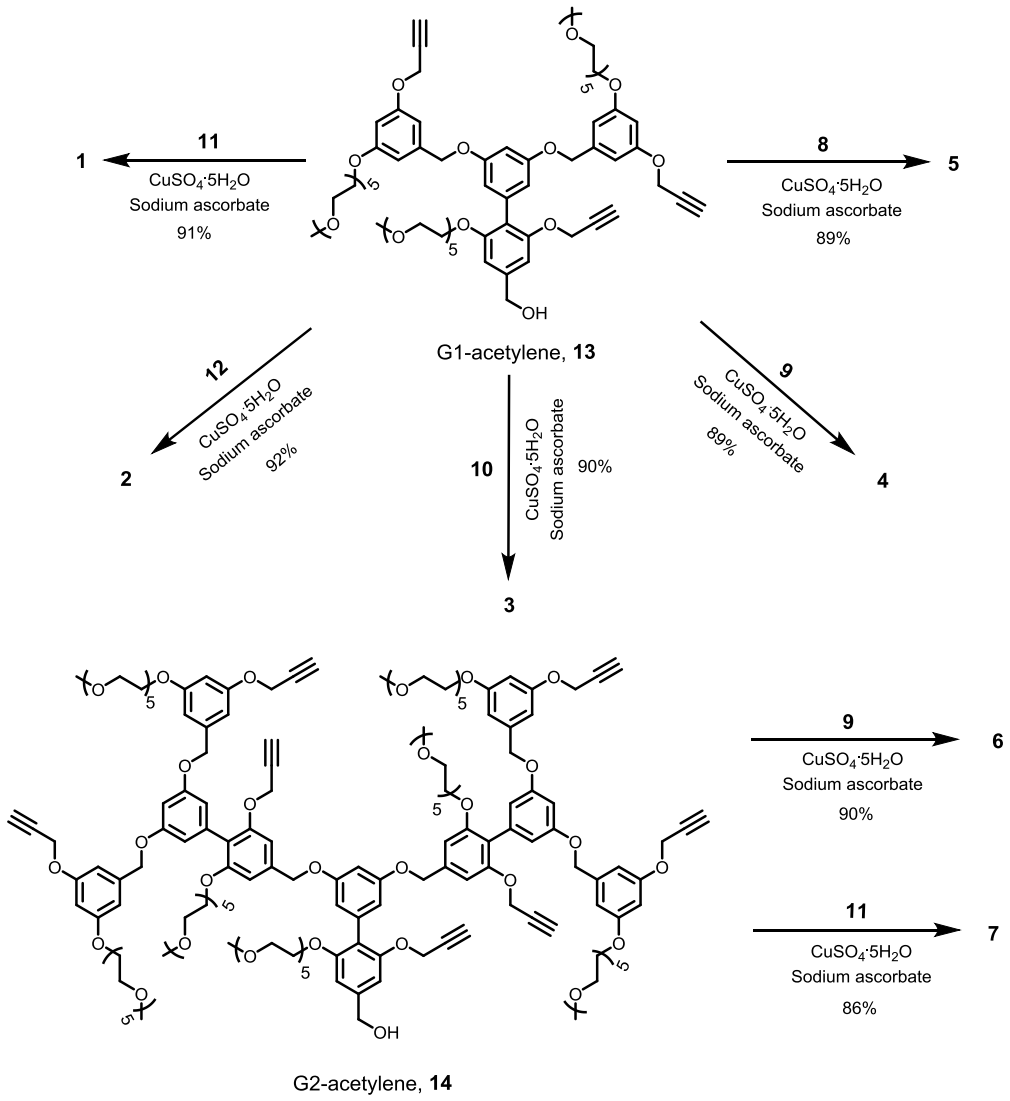

Scheme 4.2: Synthesis of dendrons (**1**-**7**).

Synthesis of compound 1:

According to general procedure for click reaction, G1-acetylene (40 mg, 0.031 mmol) was treated with compound **11** (85 mg, 0.155 mmol) to give 81 mg (89%) of dendron **1**. ^{1}H NMR (400MHz, acetone-d_6) δ: 8.54 (s, 6H), 8.36 (s, 3H), 8.09 (s, 2H), 7.84 (s, 1H), 6.94-6.57 (m, 11H), 5.18 (s, 4H), 5.13 (s, 2H), 5.04 (s, 4H), 4.64 (d, J = 5.7 Hz, 2H), 4.58-4.47 (m, 12H), 4.30 (bs, 1H), 4.15-4.13 (m, 4H), 4.07-4.05 (m, 2H), 3.90-3.80 (m, 16H), 3.66-3.42 (m, 98H), 3.26 (s, 6H), 3.25 (s, 3H); ^{13}C NMR (100 MHz, acetone-d_6) δ: 164.3, 161.2, 160.7, 159.9, 157.8, 157.2, 144.7, 144.3, 144.0, 141.1, 137.1, 133.8, 132.6 (q, J_{C-F} = 33.6 Hz), 130.6, 130.5, 127.5-127.2 (m), 125.4, 125.1, 124.0 (q, J_{C-F} = 270.6 Hz), 119.4, 111.4, 107.1, 107.1, 105.3, 105.1, 101.6, 101.5, 72.6, 71.4, 71.2, 71.1, 71.0, 70.4, 70.3, 70.1, 70.0, 69.4, 68.4, 66.1, 64.8, 63.2, 62.5, 58.8, 50.7; ^{19}F NMR (300 MHz, acetone-d_6) δ: -64.43 (s, 18H); MALDI-TOF *m/z* 2950.81, 2973.60 (calculated: M^+, 2950.16; $M+Na^+$, 2973.15).

Synthesis of compound 2:

According to general procedure for click reaction, G1-acetylene (40 mg, 0.031 mmol) was treated with compound **12** (85 mg, 0.155 mmol) to give 81 mg (89%) of dendron **2**. ^{1}H NMR (400MHz, acetone-d_6) δ: 8.51 (s, 6H), 8.38 (bs, 3H), 8.20 (s, 3H), 8.10 (s, 2H), 7.84 (s, 1H), 6.95-6.53 (m, 11H), 5.19 (s, 4H), 5.11 (s, 2H), 5.04 (s, 4H), 4.65 (d, J = 5.9 Hz, 2H), 4.58-4.56 (m, 4H), 4.50-4.47 (m, 2H), 4.33(t, J = 5.9 Hz, 1H), 4.16-4.13 (m, 4H), 4.07-4.05 (m, 2H), 3.90-3.87 (m, 4H), 3.82-3.79 (m, 6H), 3.60-3.41 (m, 110H), 3.26 (s, 6H), 3.25 (s, 3H); ^{13}C NMR (100 MHz, acetone-d_6) δ: 164.7, 161.1, 160.7, 159.8, 157.7, 157.2, 144.7, 141.0, 138.1, 137.1, 132.1 (q, J_{C-F} = 33.3 Hz), 128.9, 128.9, 125.5-125.2 (m), 124.2 (q, J_{C-F} = 270.6 Hz), 119.3, 111.4, 107.1, 107.1, 105.3, 105.1, 101.5,

101.4, 72.5, 71.3, 71.1, 71.1, 71.1, 70.9, 70.9, 70.9, 70.5, 70.4, 70.2, 70.1, 70.0, 69.3, 68.4, 64.7, 63.1, 62.4, 58.8, 50.7, 40.9; ^{19}F NMR (300 MHz, acetone-d_6) δ: -64.28 (s, 6H), -64.29 (s, 12H); MALDI-TOF *m/z* 2948.22, 3010.16 (calculated: M^+, 2947.21; $M+Na+K^+$, 3010.31).

Synthesis of dendron 3:

According to general procedure for click reaction, G1-acetylene (40 mg, 0.031 mmol) was treated with compound **10** (71 mg, 0.155 mmol) to give 75 mg (90%) of dendron **3**. ^{1}H NMR (400MHz, acetone-d_6) δ: 8.53 (s, 6H), 8.35 (s, 3H), 8.07 (s, 2H), 7.82 (s, 1H), 6.93-6.58 (m, 11H), 5.17 (s, 4H), 5.12 (s, 2H), 5.04 (s, 4H), 4.64 (d, J = 5.7 Hz, 2H), 4.56-4.46 (m, 12H), 4.25 (bs, 1H), 4.14-4.12 (m, 4H), 4.06-4.04 (m, 2H), 3.89-3.77 (m, 16H), 3.66-3.41 (m, 74H), 3.26 (s, 6H), 3.25 (s, 3H); ^{13}C NMR (100 MHz, acetone-d_6) δ: 164.4, 161.2, 160.8, 159.9, 157.8, 157.3, 144.8, 144.3, 144.0, 141.1, 137.1, 133.8, 132.6 (q, J_{C-F} = 33.6 Hz), 130.6, 130.5, 127.5-127.3 (m), 125.3, 125.0, 124.1 (q, J_{C-F} = 270.6 Hz), 119.5, 111.4, 107.2, 107.1, 105.6, 105.3, 101.6, 101.5, 72.6, 71.4, 71.3, 71.2, 71.2, 71.0, 71.0, 70.4, 70.3, 70.1, 70.1, 70.0, 69.4, 69.4, 68.4, 66.1, 64.8, 63.3, 62.5, 58.8, 50.7; ^{19}F NMR (300 MHz, acetone-d_6) δ: -64.41 (s, 6H), -64.42 (s, 12H); MALDI-TOF *m/z* 2708.41, 2709.39, 2710.37 (calculated: $M+Na^+$, 2709.0).

Synthesis of dendron 4:

According to general procedure for click reaction, G1-acetylene (40 mg, 0.031 mmol) was treated with compound **9** (58 mg, 0.155 mmol) to give 69 mg (92%) of dendron **4**. ^{1}H NMR (400MHz, acetone-d_6) δ: 8.53 (s, 4H), 8.49 (s, 2H), 8.35 (s, 2H), 8.33 (s, 1H), 8.06 (s, 2H), 7.80 (s, 1H), 6.89-6.53 (m, 11H), 5.10 (s, 4H), 5.04 (s, 2H), 5.03 (s, 4H), 4.65 (d, J = 4.5 Hz, 2H), 4.62-4.44 (m, 12H), 4.26 (bs, 1H), 4.14-4.11 (m, 4H), 4.06-4.04 (m,

2H), 4.00-3.76 (m, 16H), 3.66-3.41 (m, 50H), 3.26 (s, 6H), 3.25 (s, 3H); ^{13}C NMR (100 MHz, acetone-d_6) δ: 164.3, 161.1, 160.7, 159.9, 157.7, 157.2, 144.7, 141.1, 137.1, 133.7, 133.7, 132.6 (q, J_{C-F} = 33.6 Hz), 132.5 (q, J_{C-F} = 33.6 Hz), 130.6, 127.6-127.3 (m), 124.0 (q, J_{C-F} = 270.7 Hz), 119.4, 111.4, 107.1, 107.0, 105.3, 105.1, 101.5, 101.4, 72.6, 71.3, 71.2, 71.1, 71.1, 71.0, 70.9, 70.3, 70.2, 70.1, 70.0, 70.0, 69.4, 69.3, 68.4, 65.8, 64.7, 62.4, 58.8, 50.7; ^{19}F NMR (300 MHz, acetone-d_6) δ: -64.36 (s, 6H), -64.40 (s, 12H); MALDI-TOF *m/z* 2444.21, 2484.82 (calculated: M+Na$^+$, 2444.83; M+Na+K$^+$, 2483.93).

Synthesis of dendron 5:

According to general procedure for click reaction, G1-acetylene (40 mg, 0.031 mmol) was treated with compound **8** (53 mg, 0.155 mmol) to give 66 mg (91%) of dendron **5**. ^{1}H NMR (400MHz, acetone-d_6) δ: 8.56 (s, 4H), 8.52 (s, 2H), 8.35 (s, 2H), 8.33 (s, 1H), 8.11 (s, 2H), 7.81 (s, 1H), 6.91-6.54 (m, 11H), 5.15 (s, 4H), 5.08 (s, 2H), 5.04 (s, 4H), 4.67 (t, *J* = 6.9 Hz, 4H), 4.64 (d, *J* = 4.2 Hz, 2H),4.57 (t, *J* = 6.9 Hz, 2H), 4.48 (t, *J* = 6.1 Hz, 4H), 4.41 (t, *J* = 6.1 Hz, 2H), 4.29 (bs, 1H), 4.13-4.11 (m, 4H), 4.06-4.04 (m, 2H), 3.81-3.78 (m, 4H), 3.65-3.41 (m, 50H), 3.25 (s, 6H), 3.24 (s, 3H), 2.48 (quin, *J* = 6.4 Hz, 4H), 2.39 (quin, *J* = 6.4 Hz, 2H); ^{13}C NMR (100 MHz, acetone-d_6) δ: 164.4, 161.2, 160.7, 159.9, 157.8, 157.3, 144.8, 144.7, 144.3, 141.1, 137.1, 133.8, 133.7, 132.6 (q, J_{C-F} = 33.7 Hz), 132.5 (q, J_{C-F} = 33.7 Hz), 130.7, 130.6, 127.5-127.3 (m), 124.8, 124.5, 124.0 (q, J_{C-F} = 270.6 Hz), 119.5, 111.5, 107.1, 107.0, 105.5, 105.2, 101.6, 101.4, 72.6, 71.4, 71.2, 71.2, 71.2, 71.1, 71.0, 71.0, 70.3, 70.3, 70.1, 69.4, 68.4, 64.7, 64.0, 63.4, 62.5, 58.8, 47.7; ^{19}F NMR (300 MHz, acetone-d_6) δ: -64.35 (s, 6H), -64.41 (s, 12H); MALDI-TOF *m/z* 2331.92, 2354.72 (calculated: M$^+$, 2331.81; M+Na$^+$, 2354.80).

Synthesis of compound 6:

According to general procedure for click reaction, G2-acetylene (40 mg, 0.013 mmol) was treated with compound **9** (48 mg, 0.13 mmol) to give 67 mg (90%) of dendron **6**. ^{1}H NMR (400MHz, acetone-d_6) δ: 8.52-8.30 (m, 21H), 8.04 (s, 4H), 7.83 (s, 1H), 7.78 (s, 2H), 7.09-6.52 (m, 27H), 5.14-5.02 (m, 26H), 4.65 (d, J = 5.7 Hz, 2H), 4.61-4.41 (m, 28H), 4.31 (bs, 1H), 4.17-3.35 (m, 168H), 3.25 (s, 12H), 3.22 (s, 6H), 3.22 (s, 3H); ^{13}C NMR (100 MHz, acetone-d_6) δ: 164.3, 161.1, 160.6, 159.9, 159.9, 157.9, 157.7, 157.3, 157.2, 144.8, 144.2, 144.1, 141.0, 139.8, 137.1, 136.8, 133.7, 133.6, 133.6, 132.6 (q, J_{C-F} = 33.6 Hz), 132.5 (q, J_{C-F} = 33.6 Hz), 132.5 (q, J_{C-F} = 33.6 Hz), 130.5, 127.6-127.3 (m), 125.2, 125.0, 124.0 (q, J_{C-F} = 270.6 Hz), 120.3, 119.4, 111.5, 111.3, 107.2, 107.1, 106.5, 106.4, 105.3, 105.2, 101.8, 101.7, 101.4, 72.5, 72.5, 71.3, 71.3, 71.2, 71.1, 71.0, 71.0, 70.9, 70.9, 70.6, 70.4, 70.2, 70.0, 69.5, 69.2, 68.4, 65.8, 64.7, 63.3, 63.0, 62.4, 58.8, 50.6; ^{19}F NMR (300 MHz, acetone-d_6) δ: -64.32 (s, 18H), -64.38 (s, 24H); MALDI-TOF *m/z* 5700.77, 5722.72 (calculated: M^+, 5698.96; $M+Na^+$, 5721.94).

Synthesis of compound 7:

According to general procedure for click reaction, G2-acetylene (40 mg, 0.013 mmol) was treated with compound **11** (71 mg, 0.13 mmol) to give 78 mg (86%) of dendron **7**. ^{1}H NMR (400MHz, acetone-d_6) δ: 8.55-8.34 (m, 21H), 8.09 (s, 4H), 7.88 (s, 1H), 7.83 (s, 2H), 7.13-6.58 (m, 27H), 5.19-5.04 (m, 26H), 4.66 (d, J = 5.2 Hz, 2H), 4.58-4.45 (m, 28H), 4.35 (bs, 1H), 4.16-3.38 (m, 280H), 3.25 (s, 12H), 3.23 (s, 6H), 3.23 (s, 3H); ^{13}C NMR (100 MHz, acetone-d_6) δ: 164.4, 161.2, 160.7, 160.0, 159.9, 157.9, 157.8, 157.4, 157.3, 144.2, 144.2, 144.0, 141.0, 139.8, 137.1, 136.8, 133.8, 132.6 (q, J_{C-F} = 33.6 Hz), 130.6, 130.5, 127.5-127.2 (m), 125.4, 125.2, 124.0 (q, J_{C-F} = 270.6 Hz), 120.3, 111.5, 111.3, 107.2, 107.1, 106.6, 106.3, 101.7, 101.5, 72.6, 71.7, 71.4, 71.2, 71.0, 70.7, 70.4,

70.3, 70.0, 69.4, 68.4, 66.1, 63.3, 62.5, 58.8, 50.7; ^{19}F NMR (300 MHz, acetone-d_6) δ: -64.38 (s, 18H), -64.40 (s, 24H); MALDI-TOF *m/z* 6933.31, 6955.83 (calculated: M^+, 6931.70; $M+Na^+$, 6954.60).

4.4.3 Procedures for Preparing Probe Solutions

To a 980 µL solution of 25 mM Tris buffer was slowly added 10 µL (2.5 mM) solution of dendron in dimethyl sulfoxide (DMSO) under vigorously stirring. The solution was allowed to stir for 10 min at room temperature after the addition was complete. To prepare solutions with an enzyme, 10 µL (100 µM) solution of the enzyme in 25 mM Tris buffer was added to the above solution. To prepare solutions without enzymes, 10 µL 25 mM Tris buffer was added. Solutions were immediately taken for DLS or ^{19}F-NMR measurements, unless otherwise mentioned.

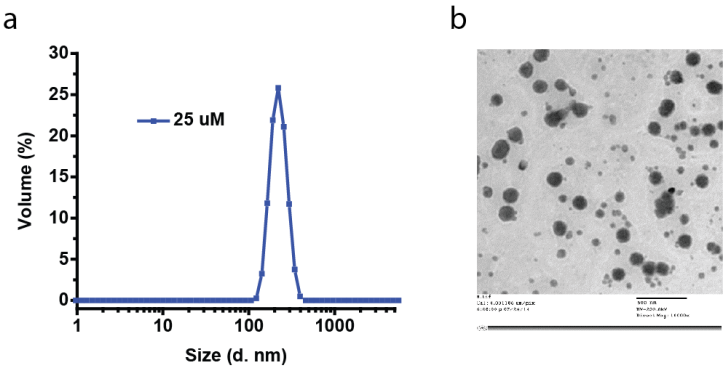

Figure 4.4: Size distribution of dendron **1** (25 µM) alone in 25 mM Tris buffer measured by (a) DLS, (b) TEM (scale bar 500 nm).

4.4.4 Control Experiment with Dendron 2

To support that the ^{19}F NMR signal generated was indeed due to the hydrolysis of ester functionalities, we performed control experiment where we utilized dendron **2** that does not contain ester functionalities. Dendron **2** (25 µM) was incubated with PLE (1 µM) for 3 hours before taking the ^{19}F NMR spectrum. The ^{19}F NMR and DLS studies upon

exposing to PLE are shown below.

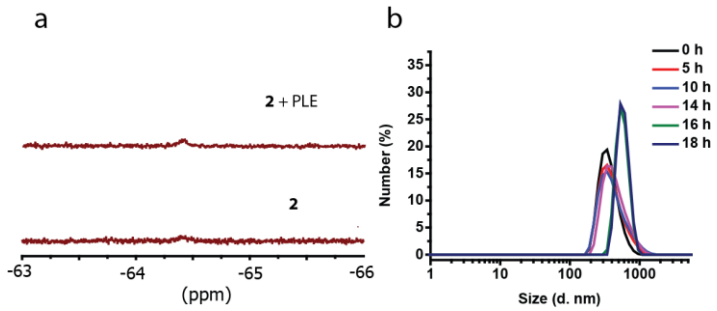

Figure 4.5: (a) ^{19}F NMR spectra of **2** (25 μM) in the presence or absence of PLE (1 μM). (b) Size evolution of **2** (25 μM) in the presence of PLE (1 μM) using DLS.

4.4.5 Enzyme Specificity Experiment

Dendron **1** was incubated with different enzymes for 3 hours before taking the ^{19}F spectra.

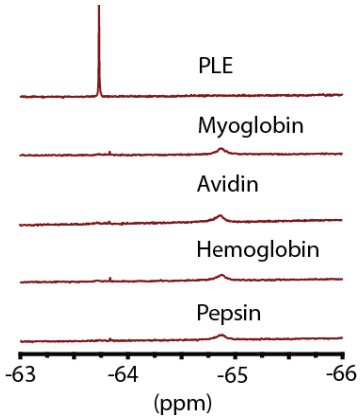

Figure 4.6: ^{19}F NMR spectra of **1** (25 μM) in the presence of different enzymes (1 μM).

4.4.6 ^{19}F-NMR Spectra of Dendron Probes

^{19}F-NMR spectra were collected on a 300 MHz Bruker NMR spectrometer using the fluorine signal of trifluoroacetic acid (δ = -76.5) as the internal standard. All spectra were taken in 25 mM Tris buffer (pH 7.4, 0.2 mM TFA, 10%D_2O (v/v)).

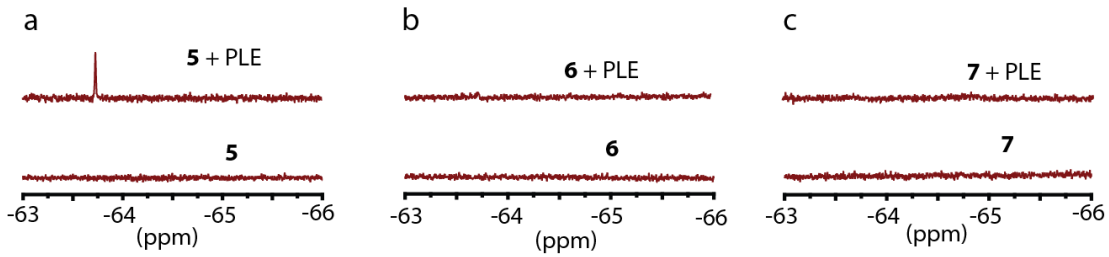

Figure 4.7: ^{19}F NMR spectra of dendrons (25 μM) before or after incubation with PLE (1 μM) for 4 days: (a) **5**, (b) **6**, (c) **7**.

4.4.7 DLS Measurements to Monitor Size Evolution of Dendron Probes

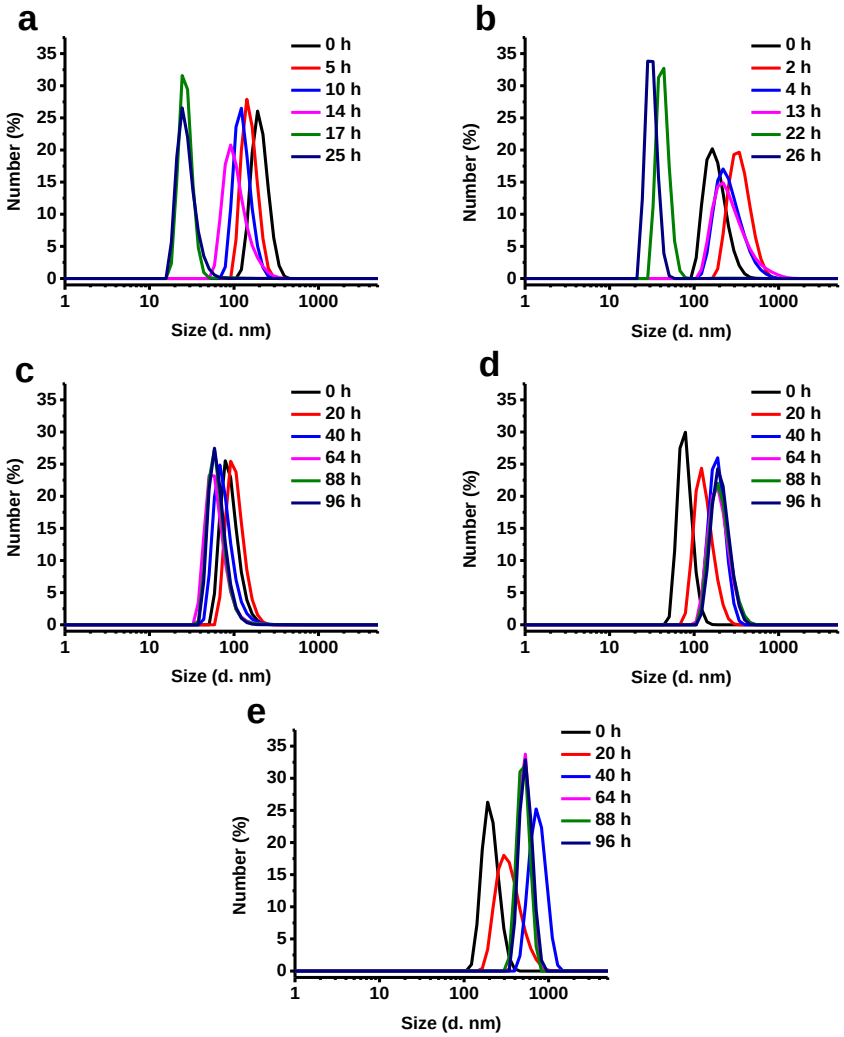

Figure 4.8: Size evolution of dendron probes (25 μM) in the presence of PLE (1 μM): (a) **3**, (b) **4**, (c) **5,** (d) **6**, and (e) **7**.

DLS experiments were performed on a Malvern Nano-ZS Zeta-sizer in 25 mM Tris buffer (pH 7.4, 0.2 mM TFA, 10%D_2O (v/v)) using a plastic cuvette (1 mL volume). First measurement was taken right after the addition of PLE. The DLS experiment was then performed during each time intervals. The temperature was maintained at 25 ^oC throughout the experiment.

4.5 References

1. Vitzthum, F.; Behrens, F.; Anderson, N. L.; Shaw, J. H. Proteomics: From Basic Research to Diagnostic Application. A Review of Requirements & Needs *J. Proteome Res.* **2005**, *4*, 1086–1097.

2. Roy R.; Yang J.; Moses M. A. Matrix Metalloproteinases as Novel Biomarkers and Potential Therapeutic Targets in Human Cancer. *J. Clin. Oncol.* **2009**, *27*, 5287–5297.

3. Lee, D.-H.; Blomhoff, R.; Jacobs, D. R. Is Serum Gamma Glutamyltransferase a Marker of Oxidative Stress? *Free Radic. Res.* **2004**, *38*, 535–539.

4. Kobayashi, H.; Ogawa, M.; Alford, R.; Choyke, P. L.; Urano, Y. New Strategies for Fluorescent Probe Design in Medical Diagnostic Imaging. *Chem. Rev.* **2010**, *110*, 2620–2640.

5. Lavis, L. D.; Raines, R. T. Bright Ideas for Chemical Biology. *ACS Chem. Biol.* **2008**, *3*, 142–155.

6. Weissleder, R.; Tung, C. H.; Mahmood, U.; Bogdanov, A. In Vivo Imaging of Tumors with Protease-Activated Near-Infrared Fluorescent Probes. *Nat. Biotechnol.* **1999**, *17*, 375–378.

7. Chen, J.; Tung, C.-H.; Allport, J. R.; Chen, S.; Weissleder, R.; Huang, P. L. Near-Infrared Fluorescent Imaging of Matrix Metalloproteinase Activity after Myocardial Infarction. *Circulation* **2005**, *111*, 1800–1805.

8. Hu, H.-Y.; Gehrig, S.; Reither, G.; Subramanian, D.; Mall, M. A.; Plettenburg, O.; Schultz, C. FRET-Based and Other Fluorescent Proteinase Probes. *Biotechnol. J.* **2014**, *9*, 266–281.

9. Gao, W.; Xing, B.; Tsien, R. Y.; Rao, J. Novel Fluorogenic Substrates for Imaging β-Lactamase Gene Expression. *J. Am. Chem. Soc.* **2003**, *125*, 11146–11147.

10. Kamiya, M.; Kobayashi, H.; Hama, Y.; Koyama, Y.; Bernardo, M.; Nagano, T.; Choyke, P. L.; Urano, Y. An Enzymatically Activated Fluorescence Probe for Targeted Tumor Imaging. *J. Am. Chem. Soc.* **2007**, *129*, 3918–3929.

11. Silvers, W. C.; Prasai, B.; Burk, D. H.; Brown, M. L.; McCarley, R. L. Profluorogenic Reductase Substrate for Rapid, Selective, and Sensitive Visualization and Detection of Human Cancer Cells that Overexpress NQO1. *J. Am. Chem. Soc.* **2013**, *135*, 309–314.

12. Perez, J. M.; Josephson, L.; O'Loughlin, T.; Högemann, D.; Weissleder, R. Magnetic Relaxation Switches Capable of Sensing Molecular Interactions. *Nat. Biotechnol.* **2002**, *20*, 816–820.

13. Louie, A. Y.; Huber, M. M.; Ahrens, E. T.; Rothbacher, U.; Moats, R.; Jacobs, R. E.; Fraser, S. E.; Meade, T. J. In Vivo Visualization of Gene Expression using Magnetic Resonance Imaging. *Nat. Biotechnol.* **2000**, *18*, 321–325.

14. Yang, C.-T.; Chuang, K.-H. Gd(III) Chelates for MRI Contrast Agents: from High Relaxivity to "Smart", from Blood Pool to Blood–Brain Barrier Permeable. *Med. Chem. Commun.* **2012**, *3*, 552–565.

15. Chang, Y. T.; Cheng, C. M.; Su, Y. Z.; Lee, W. T.; Hsu, J. S.; Liu, G. C.; Cheng, T. L.; Wang, Y. M. Synthesis and Characterization of a New Bioactivated Paramagnetic Gadolinium(III) Complex [Gd(DOTA-FPG)(H2O)] for Tracing Gene Expression. *Bioconjug. Chem.* **2007**, *18*, 1716–1727.

16. Giardiello, M.; Lowe, M. P.; Botta, M. An Esterase-Activated Magnetic Resonance Contrast Agent. *Chem. Commun.* **2007**, 4044–4046.

17. Yoo, B.; Pagel, M. D. A PARACEST MRI Contrast Agent to Detect Enzyme Activity. *J. Am. Chem. Soc.* **2006**, *128*, 14032–14033.

18. Grobner, T. Gadolinium--a Specific Trigger for the Development of Nephrogenic Fibrosing Dermopathy and Nephrogenic Systemic Fibrosis? *Nephrol. Dial. Transplant* **2006**, *21*, 1104–1108.

19. Grobner, T.; Prischl, F. C. Gadolinium and Nephrogenic Systemic Fibrosis. *Kidney Int.* **2007**, *72*, 260–264.

20. Yu, J.-X.; Hallac, R. R.; Chiguru, S.; Mason, R. P. New Frontiers and Developing Applications in ^{19}F NMR. *Prog. Nucl. Magn. Reson. Spectrosc.* **2013**, *70*, 25–49.

21. Ahrens, E. T.; Flores, R.; Xu, H.; Morel, P. A. In Vivo Imaging Platform for Tracking Immunotherapeutic Cells. *Nat. Biotechnol.* **2005**, *23*, 983–987.

22. Thurecht, K. J.; Blakey, I.; Peng, H.; Squires, O.; Hsu, S.; Alexander, C.; Whittaker, A. K. Functional Hyperbranched Polymers: Toward Targeted in Vivo ^{19}F Magnetic Resonance Imaging Using Designed Macromolecules. *J. Am. Chem. Soc.* **2010**, *132*, 5336–5337.

23. Higuchi, M.; Iwata, N.; Matsuba, Y.; Sato, K.; Sasamoto, K.; Saido, T. C. ^{19}F and ^{1}H MRI Detection of Amyloid Beta Plaques in Vivo. *Nat. Neurosci.* **2005**, *8*, 527–533.

24. Takaoka, Y.; Sakamoto, T.; Tsukiji, S.; Narazaki, M.; Matsuda, T.; Tochio, H.; Shirakawa, M.; Hamachi, I. Self-Assembling Nanoprobes that Display Off/On ^{19}F Nuclear Magnetic Resonance Signals for Protein Detection and Imaging. *Nat. Chem.* **2009**, *1*, 557–561.

25. Tanabe, K.; Harada, H.; Narazaki, M.; Tanaka, K.; Inafuku, K.; Komatsu, H.; Ito, T.; Yamada, H.; Chujo, Y.; Matsuda, T.; Hiraoka, M.; Nishimoto, S. Monitoring of Biological One-Electron Reduction by ^{19}F NMR Using Hypoxia Selective Activation of an 19F-Labeled Indolequinone Derivative *J. Am. Chem. Soc.* **2009**, *131*, 15982–15983.

26. Tanaka, K.; Kitamura, N.; Naka, K.; Chujo, Y. Multi-Modal ^{19}F NMR Probe Using Perfluorinated Cubic Silsesquioxane-Coated Silica Nanoparticles for Monitoring Enzymatic Activity. *Chem. Commun.* **2008**, 6176–6178.

27. Vutukuri, D. R.; Basu, S.; Thayumanavan, S. Dendrimers with Both Polar and Apolar Nanocontainer Characteristics. *J. Am. Chem. Soc.* **2004**, *126*, 15636–15637.

28. Aathimanikandan, S. V.; Savariar, E. N.; Thayumanavan, S. Temperature-Sensitive Dendritic Micelles. *J. Am. Chem. Soc.* **2005**, *127*, 14922–14929.

29. Azagarsamy, M. A.; Sokkalingam, P.; Thayumanavan, S. Enzyme-Triggered Disassembly of Dendrimer-Based Amphiphilic Nanocontainers. *J. Am. Chem. Soc.* **2009**, *131*, 14184–14185.

30. Azagarsamy, M. A.; Yesilyurt, V.; Thayumanavan, S. Disassembly of Dendritic Micellar Containers Due to Protein Binding. *J. Am. Chem. Soc.* **2010**, *132*, 4550–4551.

31. Yesilyurt, V.; Ramireddy, R.; Thayumanavan, S. Photoregulated Release of Noncovalent Guests from Dendritic Amphiphilic Nanocontainers. *Angew. Chem. Int. Ed. Engl.* **2011**, *50*, 3038–3042.

32. Raghupathi, K. R.; Guo, J.; Munkhbat, O.; Rangadurai, P.; Thayumanavan, S. Supramolecular Disassembly of Facially Amphiphilic Dendrimer Assemblies in Response to Physical, Chemical, and Biological Stimuli. *Acc. Chem. Res.* **2014**, *47*, 2200–2211.

33. Bloembergen, N.; Purcell, E. M.; Pound, R. V. Relaxation Effects in Nuclear Magnetic Resonance Absorption. *Phys. Rev.* **1948**, *73*, 679–679.

34. Harnoy, A. J.; Rosenbaum, I.; Tirosh, E.; Ebenstein, Y.; Shaharabani, R.; Beck, R.; Amir, R. J. Enzyme-Responsive Amphiphilic PEG-Dendron Hybrids and Their Assembly into Smart Micellar Nanocarriers. *J. Am. Chem. Soc.* **2014**, *136*, 7531–7534.

35. Grayson, S. M.; Fréchet, J. M. J. Convergent Dendrons and Dendrimers: from Synthesis to Applications. *Chem. Rev.* **2001**, *101*, 3819–3868.

36. Tomalia, D. A.; Fréchet, J. M. J. Discovery of Dendrimers and Dendritic Polymers: A Brief Historical Perspective. *J. Polym. Sci. A Polym. Chem.* **2002**, *40*, 2719–2728.

37. Svenson, S.; Tomalia, D. A. Dendrimers in Biomedical Applications--Reflections on the Field. *Adv. Drug Deliv. Rev.* **2005**, *57*, 2106–2129.

38. Newkome, G. R.; He, E.; Moorefield, C. N. Suprasupermolecules with Novel Properties: Metallodendrimers. *Chem. Rev.* **1999**, *99*, 1689–1746.

39. Bosman, A. W.; Janssen, H. M.; Meijer, E. W. About Dendrimers: Structure, Physical Properties, and Applications. *Chem. Rev.* **1999**, *99*, 1665–1688.

40. Caminade, A. M.; Majoral, J. P. Nanomaterials Based on Phosphorus Dendrimers. *Acc. Chem. Res.* **2004**, *37*, 341–348.

41. Astruc, D.; Boisselier, E.; Ornelas, C. Dendrimers Designed for Functions: From Physical, Photophysical, and Supramolecular Properties to Applications in Sensing, Catalysis, Molecular Electronics, Photonics, and Nanomedicine. *Chem. Rev.* **2010**, *110*, 1857–1959.

42. Newkome, G. R.; Yao, Z.; Baker, G. R.; Gupta, V. K. Micelles. Part 1. Cascade Molecules: a New Approach to Micelles. A [27]-Arborol. *J. Org. Chem.* **1985**, *50*, 2003–2004.

43. Hawker, C. J.; Wooley, K. L.; Fréchet, J. M. J. Unimolecular Micelles and Globular Amphiphiles: Dendritic Macromolecules as Novel Recyclable Solubilization Agents. *J. Chem. Soc., Perkin Trans. 1* **1993**, 1287–1297.

44. Tomalia, D. A.; Baker, H.; Dewald, J.; Hall, M.; Kallos, G.; Martin, S.; Roeck, J.; Ryder, J.; Smith, P. A New Class of Polymers: Starburst-Dendritic Macromolecules. *Polym. J.* **1985**, *17*, 117–132.

45. Azagarsamy, M. A.; Sokkalingam, P.; Thayumanavan, S. Enzyme-Triggered Disassembly of Dendrimer-Based Amphiphilic Nanocontainers. *J. Am. Chem. Soc.* **2009**, *131*, 14184–14185.

46. Bo, Z.; Schäfer, A.; Franke, P.; Schlüter, a. D. A Facile Synthetic Route to a Third-Generation Dendrimer with Generation-Specific Functional Aryl Bromides. *Org. Lett.* **2000**, *2*, 1645–1648.

47. Azagarsamy, M. A.; Krishnamoorthy, K.; Sivanandan, K.; Thayumanavan, S. Site-Specific Installation and Study of Electroactive Units in Every Layer of Dendrons. *J. Org. Chem.* **2009**, *74*, 9475–9485.

48. Sivanandan, K.; Aathimanikandan, S. V.; Arges, C. G.; Bardeen, C. J.; Thayumanavan, S. Probing Every Layer in Dendrons. *J. Am. Chem. Soc.* **2005**, *127*, 2020–2021.

49. Sivanandan, K.; Sandanaraj, B. S.; Thayumanavan, S. Sequences in Dendrons and Dendrimers. *J. Org. Chem.* **2004**, *69*, 2937–2944.

50. Lee, C.; Lo, S.-T.; Lim, J.; da Costa, V. C. P.; Ramezani, S.; Öz, O. K.; Pavan, G. M.; Annunziata, O.; Sun, X.; Simanek, E. E. Design, Synthesis and Biological Assessment of a Triazine Dendrimer with Approximately 16 Paclitaxel Groups and 8 PEG Groups. *Mol. Pharm.* **2013**, *10*, 4452–4461.

51. Woller, E. K.; Cloninger, M. J. Mannose Functionalization of a Sixth Generation Dendrimer. *Biomacromolecules* **2001**, 2, 1052–1054.

52. Fuller, J. M.; Raghupathi, K. R.; Ramireddy, R. R.; Subrahmanyam, A. V.; Yesilyurt, V.; Thayumanavan, S. Temperature-Sensitive Transitions below LCST in Amphiphilic Dendritic Assemblies: Host–Guest Implications. *J. Am. Chem. Soc.* **2013**, *135*, 8947–8954.

CHAPTER 5

MOLECULAR WEIGHT EFFECT ON ENZYME-INDUCED DISASSEMBLY

5.1 Introduction

Stimuli-responsive drug delivery system has been a very hot topic in recent years because its controlled release characteristics have resulted in enhanced efficacy at the target site.[1] Most of these systems in the literature respond to stimuli such as temperature, pH, light, magnetic fields, and ionic strength.[2-8] An attractive class of responsive materials involve drug delivery systems that respond to biological stimuli such as enzymes and proteins,[9-13] because aberrations in enzymatic activity or protein concentration are the primary biological imbalances associated with many diseases.[14-16]

Amphiphilic assemblies generated from dendrimers exhibit unique advantages as stimuli-responsive systems, since these assemblies not only exhibit low critical aggregate concentrations, similar to those observed with polymers, but also provide the molecular weight control seen in small molecules.[17-19] In addition, dendrimers afford a high degree of control over functional group placements within a macromolecule.[20-25] These features allow for fundamentally understanding the structure–property correlations of stimuli-responsive systems. Enzyme-responsive dendrimers have been reported, wherein an enzymatic cleavage of a chemical bond triggers a cascade of events that results in the disassembly of the dendritic molecules.[26-30] In these cases, the molecules released in response to the enzymatic reaction were covalently attached to the dendrimer. Nevertheless, it would be more advantageous and impactful to develop strategies in which the guest molecules are non-covalently attached to the amphiphilic carriers, as these greatly

simplify the molecular design as well as avoid the possibility of depotentiating the guest molecules due to covalent modification.

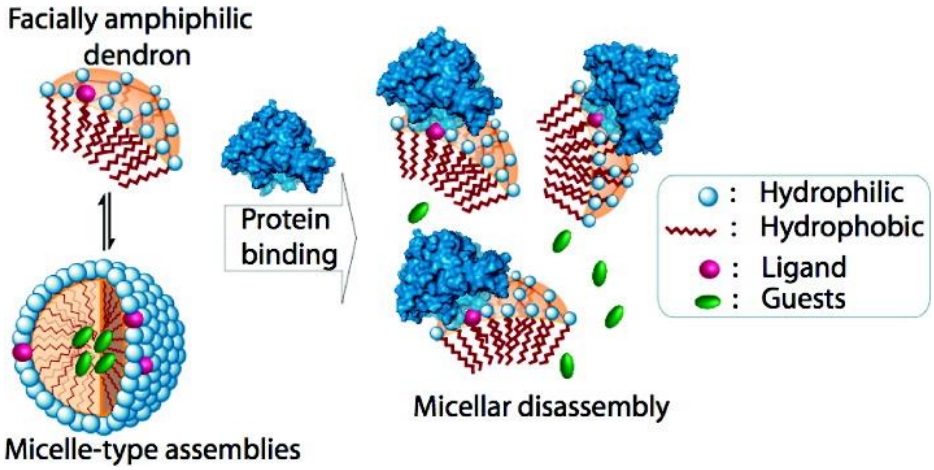

Figure 5.1: Schematic of protein-ligand binding-induced disassembly of dendritic micellar assemblies and resultant guest release.

Our research group has previously reported on such a possibility using facially amphiphilic dendrimers as the host carrier (Figure 1).[31] In this system, the guest molecules were non-covalently sequestered within the micellar assemblies formed by amphiphilic dendrimers. In the presence of the target enzyme, enzymatic cleavage of the substrate functionality caused the disassembly of micellar assemblies due to the change in the hydrophilic–lipophilic balance of the amphiphilic dendrimers and subsequent release of guest molecules. Note that the substrate functionalities for the enzyme are buried in the interior of micellar aggregates. It is critical that enzymes have access to these substrates, yet it is also important that the molecules exist mostly in the aggregate form in order to non-covalently encapsulate lipophilic guest molecules. In a later publication, we demonstrated that tunability in guest molecule release can be achieved by controlling the availability of the substrate functionalities in the dendrimers to the enzymes (Figure 2).[32]

In this work, we covalently cross-linked the micellar assemblies and found that guest molecule release rate decreased with increasing cross-linking degree. This is presumably because cross-linking reduced the accessibility of enzymes to their substrates. Besides cross-linking the assemblies, there are other factors that would dictate the availability of the substrate functionalities to the enzymes, such as HLB and molecular weight of the amphiphiles. In this chapter, we focus on effects of molecular weight of amphiphiles on the rate of enzyme-induced disassembly.

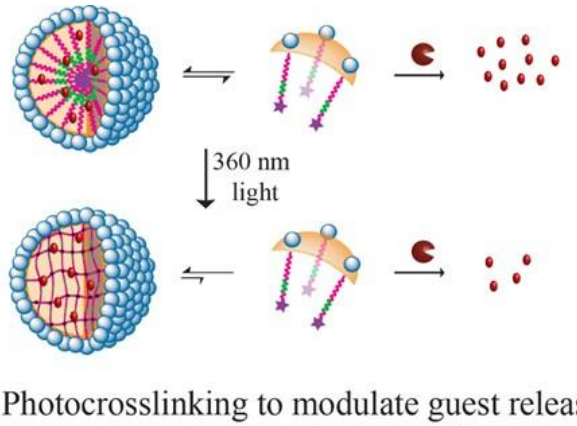

Figure 5.2: Schematic representation, showing the effect of aggregate–monomer equilibrium on enzymatic action.

5.2 Results and Discussions

5.2.1 Design and Synthesis

In order to investigate the effect of molecular weight on the rate of enzyme-induced disassembly, it is critical that the all the designed amphiphiles possess the same HLB. Even though different generations of facially amphiphilic dendrons exhibit very similar HLB, their amphiphilicities are not strictly the same, as dendrons of higher generation are slightly more hydrophobic. In addition, synthetic difficulty increases exponentially as the generation of dendron goes up. To address these challenges, we came up with new

molecular designs based on amphiphilic oligomers, which are schematically shown in Chart 1.

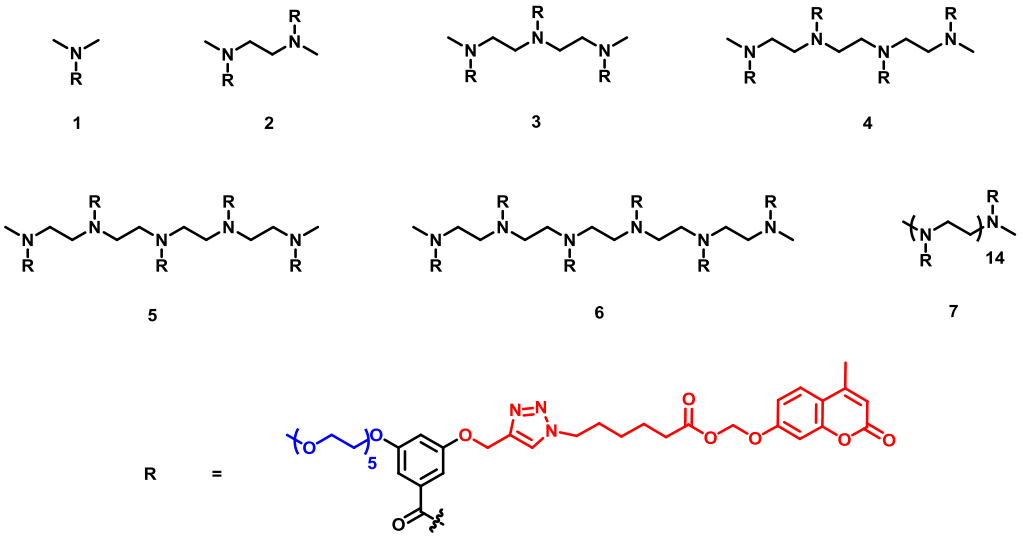

Chart 5.1: Molecular structures of amphiphilic oligomers.

In our design, we focused on variations from monomeric to hexameric amphiphiles in addition to a 14-meric amphiphile. We hypothesized that amphiphiles with higher molecular weight disassemble more slowly than their low molecular weight counterparts. This is because the residence time of amphiphiles in the aggregate form increases with their molecular weight. As a result, the accessibility of the target enzyme to their substrates is reduced, leading to a slower disassembly event. In all the amphiphiles, pentaethylene glycol monomethyl ether and alkylated coumarin moieties are attached to the meta-positions of a benzoyl building block as the hydrophilic and lipophilic moieties, respectively. This basic building block is then converted to an oligomer by attaching to the corresponding oligoamine scaffolds. Note that the coumarin moiety is bridged to the alkyl chain with an ester functionality which is a substrate for esterases. In the presence of target enzymes, the ester bond will be cleaved to afford a corresponding carboxylic acid and a

fluorescent moiety, 4-methylumbelliferone. Amphiphiles bearing a carboxylic acid end will lose their capabilities to form micellar aggregates due to the change in HLB. We will correlate the rates of enzyme-induced disassembly of each amphiphile with their rates of 4-methylumbelliferone release monitored by a fluorimeter.

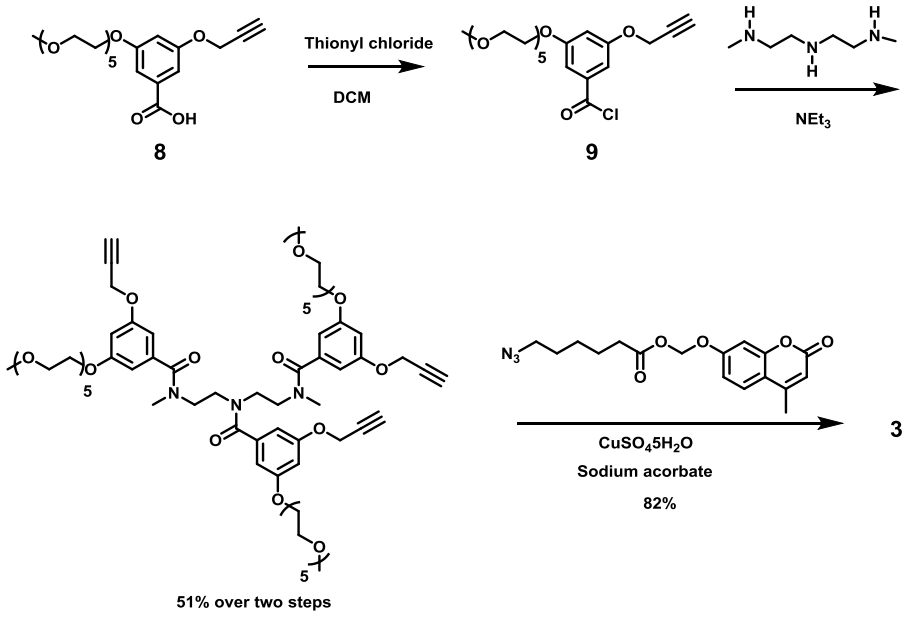

Scheme 5.1: Synthetic route for the amphiphilic oligomers, exemplified with the trimer **3**.

To synthesize the oligomers, the corresponding oligoamine was first treated with the benzoyl chloride molecule **9** under basic condition, followed by attachment of the enzyme substrate using Huisgen 1,3-dipolar cylcoaddition reaction, the so-called "click" chemistry. This is exemplified by the synthesis of trimer **3** in Scheme 1. It was necessary to conjugate the substrate in the final step as the ester functionality would not be able to sustain the acidic reaction condition used in generating the benzoyl chloride. Molecule **9** was synthesized following procedures reported by our group previously.[33] Briefly, 3,5-dihydroxybenzoic acid was first protected by converting to its ethyl ester, followed by the installation of a propargyl functionality on one of the phenolic groups through an alkylation

reaction in the presence of potassium carbonate, as shown in Scheme 2. Treatment of the mono-substituted product with penta(ethylene glycol) tosylate under similar alkylation conditions provided the precursor **10**. Hydrolysis of the ester group, followed by treatment with thionyl chloride, afforded the targeted benzoyl chloride molecule **9**.

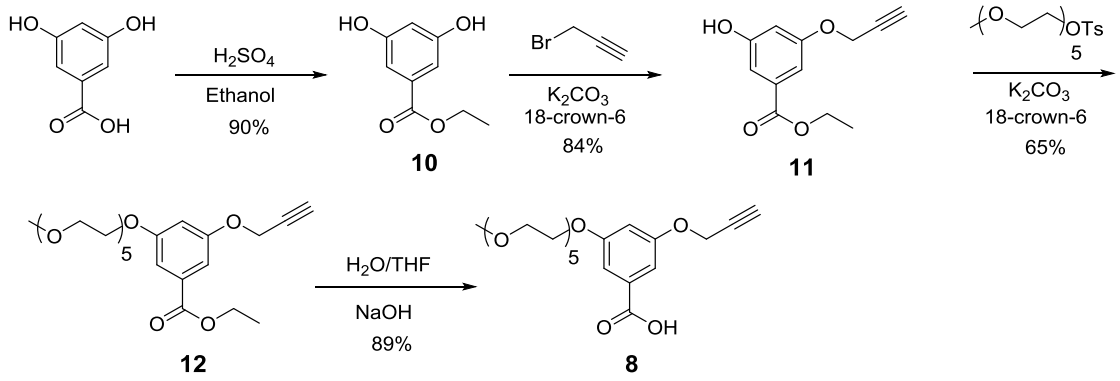

Scheme 5.2: Synthetic route of the amphiphilic building block **8**.

Note that all the oligomers in our design are terminated with secondary amines. This is necessary to ensure that all the oligomers have the same HLB. However, commercially available oligoamines are terminated with primary amines. To synthesize the target oligoamines, the corresponding commercially available oligoamines were first treated with 2-mesitylenesulfonyl chloride under a basic condition, followed by methylation of the two terminal amines with methyl iodide. Removal of the mestilenesulfonamide group using hydrobromic acid afforded the target oligoamines.

5.2.2 Critical Aggregation Concentration of Oligomers

To investigate the enzyme-induced disassembly rates, it is necessary to know above what concentrations each oligomer starts to form micelles. We first studied the micellar properties of oligomers using nile red as the spectroscopic probe. The CACs of dimer, trimer, tetramer and pentamer were found to be 66, 7.8, 2.0, and 0.74 μM, respectively.

The trend is reasonable as longer oligomers typically have lower CAC values. Attempt to measure the CAC of monomer was not successful presumably due to its relatively high CAC value, typical of small molecules.

5.2.3 Enzyme Kinetics Monitored by 4-Methylumbelliferone Release

Next, we were interested in measuring the enzymatic cleavage rates of oligomers. Since the enzymatic reaction releases a fluorescent by-product, 4-methylumbelliferone, we were able to monitor the enzymatic rates spectroscopically. For a precise comparison of the enzymatic cleavage rates, it was necessary that all the oligomer solutions contain the same concentration of enzyme substrate regardless of their molecular weights. In addition, all oligomer concentrations should be above their respective CACs. To meet these two criteria, we prepared oligomer solutions that contain 45 μM enzyme substrates, i.e. 15 μM trimer, 11.25 μM tetramer, and 9 μM pentamer. Note that dimer was not tested due to its high CAC at which other oligomers precipitated out. As shown in Figure 3, trimer had the fastest enzymatic rate over the first 10 hours. The rate of tetramer was slightly higher than that of pentamer. These preliminary results were consistent with our hypothesis that amphiphiles with higher molecular weight disassemble more slowly.

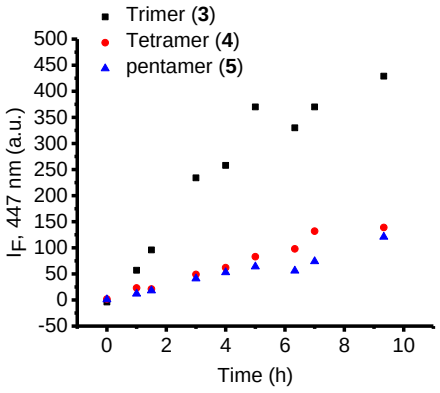

Figure 5.3: Enzymatic cleavage of amphiphilic oligomers (**3**, **4**, and **5**) monitored by fluorescence intensity of 4-methylumbelliferone (at 447 nm) over 9 hours.

To further support our hypothesis, we synthesized another set of oligomers with slightly more hydrophilicity. The new molecular design was also based on the OEG/coumarin amphiphile. However, we increased the length of OEG to endow the oligomers with a different HLB (Chart 2). The measurement of enzyme cleavage rates over 5 days showed a same trend that the release rate of 4-methylumbelliferone increased with increasing oligomer molecular weight. In these measurements, all oligomer solutions contained the same substrate concentration of 25 μM. Monomer and dimer concentrations were probably below their respective CACs which were not yet measured. Therefore, these preliminary data indicated the enzymatic cleavage rates of monomer and dimer in their monomeric forms rather than in micellar forms. Measurements of CAC and enzyme kinetics at a substrate concentration that is above each oligomer's respective CACs will be performed in the future.

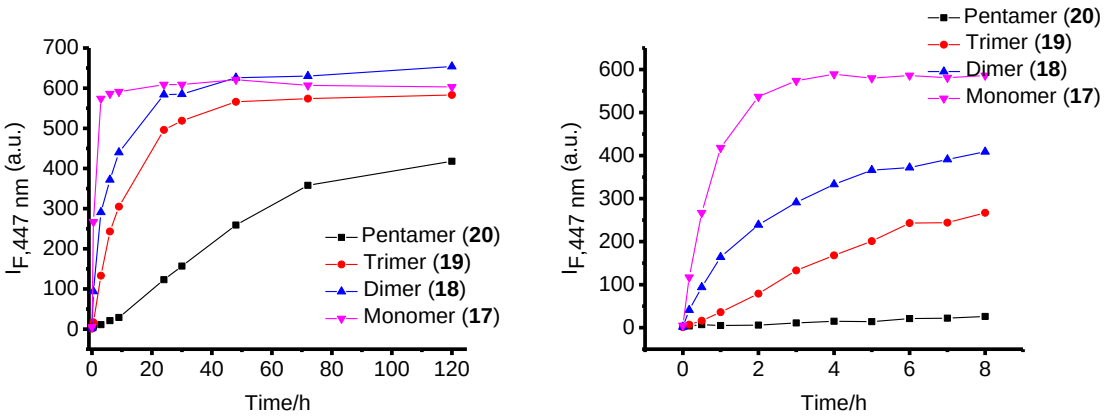

Figure 5.4: Enzymatic cleavage of amphiphilic oligomers monitored by fluorescence intensity of 4–methylumbelliferone (at 447 nm) (a) over 5 days, (b) over first 8 hours.

5.2.3 Enzyme Kinetics Monitored by Size Change

We will also study the enzyme kinetics of oligomers by monitoring their size change over time using DLS. Due to the conversion of the hydrophobic coumarin moiety

into a hydrophilic carboxylic acid by the enzymatic reaction, all oligomeric aggregates should decrease in size over time. Assessment of the rates of size evolution of each oligomer over time will allow us to compare the rates of enzyme-induced disassembly of each oligomer.

5.3 Summary

In summary, we have designed and synthesized two sets of oligomers that enabled us to investigate the effects of molecular weight on the rate of enzyme-induced disassembly. The preliminary fluorescent data showed that the rates of enzymatic cleavage decreased with increasing oligomer molecular weight, which is consistent with our hypothesis. This project is in still its preliminary stage and more experiments will be performed in the future. Overall, enzyme-induced disassembly systems developed by group have great potential in drug delivery applications. The study outlined in this chapter is very important in fundamentally understand those systems and a necessary step before we can extend them to *in vivo* applications.

5.4 Experimental

5.4.1 Materials and Methods

All chemicals and reagents were purchased from commercial sources and were used as received, unless otherwise mentioned. ^{1}H NMR spectra were recorded on a 400 MHz Bruker NMR spectrometer using the residual proton resonance of the solvent as the internal standard. Chemical shifts are reported in parts per million (ppm). Fluorescence spectra were obtained from a JASCO FP-6500 spectrofluorometer. MALDI mass spectra data were obtained at the University of Massachusetts mass spectrometry center. Oligomers and

cliclable coumarin substrate were were prepared according to previously reported procedures[32, 33].

5.4.2 Synthetic Schemes and Procedures

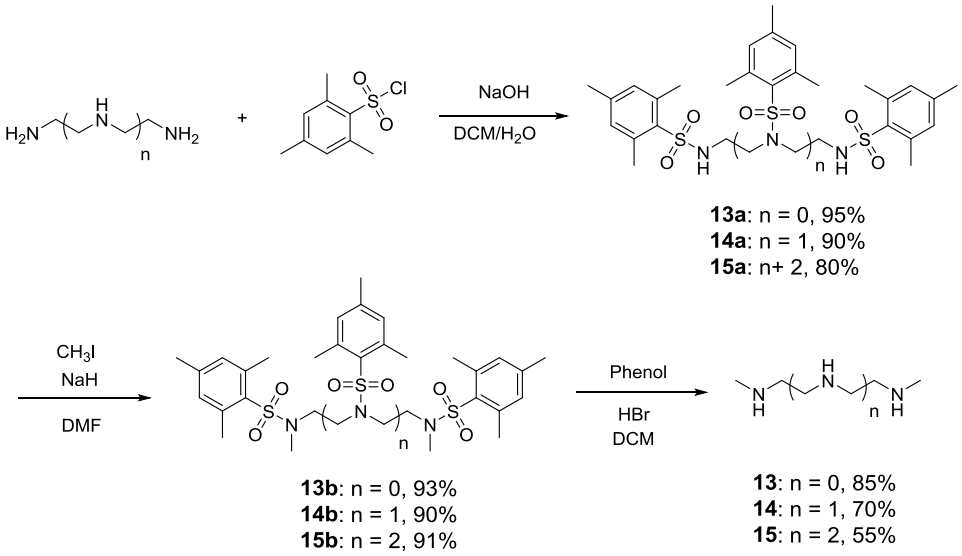

Scheme 5.3: Synthetic route of oligoamines.

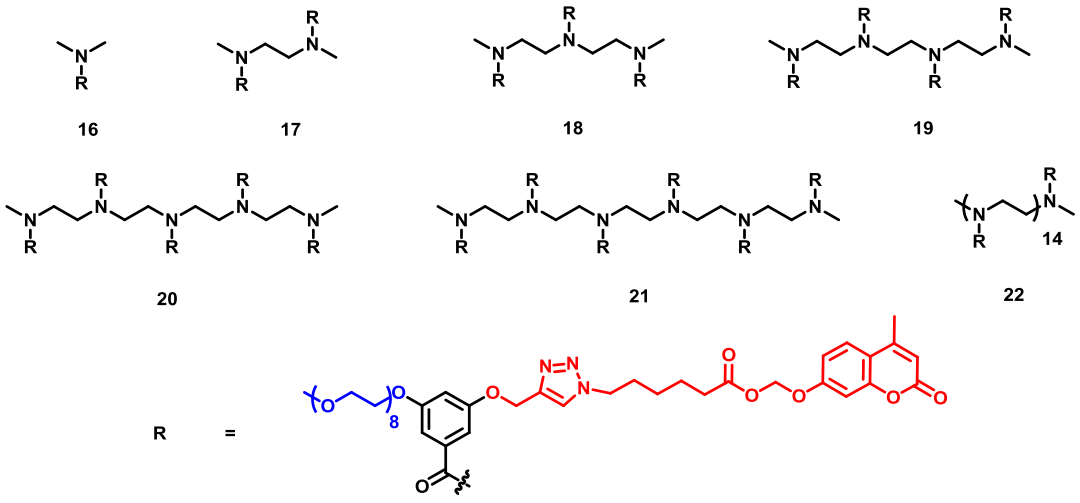

Chart 5.2: Molecular structures of amphiphilic oligomers (OEG = 8).

Synthesis of compound 13a:

To a solution of diethylenetriamine (1 equivalent) and sodium hydroxide (3.1 equivalent) in water at 0 ^{o}C was added a solution of 2-Mesitylenesulfonyl chloride (3.1 equivalent) in dichloromethane. The mixture was stirred at room temperature overnight. The aqueous layer was discarded and the organic layer was washed with brine twice. The organic layer was dried over Na_2SO_4 and evaporated to dryness. The crude product was purified by silica gel column chromatography using mixture of hexane/ethyle acetate as eluent. Yield: 95%. ^{1}H NMR (400MHz, $CDCl_3$) δ: 6.92 (s, 6H), 4.91 (bs, 2H), 3.34 (m, 4H), 2.96 (m, 4H), 2.55 (s, 12H), 2.51 (s, 6H), 2.30 (s, 9H).

Synthesis of compound 14a:

To a solution of triethylenetetraamine (1 equivalent) and sodium hydroxide (4.2 equivalent) in water at 0 ^{o}C was added a solution of 2-Mesitylenesulfonyl chloride (4.5 equivalent) in dichloromethane. The mixture was stirred at room temperature overnight. The aqueous layer was discarded and the organic layer was washed with brine twice. The organic layer was dried over Na_2SO_4 and evaporated to dryness. The crude product was purified by silica gel column chromatography using mixture of hexane/ethyle acetate as eluent. Yield: 90%. ^{1}H NMR (400MHz, $CDCl_3$) δ: 6.92 (s, 8H), 5.20 (t, 2H), 3.33 (s, 4H), 3.28 (t, 4H), 2.92 (q, 4H), 2.55 (s, 12H), 2.49 (s, 12H), 2.30 (m, 12H).

Synthesis of compound 15a:

To a solution of tetraethylenepentamine (1 equivalent) and sodium hydroxide (5.2 equivalent) in water at 0 ^{o}C was added a solution of 2-Mesitylenesulfonyl chloride (5.5 equivalent) in dichloromethane. The mixture was stirred at room temperature overnight. The aqueous layer was discarded and the organic layer was washed with brine twice. The

organic layer was dried over Na_2SO_4 and evaporated to dryness. The crude product was purified by silica gel column chromatography using mixture of hexane/ethyle acetate as eluent. Yield: 80%. ^{1}H NMR (400MHz, $CDCl_3$) δ: 6.90 (s, 10H), 5.0 (t, 2H), 3.30 (s, 8H), 3.21 (t, 4H), 2.89 (m, 4H), 2.40-2.52 (m, 30H), 2.25-2.32 (m, 15H).

Synthesis of compound 13b, 14b and 15b:

To a solution of 13a, 13a or 14a (1 equivalent) in dry DMF was added sodium hydride (3 equivalent) under argon atmosphere. The mixture was allowed to stir for 30 min, followed by addition of methyl iodide (2.5 equivalent). The reaction mixture was stirred at room temperature overnight under argon atmosphere. The reaction was quenched with water. The product was precipitated by adding excess amount of water. The precipitates were filtered and washed with hot water multiple times. The precipitates were dried to yield white solids.

*Compound **13b***, 93%. ^{1}H NMR (400MHz, $CDCl_3$) δ: 6.92 (s, 6H), 3.37 (m, 4H), 3.20 (m, 4H), 2.68 (s, 6H), 2.52 (m 18H), 2.30 (m, 9H).

*Compound **14b***, 90%. ^{1}H NMR (400MHz, $CDCl_3$) δ: 6.92 (s, 8H), 3.30 (m, 8H), 3.15 (m, 4H), 2.63 (s, 6H), 2.50 (s, 24H), 2.29 (m, 12H).

*Compound **15b***, 91%. ^{1}H NMR (400MHz, $CDCl_3$) δ: 6.90 (s, 10H), 3.31 (m, 4H), 3.22 (m, 8H), 3.12 (m, 4H), 2.62 (s, 6H), 2.40-2.52 (m, 30H), 2.22-2.31 (m, 15H).

Synthesis of compound 13, 14 and 15:

To a solution of **13b**, **14b**, or **15b** (1 equivalent) and phenol (45 equivalent) in dichloromethane was slowly added hydrobromic acid (47 equivalent). The mixture was stirred at room temperature for 1 day. Water was added to the reaction mixture and the aqueous layer was washed with dichloromethane 3 times. The aqueous portion was then

basified to pH 14 using 1 M NaOH solution and extracted with dichloromethane 6 times. The combined organic layer was dried with Na_2SO_4 and evaporated to dryness to yield the product.

*Compound **13***, 85%. ^{1}H NMR (400MHz, $CDCl_3$) δ: 2.62-2.75 (m, 8H), 2.41 (s, 6H), 1.42 (bs, 3H).

*Compound **14** (hydrochloride salt)*, 70%. ^{1}H NMR (400MHz, D_2O) δ: 3.42-3.55(m, 12H), 2.78 (s, 6H).

*Compound **15***, 55%. ^{1}H NMR (400MHz, $CDCl_3$) δ: 2.63-2.75 (m, 16H), 2.41 (s, 6H), 1.42 (bs, 5H).

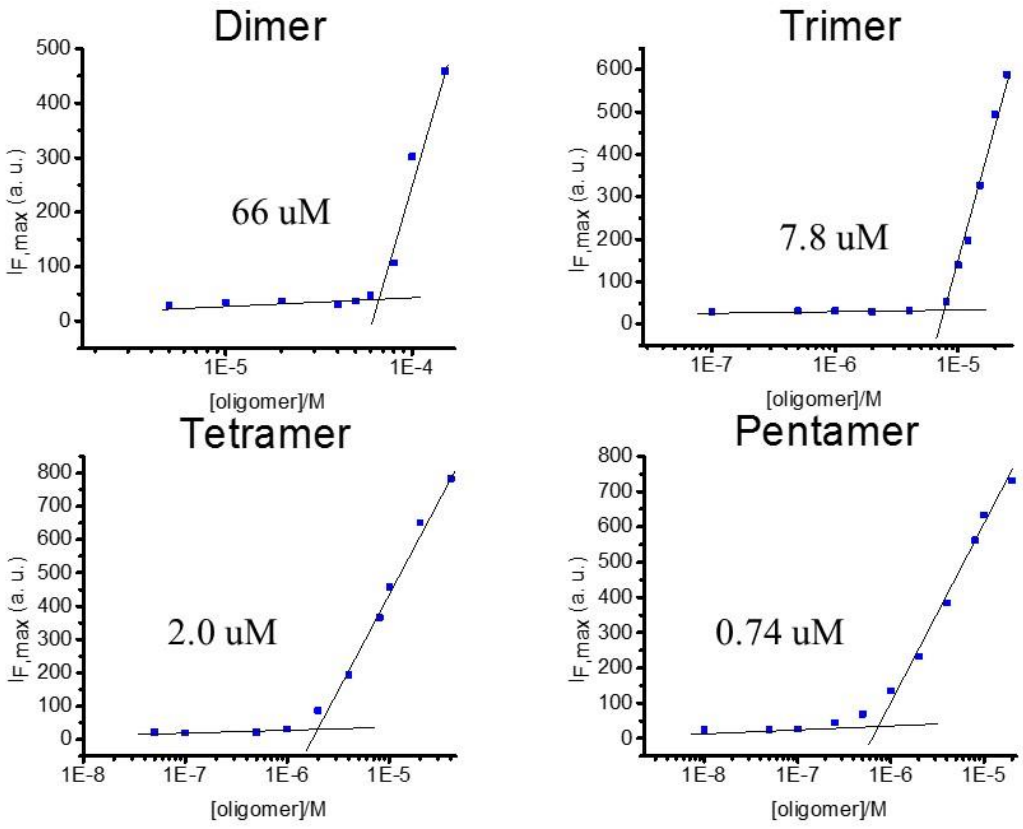

Figure 5.5: The CMC plots for dimer (**2**), trimer (**3**), tetramer (**4**), and pentamer (**5**).

5.5 References

1. Rijcken, C. J. F.; Soga, O.; Hennink, W. E.; van Nostrum, C. F. J. Triggered Destabilisation of Polymeric Micelles and Vesicles by Changing Polymers Polarity: An Attractive Tool for Drug Delivery. *J. Control. Release* **2007**, *120*, 131–148.

2. Almutairi, A.; Guillaudeu, S. J.; Berezin, M. Y.; Achilefu, S.; Fre´chet, J. M. J. Biodegradable pH-Sensing Dendritic Nanoprobes for Near-Infrared Fluorescence Lifetime and Intensity Imaging. *J. Am. Chem. Soc.* **2008**, *130*, 444–445.

3. Bae, Y.; Nishiyama, N.; Kataoka, K. In Vivo Antitumor Activity of the Folate-Conjugated pH-Sensitive Polymeric Micelle Selectively Releasing Adriamycin in the Intracellular Acidic Compartments. *Bioconjugate Chem.* **2007**, *18*, 1131–1139.

4. Wang, C.; Tam, K. C.; Jenkins, R. D.; Tan, C. B. Interactions between Methacrylic Acid/Ethyl Acrylate Copolymers and Dodecyltrimethylammonium Bromide. *J. Phys. Chem. B* **2003**, *107*, 4667–4675.

5. Lecommandoux, S.; Sandre, O.; Checot, F.; Rodriguez-Hernandez, J.; Perzynski, R. Magnetic Nanocomposite Micelles and Vesicles. *Adv. Mater.* **2005**, *17*, 712–718.

6. Schmaljohann, D. Thermo- and pH-responsive Polymers in Drug Delivery. *Adv. Drug Deliv. Rev.* **2006**, *58*, 1655–1670.

7. He, J.; Tong, X.; Zhao, Y. Photoresponsive Nanogels Based on Photocontrollable Cross-Links. *Macromolecules* **2009**, *42*, 4845–4852.

8. Yamaguchi S.; Matsumoto, S.; Ishizuka, K.; Iko, Y.; Tabata, K. V.; Arata, H. F.; Fujita, H.; Noji, H.; Hamachi, I. Thermally Responsive Supramolecular Nanomeshes for On/Off Switching of the Rotary Motion of F_1-ATPase at the Single-Molecule Level. *Chem. Eur. J.* **2008**, *14*, 1891–1896.

9. Burke, M. D.; Park, J. O.; Srinivasarao, M.; Khan, S. A. A Novel Enzymatic Technique for Limiting Drug Mobility in a Hydrogel Matrix *J. Control. Release* **2005**, *104*, 141–153.

10. Thornton, P. D.; McConnell, G.; Ulijn, R. V. Enzyme Responsive Polymer Hydrogel Beads. *Chem. Commun.* **2005**, 5913–5915.

11. Amir, R. J.; Zhong, S.; Pochan, D. J.; Hawker, C. J. Enzymatically Triggered Self-Assembly of Block Copolymers. *J. Am. Chem. Soc.* **2009**, *131*, 13949–13951.

12. Saavedra, J. E.; Shami, P. J.; Wang, L. Y.; Davies, K. M.; Booth, M. N.; Citro, M. L.; Keefer, L. K. Esterase-Sensitive Nitric Oxide Donors of the Diazeniumdiolate Family: In Vitro Antileukemic Activity. *J. Med. Chem.* **2000**, *43*, 261–269.

13. Azagarsamy, M. A.; Yesilyurt, V.; Thayumanavan, S. Disassembly of Dendritic Micellar Containers Due to Protein Binding. *J. Am. Chem.Soc.* **2010**, *132*, 4550–4551.

14. Wilson, K. E.; Langdon, S. P.; Lessells, A. M.; Miller, W. R. Expression of the Extracellular Matrix Protein Tenascin in Malignant and Benign Ovarian Tumours. *Br. J. Cancer* **1996**, *74*, 999–1004.

15. Samantaray, S.; Sharma, R.; Chattopadhyaya, T. K.; Gupta, S. D.; Ralhan, R. Increased Expression of MMP-2 and MMP-9 in Esophageal Squamous Cell Carcinoma. *J. Cancer Res. Clin. Oncol.* **2004**, *130*, 37–44.

16. Klein, H. L. The Consequences of Rad51 Overexpression for Normal and Tumor Cells. *DNA Repair* **2008**, *7*, 686–693.

17. Newkome, G. R.; Yao, Z.; Baker, G. R.; Gupta, V. K. Micelles. Part 1. Cascade Molecules: a New Approach to Micelles. A [27]-Arborol. *J. Org. Chem.* **1985**, *50*, 2003–2004.

18. Hawker, C. J.; Wooley, K. L.; Fréchet, J. M. J. Unimolecular Micelles and Globular Amphiphiles: Dendritic Macromolecules as Novel Recyclable Solubilization Agents. *J. Chem. Soc., Perkin Trans. 1* **1993**, 1287–1297.

19. Tomalia, D. A.; Baker, H.; Dewald, J.; Hall, M.; Kallos, G.; Martin, S.; Roeck, J.; Ryder, J.; Smith, P. A New Class of Polymers: Starburst-Dendritic Macromolecules. *Polym. J.* **1985**, *17*, 117–132.

20. Bo, Z.; Schäfer, A.; Franke, P.; Schlüter, a. D. A Facile Synthetic Route to a Third-Generation Dendrimer with Generation-Specific Functional Aryl Bromides. *Org. Lett.* **2000**, *2*, 1645–1648.

21. Azagarsamy, M. A.; Krishnamoorthy, K.; Sivanandan, K.; Thayumanavan, S. Site-Specific Installation and Study of Electroactive Units in Every Layer of Dendrons. *J. Org. Chem.* **2009**, *74*, 9475–9485.

22. Sivanandan, K.; Aathimanikandan, S. V.; Arges, C. G.; Bardeen, C. J.; Thayumanavan, S. Probing Every Layer in Dendrons. *J. Am. Chem. Soc.* **2005**, *127*, 2020–2021.

23. Sivanandan, K.; Sandanaraj, B. S.; Thayumanavan, S. Sequences in Dendrons and Dendrimers. *J. Org. Chem.* **2004**, *69*, 2937–2944.

24. Lee, C.; Lo, S.-T.; Lim, J.; da Costa, V. C. P.; Ramezani, S.; Öz, O. K.; Pavan, G. M.; Annunziata, O.; Sun, X.; Simanek, E. E. Design, Synthesis and Biological Assessment of a Triazine Dendrimer with Approximately 16 Paclitaxel Groups and 8 PEG Groups. *Mol. Pharm.* **2013**, *10*, 4452–4461.

25. Woller, E. K.; Cloninger, M. J. Mannose Functionalization of a Sixth Generation Dendrimer. *Biomacromolecules* **2001**, 2, 1052–1054.

26. Amir, R. J.; Shabat, D. Self-Immolative Dendrimer Biodegradability by Multi-Enzymatic Triggering. *Chem. Commun.* **2004**, 1614–1615.

27. de Groot, F. M. H.; Albrecht, C.; Koekkoek, R.; Beusker, P. H.; Scheeren, H. W. "Cascade-Release Dendrimers" Liberate All End Groups upon a Single Triggering Event in the Dendritic Core. *Angew. Chem. Int. Ed.* **2003**, *42*, 4490–4494;

28. Avital-Shmilovici, M.; Shabat, D. Self-Immolative Dendrimers: A Distinctive Approach to Molecular Amplification. *Soft Matter* **2010**, *6*, 1073–1080.

29. Niederhafner, P.; Se-bestik, J.; Jezek, J. Glycopeptide Dendrimers. Part II. *J. Pept. Sci.* **2008**, *14*, 44–65.

30. Bensel, N.; Reymond, M. T.; Reymond, J. L. Pivalase Catalytic Antibodies: Towards Abzymatic Activation of Prodrugs. *Chem. Eur. J.* **2001**, *7*, 4604–4612.

31. Azagarsamy, M. A.; Sokkalingam, P.; Thayumanavan, S. Enzyme-Triggered Disassembly of Dendrimer-Based Amphiphilic Nanocontainers. *J. Am. Chem. Soc.* **2009**, *131*, 14184–14185.

32. Raghupathi, K. R.; Azagasarmy, M. A.; Thayumanavan, S. Guest Release Control in Enzyme-Sensitive Amphiphilic Dendrimer-based Nanoparticles through Photochemical Crosslinking. *Chem. Eur. J.* **2011**, *17*, 11752–11760.

33. Wang, F.; Klaikherd, A.; Thayumanavan, S. Temperature Sensitivity Trends and Multi-Stimuli-Sensitive Behavior in Amphiphilic Oligomers. *J. Am. Chem. Soc.* **2011**, *133*, 13496–13503.

CHAPTER 6

SUMMARY AND FUTURE DIRECTIONS

This dissertation describes the design and synthesis of supramolecular assemblies and their applications in bio-sensing and drug delivery. Various materials, including surfactants, amphiphilic polymers and amphiphilic dendrimers, were utilized to form the stimuli responsive assemblies. We designed amphiphiles that self-assembled into micellar aggregates with different stabilities and demonstrated how these subtle differences are important in affecting analyte and assembly interaction. We also focused on fundamental understanding of the structure-property relationships of these materials.

6.1 Surface Functionalizable Polymer Nanoparticles

In Chapter 2, we designed and characterized a simple and versatile polymer nanoparticle platform that: (*i*) displays a versatile functional group on its surface, which can be further manipulated with a variety of complementary reactive moieties; (*ii*) is capable of non-covalently binding hydrophobic guest molecules; (*iii*) afford size tunability by simply altering the salt types and concentrations of the solution or the pH at which the nanoparticle is synthesized; (*iv*) has a very high percentage of the accessible surface moieties at smaller sizes. The nanoparticles were formed by the self-assembly of an amphiphilic random copolymer containing two orthogonally reactive functional groups, followed by cross-linking of the hydrophobic core. Two molecular designs were proposed and tested. The first design was quite robust and worked well. However, we encounter several problems with our second molecular design. Firstly, UV cross-linking of the hydrophobic coumarin moiety also caused cleavage of sulfo-NP. Secondly, hydrolysis rate

of sulfo-NP was high.

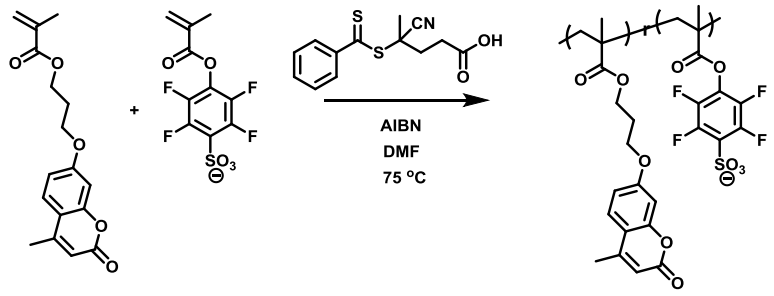

Scheme 6.1: Synthesis of sulfo-TFP containing amphiphilic random copolymer.

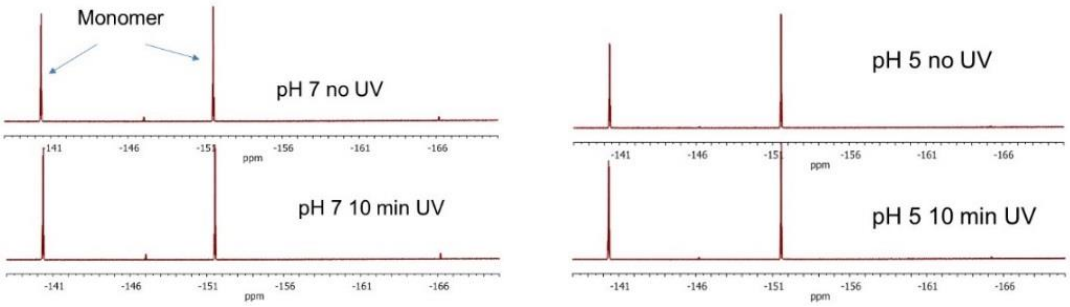

Figure 6.1: NMR spectra of sulfo-TFP monomer with and without UV irradiation at pH 7 (left), and pH 5 (right).

To address the above issues, we propose an alternative amphiphilic polymer design. Instead of sulfo-NP, we will use tetrafluoro-4-sulfophenyl ester (sulfo-TFP) as the hydrophilic activated ester group while keeping the same coumarin moiety. Similar to sulfo-NP, sulfo-TFP is a charged activated ester that is reactive toward primary amines. Although sulfo-TFP is also a phenyl ester which can still be susceptible to Photo-Fries reaction, it does not contain a nitro group, thus its absorption profile might not overlap so much with the irradiation wavelength used to cross-link the nanoparticles. To test its UV sensitivity, we UV irradiated the sulfo-TFP monomer for 10 minutes at pH 5 and 7, respectively. The ^{19}F NMR spectra showed no discernable degradation or side products. In addition, we also tested the hydrolysis of the sulfo-TFP monomer using proton NMR. Only

a little hydrolysis product was observed after 40 hours of incubation.

Besides varying the hydrophilic component of the amphiphilic random copolymer, we can design amphiphilic random copolymers with different hydrophobic components. For instance, we can cross-link the polymer nanoparticles using disulfide chemistry or azide-alkyne Huisgen cycloaddition. These two reactions should be compatible with primary-activated ester reaction used for post-functionalization. Overall, the simplicity and versatility of the surface functionalizable soft nanoparticles with host-guest capabilities will have implications in a variety of applications from materials to biology. Incorporating stimuli-responsive characteristics and expanding this method to a broader range of functional groups are among the current foci in our laboratory.

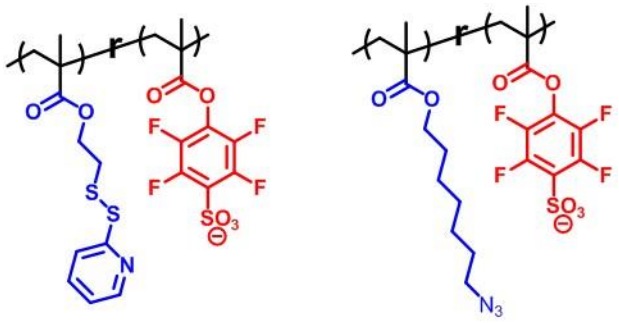

Chart 6.1: Molecular structures of amphiphilic random copolymers based on disulfide and "click" chemistry.

6.2 A Supramolecular Dissociation Strategy for Protein Sensing

In Chapter 3, we developed a new supramolecular dissociation based sensing strategy to detect specific proteins with turn-on fluorescence signals. The sensing approach is based on non-covalent encapsulation of ligand-tethered fluorophore/ quencher pair in the micellar assemblies, where the fluorescence is in the 'off' state. Protein-binding induced dissociation of the ligand-fluorophore combination away from micelle turns the

fluorescence to the 'on' state, since its proximity with the quencher is compromised. The versatility of this approach lies in its simplicity: (*i*) well-established and commercially available surfactants can be used; (*ii*) other than being hydrophobic, the fluorophore-ligand combination does not have to exhibit inherent self-assembly features and therefore does not require extensive molecular design; (*iii*) the strategy is conveniently extendable to any fluorophore-quencher combinations to modulate the colour of detection; and (*iv*) the approach is potentially extendable to most target protein analytes. We showed the sensitivity of our design was affected by both the type and concentration of amphiphiles utilized to form the micelles.

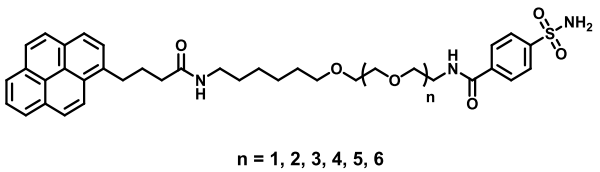

Chart 6.2: Molecular structure of probes with different HLBs.

In addition to varying the container property of the micellar host, it is also possible to improve the sensitivity by engineering the guest molecule, i.e. the probe. Here, we propose that the sensitivity can be improved by designing probes with the optimal HLB. As we mentioned earlier in Chapter 3, the partition of probe between micellar core and the bulk solution is crucial for its binding to the target protein. A probe with too much hydrophobicity would predominantly stay inside the micellar core and not be able to access the target protein. On the other hand, a probe with too much hydrophilicity would predominantly dissolved in the bulk medium and produce a high background signal since it is far away from the hydrophobic quencher residing in the micellar core. Therefore, the HLB of probes is crucial in affecting the sensitivity of the sensor. In figure 3, we probe

probes with different HLBs by incorporating different oligoethylene glycol units between the ligand and fluorophore. We anticipate that by incorporating these probes and the quencher in a same micellar assembly respectively, we will create a series of sensors with different sensitivities. These will allow us to fundamentally understand the correlation between HLB of the probe and its sensitivity.

6.3 Enzyme-Induced Disassembly

In Chapter 4, we showed that: (*i*) by incorporating fluorine-containing hydrophobic units within amphiphilic aggregates of facially amphiphilic dendrons, the ^{19}F-NMR signal can be made weak and broad; (*ii*) enzyme-induced cleavage of the fluorinated moiety results in the spontaneous generation of a strong and sharp signal; (*iii*) the signal generation is specific to the enzyme for which the linker is engineered; (*iv*) the equilibrium concentration of the unimer in the unimer-aggregate equilibrium plays a key role in the kinetics of signal generation; (*v*) the dendron probe is capable of detecting enzyme concentrations in the nanomolar range. The activatable probe described and the structural factors that control the signal generation are sufficiently general that this method can be conveniently elaborated to other enzymes.

In Chapter 5, we continued to investigate factors that affect enzyme-induced disassembly in addition to the HLB of a molecule. We designed and synthesized a series of amphiphilic oligomers with the same HLB but different molecular weights and compared their rates of enzyme-induced disassembly. While the enzyme-induced disassembly represents a covalent and irreversible modification of the hydrophilic−lipophilic balance, noncovalent interaction-based disassembly is also of great interest, as a large number of proteins that are critical in biological signal transduction

events do not have known enzymatic activity. Our group has previously introduced a protein-induced disassembly system based on amphiphilic dendrons. Similar to enzyme-induced disassembly[1], the unimer and aggregate equilibrium is also crucial for the disassembly of aggregates caused by protein binding. If we were to design a protein-binding-induced disassembly system based on an amphiphilic polymer, it would likely fail since the residence time of an amphiphile in aggregate state increases with its molecular weight.

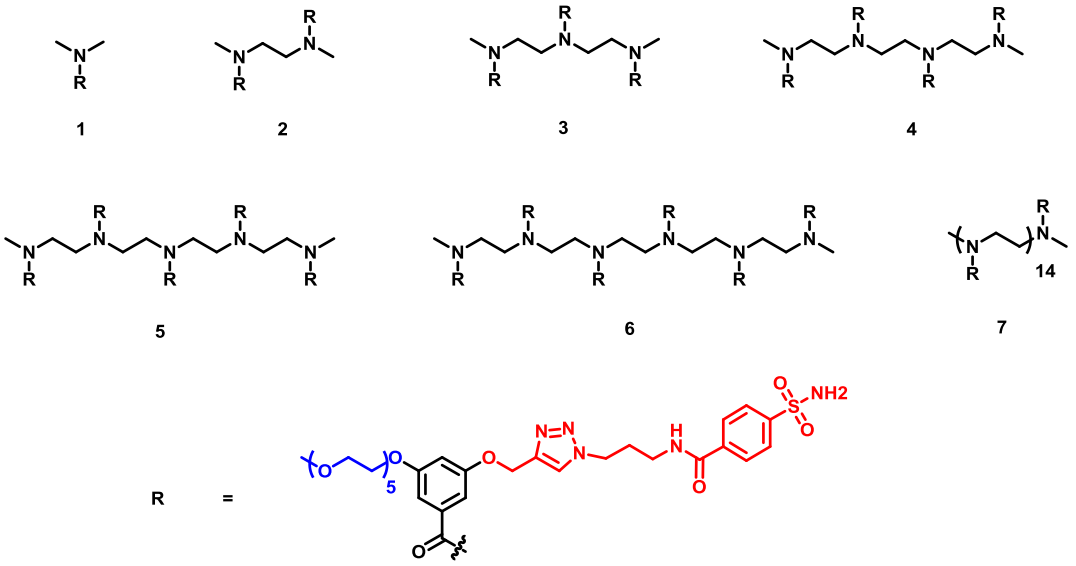

Chart 6.3: Molecular structures of sulfonamide-containing amphiphilic oligomers.

To test the effects of molecular weight on protein-binding-induced disassembly, we propose similar oligomer designs by replacing the enzyme substrate with a protein ligand. These amphiphilic oligomers should self-assemble into micelles and capable of sequestering lipophilic dye molecules. We will investigate the rate of protein-binding-induced disassembly by monitoring the rate of dye release caused by protein binding. Overall, enzyme/protein-induced disassembly systems are currently limited to amphiphilic dendrons and surfactants. Fundamental understanding of those systems is a necessary step

before we can generalize them to other materials, such as polymers, and use them for *in vivo* applications.

6.4 Reference

1. Azagarsamy, M.; Yesilyurt, V.; Thayumanavan, S. Disassembly of Dendritic Micellar Containers due to Protein Binding. *J. Am. Chem. Soc.* **2010**, *132*, 4550–4551.

BIBLIOGRAPHY

Aathimanikandan, S. V.; Savariar, E. N.; Thayumanavan, S. Temperature-Sensitive Dendritic Micelles. *J. Am. Chem. Soc.* **2005**, *127*, 14922–14929.

Adams, M.; Joyce, L.; Anslyn, E. V. *Supramolecular Chemistry: From Molecules to Nanomaterials*; Gale, P. A.; Steed, J. W., Eds.; Wiley: Chichester, 2012, Vol. 2, pp.709–732.

Ahrens, E. T.; Flores, R.; Xu, H.; Morel, P. A. In Vivo Imaging Platform for Tracking Immunotherapeutic Cells. *Nat. Biotechnol.* **2005**, *23*, 983–987.

Alarcon, C. d. l. H.; Pennadam, S.; Alexander, C. Stimuli Responsive Polymers for Biomedical Applications. *Chem. Soc. Rev.* **2005**, *34*, 276–285.

Albert, K. J.; Lewis, N. S.; Schauer, C. L.; Sotzing, G. A.; Stitzel, S. E.; Vaid, T. P.; Walt, D. R. Cross-Reactive Chemical Sensor Arrays. *Chem. Rev.* **2000**, *100*, 2595–2626.

Almutairi, A.; Guillaudeu, S. J.; Berezin, M. Y.; Achilefu, S.; Fre´chet, J. M. J. Biodegradable pH-Sensing Dendritic Nanoprobes for Near-Infrared Fluorescence Lifetime and Intensity Imaging. *J. Am. Chem. Soc.* **2008**, *130*, 444–445.

Alterio, V.; Di Fiore, A.; D'Ambrosio, K.; Supuran, C. T.; De Simone, G. Multiple Binding Modes of Inhibitors to Carbonic Anhydrases: How to Design Specific Drugs Targeting 15 Different Isoforms? *Chem. Rev.* **2012**, *112*, 4421–4468.

Amado Torres, D.; Garzoni, M.; Subrahmanyam, A.; Pavan, G. M.; Thayumanavan, S. Protein–Triggered Supramolecular Disassembly: Insights Based on Variations in Ligand Location in Amphiphilic Dendrons. *J. Am. Chem. Soc.* **2014**, *136*, 5385–5399.

Amir, R. J.; Shabat, D. Self-Immolative Dendrimer Biodegradability by Multi-Enzymatic Triggering. *Chem. Commun.* **2004**, 1614–1615.

Amir, R. J.; Zhong, S.; Pochan, D. J.; Hawker, C. J. Enzymatically Triggered Self-Assembly of Block Copolymers. *J. Am. Chem. Soc.* **2009**, *131*, 13949–13951.

Arima, H.; Motoyama, K.; Higashi, T. Polyamidoamine Dendrimer Conjugates with Cyclodextrins as Novel Carriers for DNA, shRNA and siRNA. *Pharmaceutics* **2012,** *4*, 130–148.

Astruc, D.; Boisselier, E.; Ornelas, C. Dendrimers Designed for Functions: From Physical, Photophysical, and Supramolecular Properties to Applications in Sensing, Catalysis, Molecular Electronics, Photonics, and Nanomedicine. *Chem. Rev.* **2010**, *110*, 1857–1959.

Avital-Shmilovici, M.; Shabat, D. Self-Immolative Dendrimers: A Distinctive Approach to Molecular Amplification. *Soft Matter* **2010**, *6*, 1073–1080.

Azagarsamy, M. A.; Krishnamoorthy, K.; Sivanandan, K.; Thayumanavan, S. Site-Specific Installation and Study of Electroactive Units in Every Layer of Dendrons. *J. Org. Chem.* **2009**, *74*, 9475-9485.

Azagarsamy, M. A.; Sokkalingam, P.; Thayumanavan, S. Enzyme-Triggered Disassembly of Dendrimer-Based Amphiphilic Nanocontainers. *J. Am. Chem. Soc.* **2009**, *131*, 14184–14185.

Azagarsamy, M. A.; Yesilyurt, V.; Thayumanavan, S. Disassembly of Dendritic Micellar Containers Due to Protein Binding. *J. Am. Chem. Soc.* **2010**, *132*, 4550–4551.

Bae, Y.; Nishiyama, N.; Kataoka, K. In Vivo Antitumor Activity of the Folate-Conjugated pH-Sensitive Polymeric Micelle Selectively Releasing Adriamycin in the Intracellular Acidic Compartments. *Bioconjugate Chem.* **2007**, *18*, 1131–1139.

Baldwin, R. L. How Hofmeister Ion Interactions Affect Protein Stability. *Biophys. J.* **1996**, *71*, 2056–2063.

Bandyopadhyay, P.; Ghosh, A. K. Reversible Fluorescence Quenching by Micelle Selective Benzophenone-Induced Interactions between Brij Micelles and Polyacrylic Acids: Implications for Chemical Sensors. *J. Phys. Chem. B* **2010**, *114*, 11462–11467.

Behr, J. -P. *The Lock-and-Key Principle*; The State of the Art – 100 Years On; John Wiley & Sons: Chichester, U.K., 2008.

Bell, C. A.; Smith, S. V; Whittaker, M. R.; Whittaker, A. K.; Gahan, L. R.; Monteiro, M. J. Surface-Functionalized Polymer Nanoparticles for Selective Sequestering of Heavy Metals. *Adv. Mater.* **2006,** *18*, 582–586.

Bellus, D. *Advances in Photochemistry*; John Wiley & Sons: Chichester, 1971; Vol. 8, pp. 109-159.

Bensel, N.; Reymond, M. T.; Reymond, J. L. Pivalase Catalytic Antibodies: Towards Abzymatic Activation of Prodrugs. *Chem. Eur. J.* **2001**, *7*, 4604–4612.

Bharathi, P.; Zhao, H. D.; Thayumanavan, S. Toward Globular Macromolecules with Functionalized Interiors: Design and Synthesis of Dendrons with an Interesting Twist. *Org. Lett.* **2001**, *3*, 1961−1964.

Bloembergen, N.; Purcell, E. M.; Pound, R. V. Relaxation Effects in Nuclear Magnetic Resonance Absorption. *Phys. Rev.* **1948**, *73*, 679–679.

Bo, Z.; Schäfer, A.; Franke, P.; Schlüter, a. D. A Facile Synthetic Route to a Third-Generation Dendrimer with Generation-Specific Functional Aryl Bromides. *Org. Lett.* **2000**, *2*, 1645-1648.

Bosman, A. W.; Janssen, H. M.; Meijer, E. W. About dendrimers: Structure, Physical Properties, and Applications. *Chem. Rev.* **1999**, *99*, 1665−1688.

Brannon-Peppas, L.; Blanchette, J. O. Nanoparticle and Targeted Systems for Cancer Therapy. *Adv. Drug Deliv. Rev.* **2004**, *56*, 1649–1659.

Brunsveld, L.; Folmer, B. J. B.; Meijer, E. W.; Sijbesma, R. P. Supramolecular Polymers. *Chem. Rev.* **2001**, *101*, 4071–4098.

Burke, M. D.; Park, J. O.; Srinivasarao, M.; Khan, S. A. A Novel Enzymatic Technique for Limiting Drug Mobility in a Hydrogel Matrix *J. Control. Release* **2005**, *104*, 141–153.

Cabral, H.; Nishiyama, N.; Kataoka, K. Supramolecular Nanodevices: From Design Validation to Theranostic Nanomedicine. *Acc. Chem. Res.* **2011**, *44*, 999−1008.

Caminade, A. M.; Majoral, J. P. Nanomaterials Based on Phosphorus Dendrimers. *Acc. Chem. Res.* **2004**, *37*, 341–348.

Chang, Y. T.; Cheng, C. M.; Su, Y. Z.; Lee, W. T.; Hsu, J. S.; Liu, G. C.; Cheng, T. L.; Wang, Y. M. Synthesis and Characterization of a New Bioactivated Paramagnetic Gadolinium(III) Complex [Gd(DOTA-FPG)(H2O)] for Tracing Gene Expression. *Bioconjug. Chem.* **2007**, *18*, 1716–1727.

Chen, J.; Tung, C.-H.; Allport, J. R.; Chen, S.; Weissleder, R.; Huang, P. L. Near-Infrared Fluorescent Imaging of Matrix Metalloproteinase Activity after Myocardial Infarction. *Circulation* **2005**, *111*, 1800–1805.

Chung, H. J.; Park, T. G. Self-Assembled and Nanostructured Hydrogels for Drug Delivery and Tissue Engineering. *Nano Today* **2009**, *4*, 429–437.

Daniel, M. -C.; Astruc, D. Gold Nanoparticles: Assembly, Supramolecular Chemistry, Quantum-Size-Related Properties, and Applications toward Biology, Catalysis, and Nanotechnology. *Chem. Rev.* **2004,** *104*, 293–346.

de Groot, F. M. H.; Albrecht, C.; Koekkoek, R.; Beusker, P. H.; Scheeren, H. W. "Cascade-Release Dendrimers" Liberate All End Groups upon a Single Triggering Event in the Dendritic Core. *Angew. Chem. Int. Ed.* **2003**, *42*, 4490–4494;

Dendrimer Assemblies and Supramolecular Aspects. *C.R. Chim.* **2003**, *6*, Issues 8−10, pp 709−817.

Diaz Diaz, D.; Kuhbeck, D.; Koopmans, R. J. Stimuli-Responsive Gels as Reaction Vessels and Reusable Catalysts. Chem. Soc. Rev. **2011**, *40*, 427–448.

Discher, B. M.; Won, Y. Y.; Ege, D. S.; Lee, J. C.-M.; Bates, F. S.; Discher, D. E.; Hammer, D. A. Polymersomes: Tough Vesicles Made from Diblock Copolymers. *Science* **1999**, *284*, 1143–1146.

Elghanian, R.; Storhoff, J. J.; Mucic, R. C.; Letsinger, R. L.; Mirkin, C. A. Selective Colorimetric Detection of Polynucleotides Based on the Distance-Dependent Optical Properties of Gold Nanoparticles. *Science* **1997**, *277*, 1078–1081.

Elsabahy, M.; Wooley, K. L. Design of Polymeric Nanoparticles for Biomedical Delivery Applications. *Chem. Soc. Rev.* **2012,** *41*, 2545–2561.

Evans, D. F.; Ninham, B. W. Molecular Forces in the Self-Organization of Amphiphiles. *J. Phys. Chem.* **1986**, *90*, 226−234.

Evans, D. F.; Wennerstrom, H. *The Colloidal Domain*, 2nd ed.; Wiley-VCH: New York, 1999.

Fan, C.; Plaxco, K. W.; Heeger, A. J. High-Efficiency Fluorescence Quenching of Conjugated Polymers by Proteins. *J. Am. Chem. Soc.* **2002**, *124*, 5642–5643.

Fuhrhop, J.-H.; Wang, T. Bolaamphiphiles. *Chem. Rev.* **2004**, *104*, 2901–2937.

Fuller, J. M.; Raghupathi, K. R.; Ramireddy, R. R.; Subrahmanyam, A. V.; Yesilyurt, V.; Thayumanavan, S. Temperature-Sensitive Transitions below LCST in Amphiphilic Dendritic Assemblies: Host–Guest Implications. *J. Am. Chem. Soc.* **2013**, *135*, 8947–8954.

Gao, W.; Xing, B.; Tsien, R. Y.; Rao, J. Novel Fluorogenic Substrates for Imaging β-Lactamase Gene Expression. *J. Am. Chem. Soc.* **2003**, *125*, 11146–11147.

Ge, Z.; Xie, D.; Chen, D.; Jiang, X.; Zhang, Y.; Liu, H.; Liu, S. Stimuli-Responsive Double Hydrophilic Block Copolymer Micelles with Switchable Catalytic Activity. Macromolecules **2007**, *40*, 3538–3546.

Gestwicki, J. E.; Strong, L. E.; Kiessling, L. L. Tuning Chemotactic Responses with Synthetic Multivalent Ligands. *Chem. Biol.* **2000**, *7*, 583–591.

Ghosh, P. S.; Hamilton, A. D. Supramolecular Dendrimers: Convenient Synthesis by Programmed Self-Assembly and Tunable Thermoresponsivity. *Chem. Eur. J.* **2012,** *18*, 2361–2365.

Giardiello, M.; Lowe, M. P.; Botta, M. An Esterase-Activated Magnetic Resonance Contrast Agent. *Chem. Commun.* **2007**, 4044–4046.

Giljohann, D. A.; Seferos, D. S.; Daniel, W. L.; Massich, M. D.; Patel, P. C.; Mirkin, C. A. Gold Nanoparticles for Biology and Medicine. *Angew. Chem. Int. Ed.* **2010,** *49*, 3280–3294.

Gnanaguru, K.; Ramasubbu, N.; Venkatesan, K.; Ramamurthy, V. A Study on the Photochemical Dimerization of Coumarins in the Solid State. *J. Org. Chem.* **1985,** *50*, 2337–2346.

Goodwin, S.; Gade, A. M.; Byrom, M.; Herrera, B.; Spears, C.; Anslyn, E. V.; Ellington, A. D. Next-Generation Sequencing as Input for Chemometrics in Differential Sensing Routines. *Angew. Chem. Int. Ed.* **2015**, *54*, 6339–6342.

Grayson, S. M.; Fréchet, J. M. J. Convergent Dendrons and Dendrimers: from Synthesis to Applications. *Chem. Rev.* **2001**, *101*, 3819–3868.

Grobner, T. Gadolinium--a Specific Trigger for the Development of Nephrogenic Fibrosing Dermopathy and Nephrogenic Systemic Fibrosis? *Nephrol. Dial. Transplant* **2006**, *21*, 1104–1108.

Grobner, T.; Prischl, F. C. Gadolinium and Nephrogenic Systemic Fibrosis. *Kidney Int.* **2007**, *72*, 260–264.

Gutiérrez, J.; Horrillo, M. C. Advances in Artificial Olfaction: Sensors and Applications. *Talanta* **2014**, *124*, 95–105.

Harada, A.; Kataoka, K. Supramolecular Assemblies of Block Copolymers in Aqueous Media as Nanocontainers Relevant to Biological Applications. *Progress in Poly. Sci.* **2006,** *31*, 949–982.

Harnoy, A. J.; Rosenbaum, I.; Tirosh, E.; Ebenstein, Y.; Shaharabani, R.; Beck, R.; Amir, R. J. Enzyme-Responsive Amphiphilic PEG-Dendron Hybrids and Their Assembly into Smart Micellar Nanocarriers. *J. Am. Chem. Soc.* **2014**, *136*, 7531–7534.

Hartgerink, J. D.; Beniash, E.; Stupp, S. I. Self-Assembly and Mineralization of Peptide-Amphiphile Nanofibers. *Science* **2001**, *294*, 1684−1688.

Hawker, C. J.; Wooley, K. L.; Fréchet, J. M. J. Unimolecular Micelles and Globular Amphiphiles: Dendritic Macromolecules as Novel Recyclable Solubilization Agents. *J. Chem. Soc., Perkin Trans. 1* **1993**, 1287-1297.

He, J.; Tong, X.; Zhao, Y. Photoresponsive Nanogels Based on Photocontrollable Cross-Links. *Macromolecules* **2009**, *42*, 4845–4852.

He, J.; Tremblay, L.; Lacelle, S.; Zhao, Y. Preparation of Polymer Single Chain Nanoparticles Using Intramolecular Photodimerization of Coumarin. *Soft Matter* **2011,** *7*, 2380–2386.

He, Y.; Shao, Q.; Chen, S. F.; Jiang, S. Y. Water Mobility: A Bridge between the Hofmeister Series of Ions and the Friction of Zwitterionic Surfaces in Aqueous Environments. *J. Phys. Chem. C* **2011**, *115*, 15525–15531.

Higuchi, M.; Iwata, N.; Matsuba, Y.; Sato, K.; Sasamoto, K.; Saido, T. C. ^{19}F and ^{1}H MRI Detection of Amyloid Beta Plaques in Vivo. *Nat. Neurosci.* **2005**, *8*, 527–533.

Hofmeister, F. On the Understanding of the Effects of Salts, Second report. On Irregularities in The Precipitating Effect of Salts and Their Relationship to Their Physical Behavior. *Arch. Exp. Pathol. Pharmocol.* **1888**, *24*, 247–260.

Hu, H.-Y.; Gehrig, S.; Reither, G.; Subramanian, D.; Mall, M. A.; Plettenburg, O.; Schultz, C. FRET-Based and Other Fluorescent Proteinase Probes. *Biotechnol. J.* **2014**, *9*, 266–281.

Ikeda, M.; Ochi, R.; Wada, A.; Hamachi, I. Supramolecular Hydrogel Capsule Showing Prostate Specific Antigen-Responsive Function for Sensing and Targeting Prostate Cancer Cells. *Chem. Sci.* **2010**, *1*, 491–498.

Israelachvili, J. N.; Mitchell, D. J.; Ninham, B. W. Theory of Self-Assembly of Hydrocarbon Amphiphiles into Micelles and Bilayers. *J. Chem. Soc., Faraday Trans II.* **1976**, *72*, 1525−1568.

Iyer, A. K.; Khaled, G.; Fang, J.; Maeda, H. Exploiting the Enhanced Permeability and Retention Effect for Tumor Targeting. *Drug Discov. Today* **2006**, *11*, 812–818.

Jiwpanich, S.; Ryu, J. H.; Bickerton, S.; Thayumanavan, S. Noncovalent Encapsulation Stabilities in Supramolecular Nanoassemblies. *J. Am. Chem. Soc.* **2010**, *132*, 10683–10685.

Juodkazis, S.; Mukai, N.; Wakaki, R.; Yamaguchi, A.; Matsuo, S.; Misawa, H. Reversible Phase Transitions in Polymer Gels Induced by Radiation Forces. *Nature* **2000**, *408*, 178–181.

Kamiya, M.; Kobayashi, H.; Hama, Y.; Koyama, Y.; Bernardo, M.; Nagano, T.; Choyke, P. L.; Urano, Y. An Enzymatically Activated Fluorescence Probe for Targeted Tumor Imaging. *J. Am. Chem. Soc.* **2007**, *129*, 3918–3929.

Kang, Y.; Walish, J. J.; Gorishnyy, T.; Thomas, E. L. Broad-Wavelength-Range Chemically Tunable Block-Copolymer Photonic Gels. *Nat. Mater.* **2007**, *6*, 957–960.

Kapdi, A. R.; Fairlamb, I. J. S. Synthesis of Macrocyclic Ketones Exploiting Palladium-Catalyzed Activation of Carboxylic Acids as an Enabling Step. *New J. Chem.* **2013,** *37*, 961–964.

Khandare, J.; Calderon, M.; Dagi, N. M.; Haag, R. Multifunctional Dendritic Polymers in Nanomedicine: Opportunities and Challenges. *Chem. Soc. Rev.* **2012,** *41*, 2824–2848.

Kikuchi, A.; Okano, T. Intelligent Thermoresponsive Polymeric Stationary Phases for Aqueous Chromatography of Biological Compounds. Prog. Polym. Sci. **2002**, *27*, 1165–1193.

Kim, I.-B.; Dunkhorst, A.; Bunz, U. H. F. Nonspecific Interactions of a Carboxylate-Substituted PPE with Proteins. A Cautionary Tale for Biosensor Applications. *Langmuir* **2005**, *21*, 7985–7989.

Kim, J.; Yoon, J.; Hayward, R. C. Dynamic Display of Biomolecular Patterns Through an Elastic Creasing Instability of Stimuli-Responsive Hydrogels. *Nat Mater.* **2010**, *9*, 159–164.

Klein, H. L. The Consequences of Rad51 Overexpression for Normal and Tumor Cells. *DNA Repair* **2008**, *7*, 686–693.

Kobayashi, H.; Ogawa, M.; Alford, R.; Choyke, P. L.; Urano, Y. New Strategies for Fluorescent Probe Design in Medical Diagnostic Imaging. *Chem. Rev.* **2010**, *110*, 2620–2640.

Kodadek, T.; Reddy, M. M.; Olivos, H. J.; Bachhawat-Sikder, K.; Alluri, P. G. Synthetic Molecules as Antibody Replacements. *Acc. Chem. Res.* **2004**, *37*, 711–718.

Krishnamurthy, V. M.; Kaufman, G. K.; Urbach, A. R.; Gitlin, I.; Gudiksen, K. L.; Weibel, D. B.; Whitesides, G. M. Carbonic Anhydrase as a Model for Biophysical and Physical-Organic Studies of Proteins and Protein-Ligand Binding. *Chem. Rev.* **2008**, *108*, 946–1051.

Krishnamurthy, V. M.; Semetey, V.; Bracher, P. J.; Shen, N.; Whitesides, G. M. Dependence of Effective Molarity on Linker Length for an Intramolecular Protein−Ligand System. *J. Am. Chem. Soc.* **2007**, *129*, 1312–1320.

Kwon, I. C.; Bae, Y. H.; Kim, S. W. Electrically Credible Polymer Gel for Controlled Release of Drugs. *Nature* **1991**, *354*, 291–293.

Langer, R. New Methods of Drug delivery. *Science* **1990**, *249*, 1527–1533.

Lavis, L. D.; Raines, R. T. Bright Ideas for Chemical Biology. *ACS Chem. Biol.* **2008**, *3*, 142–155.

Lecommandoux, S.; Sandre, O.; Checot, F.; Rodriguez-Hernandez, J.; Perzynski, R. Magnetic Nanocomposite Micelles and Vesicles. *Adv. Mater.* **2005**, *17*, 712–718.

Lee, C.; Lo, S.-T.; Lim, J.; da Costa, V. C. P.; Ramezani, S.; Öz, O. K.; Pavan, G. M.; Annunziata, O.; Sun, X.; Simanek, E. E. Design, Synthesis and Biological Assessment of a Triazine Dendrimer with Approximately 16 Paclitaxel Groups and 8 PEG Groups. *Mol. Pharm.* **2013**, *10*, 4452-4461.

Lee, D.-H.; Blomhoff, R.; Jacobs, D. R. Is Serum Gamma Glutamyltransferase a Marker of Oxidative Stress? *Free Radic. Res.* **2004**, *38*, 535–539.

Lee, H. C.; Kim, S.-J.; Kim, K.-S.; Shin, H.-C.; Yoon, J.-W. Remission in Models of Type 1 Diabetes by Gene Therapy Using a Single-Chain Insulin Analogue. *Nature* **2000**, *408*, 483–488.

Lee, M.; Cho, B.-K.; Zin, W.-C. Supramolecular Structures from Rod−Coil Block Copolymers. *Chem. Rev.* **2001**, *101*, 3869–3892.

Li, L.; Ryu, J.; Thayumanavan, S. Effect of Hofmeister Ions on the Size and Encapsulation Stability in Polymer Nanogels. *Langmuir*, **2013**, *29*, 50–55.

Liu, J.; Lu, Y. Stimuli-Responsive Disassembly of Nanoparticle Aggregates for Light-Up Colorimetric Sensing. *J. Am. Chem. Soc.* **2005**, *127*, 12677–12683.

Louie, A. Y.; Huber, M. M.; Ahrens, E. T.; Rothbacher, U.; Moats, R.; Jacobs, R. E.; Fraser, S. E.; Meade, T. J. In Vivo Visualization of Gene Expression using Magnetic Resonance Imaging. *Nat. Biotechnol.* **2000**, *18*, 321–325.

Ma, X.; Zhao, Y. Biomedical Applications of Supramolecular Systems Based on Host–Guest Interactions. *Chem. Rev.* **2015**, *115*, 7794–7839.

Maeda, H.; Bharate, G. Y.; Daruwalla, J. Polymeric Drugs for Efficient Tumor-Targeted Drug Delivery based on EPR-Effect. *Eur. J. Pharm. Biopharm.* **2009**, *71*, 409–419.

Maeda, H.; Wu, J.; Sawa, T.; Matsumura, Y.; Hori, K. Tumor Vascular Permeability and the EPR Effect in Macromolecular Therapeutics: A Review. *J. Control. Release* **2000**, *65*, 271–284.

Magnusson, J. P.; Khan, A.; Pasparakis, G.; Saeed, A. O.; Wang, W. X.; Alexander, C. Ion-sensitive "Isothermal" Responsive Polymers Prepared in Water. *J. Am. Chem. Soc.* **2008**, *130*, 10852–10853.

Mammen, M.; Choi, S. K.; Whitesides, G. M. Polyvalent Interactions in Biological Systems: Implications for Design and Use of Multivalent Ligands and Inhibitors. *Angew. Chem., Int. Ed.* **1998**, *37*, 2754–2794.

Matulis, D.; Kranz, J. K.; Salemme, F. R.; Todd, M. J. Thermodynamic Stability of Carbonic Anhydrase: Measurements of Binding Affinity and Stoichiometry using ThermoFluor. *Biochemistry* **2005**, *44*, 5258–5266.

Mehlich, J.; Ravoo, B. J. Click Chemistry by Microcontact Printing on Self-Assembled Monolayers: A Structure–Reactivity Study by Fluorescence Microscopy. *Org. Biomol. Chem.* **2011,** *9,* 4108–4115.

Meng, F.; Zhong, Z.; Feijen, J. Stimuli-Responsive Polymersomes for Programmed Drug Delivery. *Biomacromolecules* **2009**, *10*, 197–209.

Menger, F. M. The Structure of Micelles. *Acc. Chem. Res.* **1979**, *12*, 111–117.

Micheli, M.-Rita; Bova, R.; Magini, A.; Polidoro, M.; Emiliani, C. Lipid-Based Nanocarriers for CNS-Targeted Drug Delivery. *Recent Pat. CNS Drug Discov.* **2012,** *7*, 71–86.

Miyake, M.; Yamada, K.; Oyama, N. Self-Assembling of Guanidine-Type Surfactant. *Langmuir* **2008**, *24*, 8527–8532.

Moffitt, M.; Khougaz, K.; Eisenberg, A. Micellization of Ionic Block Copolymers. *Acc. Chem. Res.* **1996**, *29*, 95–102.

Mourez, M.; Kane, R. S.; Mogridge, J.; Metallo, S.; Deschatelets, P.; Sellman, B. R.; Whitesides, G. M.; Collier, R. J. Nat. Designing a Polyvalent Inhibitor of Anthrax Toxin. *Biotechnol.* **2001**, *19*, 958–961.

Muthuramu, K.; Ramamurthy, V. Photodimerization of Coumarin in Aqueous and Micellar Media. *J. Org. Chem.* **1982,** *47*, 3976–3979.

Nagarajan, R. Molecular Packing Parameter and Surfactant Self-assembly: The Neglected Role of the Surfactant Tail. *Langmuir* **2002**, *18*, 31−38.

Nanoparticles: Building Blocks for Nanotechnology; Rotello, V. M., Ed.; Springer: 2003.

Nanoparticles: From Theory to Application; Schmid, G., Ed.; Wiley-VCH: Essen, 2004.

Neiser, M. W.; Muth, S.; Kolb, U.; Harris, J. R.; Okuda, J.; Schmidt, M. Micelle Formation from Amphiphilic "Cylindrical Brush"–Coil Block Copolymers Prepared by Metallocene Catalysis. *Angew. Chem., Int. Ed.* **2004**, *43*, 3192–3195.

Newkome, G. R.; He, E.; Moorefield, C. N. Suprasupermolecules with Novel Properties: Metallodendrimers. *Chem. Rev.* **1999**, *99*, 1689–1746.

Newkome, G. R.; Yao, Z.; Baker, G. R.; Gupta, V. K. Micelles. Part 1. Cascade Molecules: a New Approach to Micelles. A [27]-Arborol. *J. Org. Chem.* **1985**, *50*, 2003-2004.

Niederhafner, P.; Se-bestik, J.; Jezek, J. Glycopeptide Dendrimers. Part II. *J. Pept. Sci.* **2008**, *14*, 44–65.

Oh, K. J.; Cash, K. J.; Plaxco, K. W. Excimer-Based Peptide Beacons: A Convenient Experimental Approach for Monitoring Polypeptide−Protein and Polypeptide−Oligonucleotide Interactions. *J. Am. Chem. Soc.* **2006**, *128*, 14018–14019.

Okhapkin, I. M.; Makhaeva, E. E.; Khokhlov, A. R. Water Solutions of Amphiphilic Polymers: Nanostructure Formation and Possibilities for Catalysis. *Adv. Polym. Sci.* **2006**, *195*, 177–210.

O'Reilly, R. K.; Hawker, C. J.; Wooley, K. L. Cross-Linked Block Copolymer Micelles: Functional Nanostructures of Great Potential and Versatility. *Chem. Soc. Rev.* **2006,** *35*, 1068–1083.

Owen, S. C.; Chan, D. P. Y.; Shoichet, M. S. Polymeric Micelle Stability. *Nano Today* **2012,** *7*, 53–65.

Perez, J. M.; Josephson, L.; O'Loughlin, T.; Högemann, D.; Weissleder, R. Magnetic Relaxation Switches Capable of Sensing Molecular Interactions. *Nat. Biotechnol.* **2002**, *20*, 816–820.

Raghupathi, K. R.; Azagarsamy, M. A.; Thayumanavan, S. Guest-Release Control in Enzyme-Sensitive, Amphiphilic-Dendrimer-Based Nanoparticles through Photochemical Crosslinking. *Chem. Eur. J.* **2011,** *17*, 11752–11760.

Raghupathi, K. R.; Guo, J.; Munkhbat, O.; Rangadurai, P.; Thayumanavan, S. Supramolecular Disassembly of Facially Amphiphilic Dendrimer Assemblies in Response to Physical, Chemical, and Biological Stimuli. *Acc. Chem. Res.* **2014**, *47*, 2200–2211.

Rijcken, C. J. F.; Soga, O.; Hennink, W. E.; van Nostrum, C. F. J. Triggered Destabilisation of Polymeric Micelles and Vesicles by Changing Polymers Polarity: An Attractive Tool for Drug Delivery. *J. Control. Release* **2007**, *120*, 131–148.

Roy R.; Yang J.; Moses M. A. Matrix Metalloproteinases as Novel Biomarkers and Potential Therapeutic Targets in Human Cancer. *J. Clin. Oncol.* **2009**, *27*, 5287–5297.

Roy, D.; Sumerlin, B. S. Glucose-Sensitivity of Boronic Acid Block Copolymers at Physiological pH. *ACS Macro Lett.* **2012,** *1,* 529–532.

Ryu, J.-H.; Chacko, R.; Jiwpanich, S.; Bickerton, S.; Babu, R. P.; Thayumanavan, S. Self-Crosslinked Polymer Nanogels: a Versatile Nanoscopic Drug Delivery Platform. *J. Am. Chem. Soc.* **2010**, *132*, 17227–17235.

Ryu, J.-H.; Jiwpanich, S.; Chacko, R.; Bickerton, S.; Thayumanavan, S. Surface-Functionalizable Polymer Nanogels with Facile Hydrophobic Guest Encapsulation Capabilities. *J. Am. Chem. Soc.* **2010**, *132*, 8246–8247.

Saavedra, J. E.; Shami, P. J.; Wang, L. Y.; Davies, K. M.; Booth, M. N.; Citro, M. L.; Keefer, L. K. Esterase-Sensitive Nitric Oxide Donors of the Diazeniumdiolate Family: In Vitro Antileukemic Activity. *J. Med. Chem.* **2000**, *43*, 261–269.

Saha, K.; Agasti, S. S.; Kim, C.; Li, X.; Rotello, V. M. Gold Nanoparticles in Chemical and Biological Sensing. *Chem. Rev.* **2012,** *112*, 2739–2779.

Samantaray, S.; Sharma, R.; Chattopadhyaya, T. K.; Gupta, S. D.; Ralhan, R. Increased Expression of MMP-2 and MMP-9 in Esophageal Squamous Cell Carcinoma. *J. Cancer Res. Clin. Oncol.* **2004**, *130*, 37–44.

Sandanaraj, B. S.; Demont, R.; Aathimanikandan, S. V.; Savariar, E. N.; Thayumanavan, S. Selective Sensing of Metalloproteins from Non-selective Binding using a Fluorogenic Amphiphilic Polymer. *J. Am. Chem. Soc.* **2006**, *128*, 10686–10687.

Sandanaraj, B. S.; Demont, R.; Thayumanavan, S. Generating Patterns for Sensing Using a Single Receptor Scaffold. *J. Am. Chem. Soc.* **2007**, *129*, 3506–3507.

Sawant, R. R.; Torchilin, V. P. Liposomes as 'Smart' Pharmaceutical Nanocarriers. *Soft Matter* **2010,** *6*, 4026–4044.

Schmaljohann, D. Thermo- and pH-responsive Polymers in Drug Delivery. *Adv. Drug Deliv. Rev.* **2006**, *58*, 1655–1670.

Schulze, A.; Giannis, A. IBX-Mediated Conversion of Primary Alcohols and Aldehydes to N-Hydroxysuccinimide Esters. *Adv. Synth. Catal.* **2004,** *346*, 252–256.

Searle N. *Environmental Effects on Polymeric Materials*; Plastics and the Environment; Andrade, A., Ed.; Wiley: 2003; pp. 313-358.

Seyrek, E.; Dubin, P. L.; Tribet, C.; Gamble, E. A. Ionic Strength Dependence of Protein-Polyelectrolyte Interactions. *Biomacromolecules* **2003**, *4*, 273–282.

Shchukin, D. G.; Grigoriev, D. O.; Mohwald, H. Application of Smart Organic Nanocontainers in Feedback Active Coatings. Soft Matter **2010**, *6*, 720–725.

Silvers, W. C.; Prasai, B.; Burk, D. H.; Brown, M. L.; McCarley, R. L. Profluorogenic Reductase Substrate for Rapid, Selective, and Sensitive Visualization and Detection of Human Cancer Cells that Overexpress NQO1. *J. Am. Chem. Soc.* **2013**, *135*, 309–314.

Simoni, E.; Daniele, S.; Bottegoni G.; Pizzirani D.; Trincavelli, M. L.; Goldoni, L.; Tarozzo, G.; Reggiani, A.; Martini, C.; Piomelli, D.; Melchiorre, C.; Rosini, M.; Cavall, A. Combining Galantamine and Memantine in Multitargeted, New Chemical Entities Potentially Useful in Alzheimer's Disease. *J. Med. Chem.* **2012,** *55*, 9708–9721.

Sivanandan, K.; Aathimanikandan, S. V.; Arges, C. G.; Bardeen, C. J.; Thayumanavan, S. Probing Every Layer in Dendrons. *J. Am. Chem. Soc.* **2005**, *127*, 2020-2021.

Sivanandan, K.; Sandanaraj, B. S.; Thayumanavan, S. Sequences in Dendrons and Dendrimers. *J. Org. Chem.* **2004**, *69*, 2937-2944.

Soussan, E.; Cassel, S.; Blanzat, M.; Rico-Lattes, I. Drug Delivery by Soft Matter: Matrix and Vesicular Carriers. *Angew. Chem., Int. Ed.* **2009**, *48*, 274−288.

Stockwell, B. R. Exploring Biology with Small Organic Molecules. *Nature* **2004**, *432,* 846–854.

Stuart, M. A. C.; Huck, W. T. S.; Genzer, J.; Muller, M.; Ober, C.; Stamm, M.; Sukhorukov, G. B.; Szleifer, I.; Tsukruk, V. V.; Urban, M.; Winnik, F.; Zauscher, S.; Luzinov, I.; Minko, S. Emerging Applications of Stimuli-Responsive Polymer Materials. *Nat. Mater.* **2010**, *9*, 101–113.

Sun, W.; Bandmann, H.; Schrader, T. A Fluorescent Polymeric Heparin Sensor. *Chem. Eur. J.* **2007,** *13,* 7701–7707.

Suwa, K.; Yamamoto, K.; Akashi, M.; Takano, K.; Tanaka, N.; Kunugi, S. Effects of Salt on the Temperature and Pressure Responsive Properties of Poly(N-vinylisobutyramide) Aqueous Solutions. *Colloid Polym. Sci.* **1998**, *276*, 529–533.

Svenson, S.; Tomalia, D. A. Dendrimers in Biomedical Applications--Reflections on the Field. *Adv. Drug Deliv. Rev.* **2005**, *57*, 2106–2129.

Swann, J. M. G.; Bras, W.; Topham, P. D.; Howse, J. R.; Ryan, A. J. Effect of the Hofmeister Anions Upon the Swelling of a Self-Assembled pH-Responsive Hydrogel. *Langmuir* **2010**, *26*, 10191–10197.

Takaoka, Y.; Sakamoto, T.; Tsukiji, S.; Narazaki, M.; Matsuda, T.; Tochio, H.; Shirakawa, M.; Hamachi, I. Self-Assembling Nanoprobes that Display off/on ^{19}F Nuclear Magnetic Resonance Signals for Protein Detection and Imaging. *Nat. Chem.* 2009, **1**, 557–561.

Tanabe, K.; Harada, H.; Narazaki, M.; Tanaka, K.; Inafuku, K.; Komatsu, H.; Ito, T.; Yamada, H.; Chujo, Y.; Matsuda, T.; Hiraoka, M.; Nishimoto, S. Monitoring of Biological One-Electron Reduction by ^{19}F NMR Using Hypoxia Selective Activation of an 19F-Labeled Indolequinone Derivative *J. Am. Chem. Soc.* **2009**, *131*, 15982–15983.

Tanaka, K.; Kitamura, N.; Naka, K.; Chujo, Y. Multi-Modal ^{19}F NMR Probe Using Perfluorinated Cubic Silsesquioxane-Coated Silica Nanoparticles for Monitoring Enzymatic Activity. *Chem. Commun.* **2008**, 6176–6178.

Tandon, N.; Cannizzaro, C.; Chao, P.-H. G.; Maidhof, R.; Marsano, A.; Au, H. T. H.; Radisic, M.; Vunjak-Novakovic, G. Electrical Stimulation Systems for Cardiac Tissue Engineering. *Nat. Protoc.* **2009**, *4*, 155–173.

Taylor, P. W.; King, R. W.; Burgen, A. S. V. Kinetics of Complex Formation between Human Carbonic Anhydrases and Aromatic Sulfonamides. *Biochemistry* **1970**, *9*, 2638–2645.

Thornton, P. D.; McConnell, G.; Ulijn, R. V. Enzyme Responsive Polymer Hydrogel Beads. *Chem. Commun.* **2005**, 5913–5915.

Thurecht, K. J.; Blakey, I.; Peng, H.; Squires, O.; Hsu, S.; Alexander, C.; Whittaker, A. K. Functional Hyperbranched Polymers: Toward Targeted in Vivo ^{19}F Magnetic Resonance Imaging Using Designed Macromolecules. *J. Am. Chem. Soc.* **2010**, *132*, 5336–5337.

Thurley, S.; Röglin, L.; Seitz, O. Hairpin Peptide Beacon: Dual-Labeled PNA-Peptide-Hybrids for Protein Detection. *J. Am. Chem. Soc.* **2007**, *129*, 12693–12695.

Tomalia, D. A.; Baker, H.; Dewald, J.; Hall, M.; Kallos, G.; Martin, S.; Roeck, J.; Ryder, J.; Smith, P. A New Class of Polymers: Starburst-Dendritic Macromolecules. *Polym. J.* **1985**, *17*, 117-132.

Tomalia, D. A.; Fréchet, J. M. J. Discovery of Dendrimers and Dendritic Polymers: A Brief Historical Perspective. *J. Polym. Sci. A Polym. Chem.* **2002**, *40*, 2719–2728.

Torchilin, V. P. Structure and Design of Polymeric Surfactant-based Drug Delivery Systems. *J. Control. Release* **2001**, *73*, 137−172.

Trenor, S. R.; Shultz, A. R.; Love, B. J.; Long, T. E. Coumarins in Polymers: From Light Harvesting to Photo-Cross-Linkable Tissue Scaffolds. *Chem. Rev.* **2004,** *104*, 3059–3078.

Tung, S. H.; Lee, H. Y.; Raghavan, S. R. A Facile Route for Creating “Reverse” Vesicles: Insights into “Reverse” Self-Assembly in Organic Liquids. *J. Am. Chem. Soc.* **2008**, *130*, 8813– 8817.

Udenfriend, S.; Stein, S.; Böhlen, P.; Dairman, W.; Leimgruber, W.; Weigele, M. Fluorescamine: A Reagent for Assay of Amino Acids, Peptides, Proteins, and Primary Amines in the Picomole Range. *Science* **1972,** 178, 871–872.

Van Nostrum, C. F. Covalently Cross-Linked Amphiphilic Block Copolymer Micelles. *Soft Matter* **2011,** *7*, 3246–3259.

Vauthey, S.; Santoso, S.; Gong, H.; Watson, N.; Zhang, S. Molecular Self-Assembly of Surfactant-like Peptides to Form Nanotubes and Nanovesicles. *Proc. Natl. Acad. Sci. U.S.A.* **2002**, *99*, 5355–5360.

Vitzthum, F.; Behrens, F.; Anderson, N. L.; Shaw, J. H. Proteomics: From Basic Research to Diagnostic Application. A Review of Requirements & Needs *J. Proteome Res.* **2005**, *4*, 1086–1097.

Von Hippel, P. H.; Wong., K. Y. Neutral Salts: The Generality of Their Effects on the Stability of Macromolecular Conformations. *Science* **1964**, *145*, 577–580.

Vutukuri, D. R.; Basu, S.; Thayumanavan, S. Dendrimers with Both Polar and Apolar Nanocontainer Characteristics. *J. Am. Chem. Soc.* **2004**, *126*, 15636–15637.

Wahlund, P. O.; Galaev, I. Y.; Kazakov, S. A.; Lozinsky, V. I.; Mattiasson, B. "Protein-Like" Copolymers: Effect of Polymer Architecture on the Performance in Bioseparation Process. *Macromol. Biosci.* **2002**, *2*, 33–42.

Wang, C.; Tam, K. C.; Jenkins, R. D.; Tan, C. B. Interactions between Methacrylic Acid/Ethyl Acrylate Copolymers and Dodecyltrimethylammonium Bromide. *J. Phys. Chem. B* **2003**, *107*, 4667–4675.

Wang, F.; Klaikherd, A.; Thayumanavan, S. Temperature Sensitivity Trends and Multi-Stimuli-Sensitive Behavior in Amphiphilic Oligomers. *J. Am. Chem. Soc.* **2011**, *133*, 13496–13503.

Weissleder, R.; Tung, C. H.; Mahmood, U.; Bogdanov, A. In Vivo Imaging of Tumors with Protease-Activated Near-Infrared Fluorescent Probes. *Nat. Biotechnol.* **1999**, *17*, 375–378.

Wilson, J. N.; Wang, Y.; Lavigne, J. J.; Bunz, U. H. F. A Biosensing Model System: Selective Interaction of Biotinylated PPEs with Streptavidin-Coated Polystyrene Microspheres. *Chem. Commun.* **2003**, 1626–1627.

Wilson, K. E.; Langdon, S. P.; Lessells, A. M.; Miller, W. R. Expression of the Extracellular Matrix Protein Tenascin in Malignant and Benign Ovarian Tumours. *Br. J. Cancer* **1996**, *74*, 999–1004.

Woller, E. K.; Cloninger, M. J. Mannose Functionalization of a Sixth Generation Dendrimer. *Biomacromolecules* **2001**, 2, 1052-1054.

Yamaguchi S.; Matsumoto, S.; Ishizuka, K.; Iko, Y.; Tabata, K. V.; Arata, H. F.; Fujita, H.; Noji, H.; Hamachi, I. Thermally Responsive Supramolecular Nanomeshes for On/Off Switching of the Rotary Motion of F_1-ATPase at the Single-Molecule Level. *Chem. Eur. J.* **2008**, *14*, 1891–1896.

Yang, C.-T.; Chuang, K.-H. Gd(III) Chelates for MRI Contrast Agents: from High Relaxivity to "Smart", from Blood Pool to Blood–Brain Barrier Permeable. *Med. Chem. Commun.* **2012**, *3*, 552–565.

Yashima, E.; Maeda, K. Chirality-Responsive Helical Polymers. *Macromolecules* **2007**, *41*, 3–12.

Yesilyurt, V.; Ramireddy, R.; Thayumanavan, S. Photoregulated Release of Noncovalent Guests from Dendritic Amphiphilic Nanocontainers. *Angew. Chem. Int. Ed. Engl.* **2011**, *50*, 3038–3042.

Yoo, B.; Pagel, M. D. A PARACEST MRI Contrast Agent to Detect Enzyme Activity. *J. Am. Chem. Soc.* **2006**, *128*, 14032–14033.

Yoshii, T.; Mizusawa, K.; Takaoka, Y.; Hamachi, I. Intracellular Protein-Responsive Supramolecules: Protein Sensing and In-Cell Construction of Inhibitor Assay System. *J. Am. Chem. Soc.* 2014, **136**, 16635–16642.

You, C.-C.; Miranda, O. R.; Gider, B.; Ghosh, P. S.; Kim, I.-B.; Erdogan, B.; Krovi, S. A.; Bunz, U. H. F.; Rotello, V. M. Detection and Identification of Proteins Using Nanoparticle–Fluorescent Polymer 'Chemical Nose' Sensors. *Nat. Nanotechnol.* **2007**, *2*, 318–323.

You, L.; Zha, D.; Anslyn, E. V. Recent Advances in Supramolecular Analytical Chemistry Using Optical Sensing. *Chem. Rev.* **2015**, *115*, 7840–7892.

Yu, J.-X.; Hallac, R. R.; Chiguru, S.; Mason, R. P. New Frontiers and Developing Applications in ^{19}F NMR. *Prog. Nucl. Magn. Reson. Spectrosc.* **2013**, *70*, 25–49.

Zhang, J.; Wang, Z.-l.; Liu, J.; Chen, S.; Liu, G.-y. *Self-Assembled Nanostructures*; Nanostructure Science and Technology Series; Springer: 2002.

Zhang, L.; Yu, K.; Eisenberg, A. Ion-Induced Morphological Changes in "Crew-Cut" Aggregates of Amphiphilic Block Copolymers. *Science* **1996**, *272*, 1777–1779.

Zhang, Y. J.; Furyk, S.; Bergbreiter, D. E.; Cremer, P. S. Specific Ion Effects on the Water Solubility of Macromolecules: PNIPAM and the Hofmeister Series. *J. Am. Chem. Soc.* **2005**, *127*, 14505–14510.

Zhang, Y.; Furyk, S.; Sagle, L. B.; Cho, Y.; Bergbreiter, D. E.; Cremer, P. S. Effects of Hofmeister Anions on the LCST of PNIPAM as a Function of Molecular Weight. *J. Phys. Chem. C* **2007**, *111*, 8916–8924.

Zhu, Z.; Sukhishvili, S. A. Layer-by-Layer Films of Stimuli-Responsive Block Copolymer Micelles. *J. Mat. Chem.* **2012,** *22*, 7667–7671.

Zhuang, J.; Gordon, M.; Ventura, J.; Li, L. Thayumanavan, S. Multi-Stimuli Responsive Macromolecules and Their Assemblies. *Chem. Soc. Rev.* **2013**, *42*, 7421–7435.